MECA WORKSHOP ON

DUST ON MARS II

MECA

LPI Technical Report Number 86-09

LUNAR AND PLANETARY INSTITUTE 3303 NASA ROAD 1 HOUSTON, TEXAS 77058-4399

MECA WORKSHOP ON

DUST ON MARS II

Edited by

Steven Lee

Sponsored by
The Lunar and Planetary Institute
National Aeronautics and Space Administration

Hosted by
Arizona State University
Tempe, Arizona
February 24–26, 1986

Lunar and Planetary Institute 3303 NASA Road 1 Houston, Texas 77058-4399

LPI Technical Report 86-09

Compiled in 1986 by the
LUNAR AND PLANETARY INSTITUTE

The Institute is operated by Universities Space Research Association under Contract NASW-4066 with the National Aeronautics and Space Administration.

This report may be cited as:
Lee S. ed. (1986) *MECA Workshop on Dust on Mars II.* LPI Tech. Rpt. 86-09. Lunar and Planetary Institute, Houston. 79 pp.

Papers in this report may be cited as:
Author A. A. (1986) Title of paper. In *MECA Workshop on Dust on Mars II* (S. Lee, ed.), pp. xx–yy. LPI Tech Rpt. 86-09. Lunar and Planetary Institute, Houston.

This report is distributed by:

LIBRARY/INFORMATION CENTER
Lunar and Planetary Institute
3303 NASA Road I
Houston, TX 77058-4399

Mail order requestors will be invoiced for the cost of postage and handling.

Contents

Program

Monday, February 24
9:00 a.m. - 12:15 p.m.

Session I: Physical and Chemical Properties of Dust
Chairman: Alan Peterfreund

J. Tillman
Martian atmospheric dust over three years as inferred from Lander meteorology measurements

T. Martin
Infrared opacity of dust in the Mars atmosphere

R. Kahn
The varying properties of martian aerosols

F. Jaquin
The vertical distribution of aerosols during the growth phase of a global dust storm

J. Gooding
Condensation of frosts on martian dust particles

D. Colburn, J. B. Pollack, and R. M. Haberle
Influence of dust on water condensation at Mars

A. Banin
Constraining Mars-dust mineralogy on the basis of Viking biology simulations and Mars spectral reflectance

R. Morris, H. V. Howard, Jr., D. G. Agresti, and J. A. Newcomb
Spectral properties of "dust" produced in the dry valleys of Antarctica; A martian analog?

Monday, February 24
1:30 - 4:30 p.m.

Session II: Atmospheric Dust Transport and Redistribution
Chairman: Robert Haberle

L. Martin and P. B. James
Dust clouds of a different nature

P. James and L. J. Martin
Interannual variability in Mars' South Polar recessions and possible correlations with major duststorms

D. Paige
Dust in the spring season polar atmospheres: A north-south comparison

J. Barnes and J. L. Hollingsworth
Implications of a polar warming for dust transport into the North Polar region of Mars

R. Haberle
The development of global dust storms on Mars: The role of the mean meridional circulation

R. Zurek and R. M. Haberle
Cross-equatorial transport during a martian great dust storm

J. Pollack, R. M. Haberle, J. Barnes, M. Schlesinger, R. Zurek, C. B. Leovy, J. White, J. Schaeffer, and K. Bilski
Influence of dust on the general circulation of the martian atmosphere

Tuesday, February 25
9:00 a.m. - 12:15 p.m.

Session III: Dust Erosion, Deposition, Sources, and Sinks
Chairman: Peter Thomas

R. Greeley
Toward an understanding of the martian dust cycle

R. Arvidson
On the rate of formation of sedimentary debris on Mars

H. Moore
Martian miniature landslides, Mutch Memorial Station

J. Zimbelman
Physical properties of aeolian features in the Elysium-Amazonis region of Mars

B. Jakosky and P. Christensen
Are the Viking Lander sites representative of the surface of Mars?

P. Christensen
Surface albedo variations on Mars: Implications for yearly dust deposition and removal

S. Lee
Viking observations of regional sources and sinks of dust on Mars

L. Roth, R. S. Saunders, and T. W. Thompson
Radar reflectivity of a variable dust cover

T. Thompson, R. F. Jurgens, L. Roth, and L. Robinett
Possible Goldstone radar observations of Mars: 1986 and 1988 oppositions

Tuesday, February 25
1:30 - 4:30 p.m.

Session : General Discussion/Overview/Questions

(1) How many dust components are there on Mars, and what are their properties?
(Discussion Leader: Alan Peterfreund)

(2) How does the global atmospheric circulation affect dust redistribution?
(Discussion Leader: Robert Haberle)

(3) How do dust sources and sinks vary with time?
(Discussion leader: Peter Thomas)

Summary of Technical Sessions and Discussions

A MECA workshop, "Dust on Mars II," was sponsored by NASA through the Lunar and Planetary Institute and hosted by Arizona State University on February 24–25, 1986. Following the recommendations of the participants in the previous MECA "dust" workshop (held at ASU on February 4–5, 1985), the goal of this workshop was to discuss the following questions:

(1) How many components of dust are there on Mars, and what are their properties?
(2) How is dust ejected from the surface into the atmosphere?
(3) How does the global atmospheric circulation affect the redistribution of dust?
(4) Are there sources and sinks of dust? If so, how do they vary with time?

Forty-three people attended the meeting and engaged in the discussion sections; of these, twenty-four presented summaries of their dust-related research.

The first workshop session considered the physical and chemical properties and the distribution (both temporal and spatial) of dust and condensates. Several "observational" presentations focused on detailed analyses of Viking data. Pressure data recorded over four martian years at Viking Lander 1 and two years at Viking Lander 2 have been studied by J. Tillman with particular attention to the major transient events related to two global dust storms in 1977 (Year 1) and one in 1982 (Year 4). The 1982 event was similar in season to the first 1977 storm (L_s ~200°) but was more intense than this storm, appearing instead to be similar to the second 1977 storm. The 1982 storm was noted as having a unique pressure signature, suggesting a second surge of intense activity a week after the initial change in pressures was noted. T. Martin presented a dust opacity history based on a global data analysis using the 7, 9, and 15 μm data collected by the Orbiters' Infrared Thermal Mappers (IRTM). The resultant maps of opacity depict the spatial and temporal variations of atmospheric dust loading throughout the Viking missions. Detailed maps during the 1977 dust storm season suggest large local variability of opacity in many areas.

Evidence for H_2O ice in the Mars atmosphere has been inferred from a variety of optical observations using the Landers and Orbiters. Limb observations show that a detached haze fluctuates in height and opacity with time and location. R. Kahn modelled the properties of these hazes during the non-dust storm periods with consideration of mean optical depth, condensation level, mean particle size, and eddy diffusion. Correlation of the cloud height with MAWD column water vapor abundance implies that water controls the location of the cloud base. The mean particle sizes increase as condensation heights decrease in such a way that the average fall time is always about 1/4 day. F. Jaquin reported on analysis of the limb observations made by the Orbiter cameras over three Mars years. Profiles of reflectance vs. elevation above the surface show the buildup of dust with height as a function of time and latitude. During the 1977 dust storm season, continuous haze up to 50 km altitude is seen in the northern hemisphere with a weak detached haze above that. The detached haze (probably condensates) is better defined in the southern hemisphere.

The second set of speakers reported on "laboratory and theoretical" results. J. Gooding has been performing experiments and modelling the heterogeneous nucleation of condensates on mineral grains. Favorable conditions for condensation appear to be related to crystallographic compatibility (with respect to structure and number of "active" sites) and the nature of chemical bonds. Details for mineral classes and for given minerals, especially clays, show the complexities of the nucleation process as a function of condensate type. Furthermore, as nucleation occurs the initial condensates will change conditions associated with subsequent nucleation. D. Colburn discussed the influence of dust on water condensation using Lander optical depth measurements. Both seasonal and diurnal effects appear to be factors in the amount of water condensation. Also, most condensation appears to occur aloft as opposed to near-surface, and is strongly related to dust abundance. Simulating results from the labeled-release biology experiment aboard the Landers, A. Banin inferred properties of martian dust. Smectite minerals (montmorillonite and nontronite) that were ion-modified were found to best simulate the kinetic results of the biology experiment.

The ion-modification served to exchange calcium and sodium ions with iron. This modification is consistent with Lander chemical analyses. These experiments suggest that: (1) the pH of martian soil is less than 4.5; (2) $CaCO_3$ probably cannot be in soil at concentrations larger than ~1.0%; (3) montmorillonite is apparently essential for causing rapid decomposition on clay surfaces. According to results presented by R. Morris, the spectra of martian bright regions suggest that "dust" produced in the dry valleys of Antarctica may be a reasonable martian analogue. Weathering on Mars, assuming analogous processes to those in Antarctica, results in more highly oxidized material, but in general appears to be similar to that for ferric products that were studied. Further, the presence of hematite as a component of martian dust is strongly suggested.

The second workshop session addressed topics of atmospheric dust transport and redistribution. L. Martin led off the session discussing equatorial dust clouds imaged by Viking that differed from other dust clouds because of their persistent association with a small canyon. Downslope katabatic-type winds may be responsible for the clouds' origin; in some cases they appeared to flow into the canyon floor. The potential of the telescopic record for revealing interannual variation in the CO_2 cycle was the subject of the presentation given by P. James. The signature of this variability appears as differences in the retreat rate of the south polar cap (readily observed during favorable oppositions). Comparison of data for the 1956, 1971, 1973, and 1977 dust storm years shows some variability with the cap retreating slower than the median in 1971 and 1977 and faster than the median in 1956 and 1973. The extent to which this variability would affect pressure variations is evidently small, however, given the high degree of repeatability in the seasonal pressure data from the Lander sites. D. Paige discussed his analysis of IRTM data at the north and south poles during the spring season. By constraining a radiative equilibrium model he developed to reproduce the brightness temperatures in the various IRTM channels, he concluded that dust in both polar regions is similar in composition to that observed in the tropics (the so called "Toon-Pollack" dust). He also found that unless the dust was confined to the lowest 5 km, it was not possible to reproduce the observed 15 micron brightness temperatures. This problem was even more difficult in the north where additional cooling, perhaps due to water ice, is needed.

J. Barnes focused attention on the transport implications of the warming of the north polar atmosphere during the second global dust storm of 1977. Based on models that follow the actual motion of air parcels, the observed warming must be accompanied by sinking motion; to conserve mass, poleward transport from lower latitudes is required. Barnes also discussed other modelling that implies that vertically-propagating forced stationary waves may play an important role in the heat budget of the polar atmosphere during global dust storms. In the next paper, R. Haberle presented a mechanism for interannual variability of global dust storms. His nearly inviscid zonally-symmetric circulation model suggests the following scenario: First, global dust storms transport dust into the northern hemisphere. This dust is then available for raising by baroclinic waves in the following years. During the post-dust-storm years the cross-equatorial Hadley circulation is therefore weakened due to heating by dust suspended in its descending branch. When the supply of dust is exhausted, the full strength of the Hadley circulation, and the likelihood of global dust storms, is restored. R. Zurek then spoke about how tidal forcing of the mean meridional circulation may break up the otherwise smooth structure of the cross-equatorial Hadley cell. During relatively dusty periods, tides produce significant accelerations of the zonal and meridional wind fields, and these accelerations have considerable vertical structure. When included in Haberle's 2D model, several vertically-stacked Hadley-type cells were produced. Zurek suggested that by changing the structure of the Hadley circulation, the tides could effectively limit the flux of dust into the northern hemisphere during a global dust storm, explaining the decay patterns seen at the Lander sites. Completing the "theoretical" presentations of this session, J. Pollack gave a progress report on the Mars general circulation model (GCM) and presented some preliminary results. Work on the GCM during the past several years has focused on including dust as a radiatively active constituent, generalizing the model to an arbitrary number of layers, and improving the numerical methods for calculating infrared fluxes. All of these changes have been implemented and tested, and the current effort has shifted to determining the model's performance in a variety of configurations and examining how dust affects the behavior of large-scale atmospheric eddies.

During the final session of the workshop, the participants turned their attention to the study of dust sedimentation and erosion on Mars. The research that was discussed is being conducted in three general areas: photointerpretation of sedimentary and erosional features, surface properties determined from thermal inertia, albedo, and radar data, and laboratory and theoretical work on the processes involved in wind transport of dust. R. Greeley tied together the various laboratory and theoretical studies applicable to the martian dust cycle. In particular, the continuing question of the role of volatiles in any aggregation of dust particles and in ejection of dust from the surface was considered. R. Arvidson presented results of a study of the morphology and statigraphy of south polar pitted and layered terrains that indicates deposition in two very different phases extending over about half of martian history. The radically different layered and unlayered pitted deposits suggest substantial differences in sedimentary regimes. At another size scale, H. Moore reported that the morphology of small landslides at the VL1 site is diagnostic of surface layers of very low cohesiveness that are probably recent aeolian deposits. Slope failure of such layers may be an important mechanism for producing a surface that is not in equilibrium with martian wind regimes, thereby enhancing the possibility of aeolian erosion.

Several specific regions of the planet were discussed in detail. The physical properties of aeolian features in the Elysium-Amazonis area were examined by J. Zimbelman. Analysis of the thermal inertia of wind streaks in the region suggests a long-lived movement of fine to medium sand-sized materials in the observed depositional dark streaks and possible dust deposits of significant thickness accumulating in bright streaks. B. Jakosky reported on a study relating the characteristics of the Lander sites to the global data on thermal inertia, albedo, and color; the sites apparently do not match the general planet-wide trends in these data sets. In particular, the VL1 site is intermediate between bright areas assumed to accumulate dust and those dark areas that are thought to be swept relatively clear. P. Christensen discussed the albedo variation of several areas on the planet using the IRTM albedo channel. He found that northern hemisphere dark regions showed a long period of progressive dust removal after global dust storms, while southern hemisphere dark regions show a rapid return to pre-storm albedos. S. Lee investigated regional sources and sinks using IRTM albedo data and Orbiter images. The patterns of temporal changes indicate that Syrtis Major, through much of the year, acts as a source region for dust redeposited in neighboring Arabia. In the Solis Planum region, removal of dust is restricted to periods of major dust-storm activity.

The ability of radar to detect seasonal variability in surface dust cover was examined by L. Roth. A theoretical study of radar reflectivity as a function of dust layer thickness concludes that time-variable reflectivity data would be consistent with significant changes in dust layer thickness only under very restricted conditions of layer geometry and continuity. The session was concluded with T. Thompson's review of future opportunities for radar observations of Mars. The 1986 and 1988 oppositions will greatly extend the southern hemisphere coverage available from previous years, while upgrades in the Goldstone radar should significantly improve resolution and allow both X- and S-band observations.

The final afternoon of the workshop consisted of an open discussion of the major questions posed during the preceding two days. Much of the discussion centered around the possibilities for interdisciplinary cooperation. For example, observations of regional dust sources and sinks, and tracking the location, timing, and growth of local and great dust storms, should provide useful input and constraints for atmospheric circulation models. The mineralogical properties of dust may greatly influence the formation of condensates; hence, knowledge of such properties may play major roles in modelling the production of atmospheric hazes and polar deposits. It was agreed that defining the frequency and characteristics of local and "global" dust storms, the distribution (temporal and spatial) of dust on the surface, and the physical and chemical properties of dust along with inclusion of dust related effects in atmospheric circulation models, are all areas in which continued research and communication among the various interested groups would be fruitful for the entire community. The research discussed at the workshop is clearly moving in the direction of posing questions for the Mars Observer mission, while showing that Viking Orbiter and Earth-based data provide an excellent basis for formulation of Mars Observer experiment strategies.

ABSTRACTS

ON THE RATE OF FORMATION OF SEDIMENTARY DEBRIS ON MARS; Raymond E. Arvidson, McDonnell for the Space Sciences, Department of Earth and Planetary Sciences, Washington University, St. Louis, MO 63130

We now have enough information to place rather meaningful constraints on the current rates of aeolian redistribution of fine grained debris on Mars. For example, from the three years of Viking Lander 1 observations, typical values of sediment redistribution are micrometers per year, although centimeters of loose, disturbed material were removed during a brief interval in the third year (1). Rates of erosion of rocks were too small to be observed, either by tracking changes in morphologies or by tracking changes in rock photometric properties. Consideration of the large number of pristine-looking, small bowl-shaped craters at the Lander 1 site suggests a rate of rock breakdown and removal of only meters over the lifetime of the surface. Thus, averaged over the lifetime of the Chryse Plains, rock breakdown and removal has been meters per billions of years, orders of magnitude lower than the micrometers per year for soils (2). Most of the equatorial regions of Mars likewise preserves ancient surfaces, with craters even at small sizes seemingly in production. Thus, rock breakdown and removal over the equatorial terrains has been quite small for much of geological time. Even the fretted terrains have probably been inactive for a long while, considering that the crater abundances in much of fretted terrain are second in abundance only to the cratered terrains (3). The younger fretted areas seem to be embayed by younger deposits (4) or to be in areas of relatively recent tectonic activity, such as the chaotic terrains. By areal extent, most of the equatorial terrains of Mars have been subjected to very low erosion rates, significantly less than the debris redistribution rates witnessed by Viking Lander 1. Thus, as noted by (2), differential aeolian erosion on Mars is a major geological process, with debris deposits accumulating and eroding to depths of hundreds of meters over geological time, while rock breakdown has been occurring in most regions at vanishingly small rates. Given the low rates of production of new debris, one is forced to conclude that Mars has had a decidedly non-linear history of debris production. In particular, most sedimentary debris must have been produced relatively early, perhaps in the first billion years of geological time. Impact cratering, production of volcanic ash, and chemical corrosion may all have been important debris-forming processes. Given that the mineralogy of martian debris has apparently not come into equilibrium with the present ambient conditions (5), we may have some chance of deciphering the relative importance of various debris forming processes. For example, if analyses of Mars Observer Imaging Spectrometer data show a dominance of palagonitic materials, then early volcanism would be indicated.

REFERENCES

1. Arvidson, R. and others, 1983, Science, v.222, p.463-468.
2. Arvidson, R. and others, 1979, Nature, v.278, p.533-535.
3. Coradini, M. and R. Arvidson, 1976, Proceed., Int. Colloq. Planetary Geology, Geol. Romana, v.15, p.377-381.
4. Frey, H. and A. Seneniuk, 1985, Geol. Soc. Am., Abstracts, p.586.
5. Gooding, J., 1978, Icarus, v.33, p.483-513.

CONSTRAINING MARS-DUST MINERALOGY ON THE BASIS OF VIKING BIOLOGY SIMULATIONS AND MARS SPECTRAL REFLECTANCE.

A. Banin, Hebrew University, P.O. Box 12, Rehovot, Israel

Among the prime, unresolved and often debated issues related to Mars is the question of the composition and properties of its fine, dusty surface materials. Unfortunately, no direct and definitive mineralogical analysis has been done on the soil and dust of Mars as yet. Various indirect approaches were used, however, to arrive at Mars dust mineralogy. These included direct chemical analyses, chemical modeling, simulations of the chemical interaction with water and solutes, and a multitude of spectroscopic observations from Earth, orbiters and landers. In the following we will briefly review these, specifically emphasizing the chemical simulations and present our current thinking on the mineral composition of the Martian dust.

Chemical composition of the Martian fine surface material: Quite probably, the most directly related available evidence regarding soil and dust mineralogy, is the inorganic chemical analysis (ICA) obtained by X-ray fluorescence analyzers aboard the Viking landers. The analyses have shown elemental abundances, (given as oxides), of 40-45% SiO_2, 7-7.5% Al_2O_3, 17-19% Fe_2O_3, 5-7% MgO, 5-6% CaO, 0.4-0.7% TiO_2, traces of K, 6-9% SO_4 and 0.3-0.9% Cl (1). The chemical composition of the soil in the two Viking landing sites, and of different samples taken from each site, was found to be strikingly similar. On the basis of the chemical data, several combinations of minerals have been suggested initially (2,3,4). These characteristically contained about 60-80% clay minerals of the smectite group, mixed with various soluble salts such as kieserite ($MgSO_4$) and halite (NaCl). Suggested accessory minerals were: iron oxides(Fe_2O_3), calcite ($CaCO_3$), and quartz (SiO_2).

Simulation of the Viking Biology experiments: The Viking Biology experiments turned out to be (and still are) an important and unique source of chemical information on Martian dust and soil because of the direct "wet chemistry" that was conducted on the soil and the information obtained on the interaction of the Mars minerals with water, salts and organics. Although no clear evidence for life was found, the Viking Biology experiments showed that the minerals in the Mars soil were chemically reactive and capable of decomposing various organic acids, catalyzing photochemical fixation of CO_2/CO, and releasing oxygen upon wetting (5,6).

The simulation of the Viking Biology experiments, conducted between 1977 and 1979 gave somewhat diverse results. Levin and his colleagues reported that the Mars soil analogs provided by the ICA Team did not simulate the Labeled Release (LR) Viking experiment (7). On the other hand, Banin and his colleagues, using ion-modified clays, succeeded in the kinetic simulations of this experiment (8,9,10). The clay modification by Banin et al. (11,12) involved the exchange of calcium and sodium ions, the primary adsorbed ions of clays on Earth, with iron, a ubiquitous and abundant element in the Martian soil. In addition to affecting the chemical and catalytic properties of the clay, this exchange resulted in a pronounced color change from gray to reddish-orange, making the clay very similar in color and spectral characteristics to the Martian soil (13,14).

Our detailed experimental studies showed (10,13,14,15) that among the many mixtures of clays and various salts whose combinations give elemental compositions similar to the Mars soil, only iron smectites, and particularly montmorillonite, reasonably simulated the chemical reactivity in the Viking Biology LR experiment. These simulations showed that if any CO_2 was to be released in the LR Viking experiment, calcite ($CaCO_3$) could not be present in

the dusty surface materials at concentrations higher than about 0.5%, and the pH of the soil could not be above ca. 5.

In separate simulation experiments, Hubbard (16), using the modified clays of Banin, detected photochemical fixation of atmospheric ^{14}C, and its incorporation into organics in the soil. This photochemical fixation was similar to the observations on Mars in the Viking Pyrolytic Release (PR) experiment. Other candidates for Mars soil components which were suggested using Viking Biology results as the guideline were carbon suboxide (17) and various mafic silicate minerals (18).

Spectroscopic evidence: Earth-based visible and near infrared reflectance data were accumulated through telescopic measurements of McCord's group in Hawaii (19,20). Since the termination of the Viking extended mission in 1978, this spectral information became the major if not the sole source of new experimental data on Mars soils mineralogy. The Mars reflectance spectrum was found to show opacity and band saturation (no reflectance) in the near UV-visible range (0.3-0.5 μm) with increasing transparency (increasing reflectance) in the long-wavelength visible and near infrared range (0.5-0.9 μm). However, it was lacking any clear and pronounced absorption features throughout this range. Spectra of crystalline, pure iron oxides such as hematite and goethite were found by Singer (21) and by Sherman et al. (22) to exhibit significant deviations from the Mars reflectance spectrum measured from Earth. However, several iron-containing minerals have been found to bear significant similarity to the Mars reflectance spectrum. These include amorphous iron-silica gels (23,24), palagonite (21), iron-containing aluminum oxy-hydroxide (25), and iron saturated montmorillonite clay (14). A feature common to all of the candidates is that they contain ferric iron in a matrix of oxy-hydroxide which is not well crystallized, or has only short-range ordering. Unfortunately, on the basis of the spectral comparison alone, there is yet no obvious way to choose among the various candidates, and additional properties and characteristics of the Martian soil and its Earth analogs have to be studied in order to further constrain the possible Martian mineralogical composition.

References: 1) Clark, B.C. et al. (1982) JGR 87, 10,059-10,067. 2) Toulmin, P. Jr. et al. (1977) JGR 82, 4625-4634. 3) Clark, B.C. et al. (1977) JGR 82, 4577-4594. 4) Clark, B.C. et al. (1976) Science 194, 1283-1288. 5) Klein, H.P. (1977) JGR 82, 4677-4680. 6) Klein, H.P. (1979) Rev. Geophys. Space Phys. 17, 1655-1662. 7) Levin, G.V. and Straat, P.A. (1977) Biosystems 9, 165-174. 8) Banin, A. and Rishpon, J. (1978) COSPAR, Life Sci. Space Res. XVII, 59-64. 9) Banin, A. and Rishpon, J. (1979) J. Mol. Evol. 14, 133-152. 10) Banin, A. et al. (1981) Proc. Third Intern. Coll. Mars Publ. 441 Lunar Planet. Inst., Houston, pp. 16-18. 11) Banin, A. (1973) U.S. Patent 3, 725,528, 14 pp. 12) Gerstl, Z. and Banin, A. (1980) Clays & Clay Min. 28, 335-345. 13) Banin, A. et al. (1984) Proc. Lunar Planet Sci. Conf. (15th) 31-32. 14) Banin, A. et al. (1985) JGR 90, (supplement) C771-C774. 15) Banin, A. and Margulies, L. (1983) Nature 305, 523-526. 16) Hubbard, J.S. (1979) J. Mol. Evol.14, 211-222. 17) Oyama, V.I. et al. (1978) COSPAR, Life Sci. Space Res. XVI, 3-8. 18) Huguenin, R.L. (1982) JGR 87, 10,069-10,082. 19) McCord, T.B. et al. (1982) JGR 87, 3021-3032. 20) Singer, R.B. et al. (1979) JGR 84, 8415-8426. 21) Singer, R.B. (1982) JGR 87, 10,159-10,168. 22) Sherman, D.M et al. (1979) JGR 84, 8415-8426. 23) Evans, D.L. and Adams, J.B. (1979) Proc. Lunar Planet. Sci. Conf. (10th), 1829-1834. 24) Evans, D.L. and Adams, J.B. (1980) Proc. Lunar Planet. Sci. Conf. (11th), 757-763. 25) Morris, et al. (1983) Proc. Lunar Planet. Sci. Conf. (14th), 526-527. This work was supported in part by NASA grant NSG-7512 and NASA Cooperative Agreement NCC 2-352 (Ames Research Center).

IMPLICATIONS OF A POLAR WARMING FOR DUST TRANSPORT INTO THE NORTH POLAR REGION OF MARS; J.R. Barnes and J.L. Hollingsworth, Department of Atmospheric Sciences, Oregon State University, Corvallis, OR 97331

The layered terrains in the polar regions of Mars have been widely interpreted as records of quasi-periodic variations in the Mars climate system driven by orbital element variations (see, e.g., Pollack and Toon, 1982). It has been suggested that the polar laminae in the north are being formed at present and that perhaps the bulk of the deposited dust and water ice is transported to the pole during global dust storms (Cutts, 1973; Pollack et al., 1979), which currently occur during the growth phase of the seasonal CO_2 frost cap. Pollack et al. hypothesized that CO_2 and water ice condensation onto dust grains would consitute a very effective mechanism for removing the dust to the surface in the polar regions. Paige (1985) carried out analyses of Viking IRTM observations and concluded that deposition of dust did occur (probably in conjunction with CO_2 condensation in the atmosphere) in the region of the north residual cap during the winter solstice (the second) dust storm of 1977. The magnitude of this deposition is uncertain, however, Jakosky (1983) and Jakosky and Martin (1984) have argued that the transport of dust (and water) onto the north residual cap during global dust storms is insignificant.

The deposition of dust onto the seasonal polar cap is also of considerable importance, because of the effects on the polar cap albedo and thus the radiation budget of the subliming cap. Additionally, the dust loading of the polar atmosphere is significant because of its effects on the radiation budget of the cap: the enhanced emissivity of the atmosphere implies enhanced downward IR fluxes.

The intense warming of the polar atmosphere which was observed by the Viking IRTM during the winter solstice dust storm of 1977 (Martin and Kieffer, 1979; Jakosky and Martin, 1984) must have been the result of substantial dynamical transports of heat into the north polar region. The warming at the pole (~50 K in magnitude in the vicinity of the 25 km level) must have been produced by compressional heating associated with downward - in a Lagrangian sense - motion of air parcels. An accompanying poleward flow is then also implied. Such a Lagrangian motion pattern implies poleward and downward transport of tracers such as dust and water.

Numerical simulations conducted with a simplified beta-plane wave-mean flow model strongly suggest that the polar warming could have been induced by a forced, vertically propagating, planetary-scale (zonal wavenumber 1) wave (Barnes and Hollingsworth, 1985). The dynamics of such a warming are most clearly viewed in the so-called transformed Eulerian-mean system, instead of the traditional Eulerian one. In the transformed system, the warming is produced by downward vertical motions - rather than eddy transport of heat. [The transformed Eulerian-mean vertical motion field is generally a good approximation to the true Lagrangian-mean vertical motion field - unlike the Eulerian-mean verical motion field.] The mean meridional circulation in the transformed Eulerian-mean system, the so-called residual mean meridional circulation, is characterized by poleward and downward flow into the polar interior during the simulated warmings. This poleward and downward flow takes place throughout a very deep region as the warming occurs, with the much weaker return flow confined to low levels. The residual mean meridional circulation should constitute a good first approximation

appropriate to the transport of tracers (Holton, 1981), thus implying transport into the polar interior of a tracer initially located largely equatorward of the cap boundary (e.g., dust or water).

Full tracer (dust) transport simulations corresponding to the dynamical warming simulations are planned. These will allow a quantitative examination of the transport of dust into the polar region in association with a polar warming event.

REFERENCES

Barnes, J.R. and J.L. Hollingsworth (1985) Dynamical modeling of a Martian polar warming. Bull. Amer. Astron. Soc., 17, 3: 733.

Cutts, J.A. (1973) Nature and origin of layered deposits of the Martian polar regions. J. Geophys. Res., 78, 4231-4249.

Holton, J.R. (1981) An advective model for two-dimensional transport of stratospheric trace species. J. Geophys. Res., 86, 11, 989-11, 994.

Jakosky, B.M. (1983) Mars north polar cap: Net annual source or sink? Bull. Amer. Astron. Soc., 15, 846.

Jakosky, B.M. and T.Z. Martin (1984) Mars: Polar atmospheric temperatures and the net transport of water and dust. Unpublished manuscript.

Martin, T.Z. and H.H. Kieffer (1979) Thermal infrared properties of the Martian atmosphere. 2. The 15 μm band measurements. J. Geophys. Res., 84, 2843-2852.

Pollack, J.B., D.S. Colburn, F.M. Flasar, R. Kahn, C.E. Carlston, and D. Pidek (1979) Properties and effects of dust particles suspended in the Martian atmosphere. J. Geophys. Res., 84, 2929-2945.

Paige, D.A. (1985) The annual heat balance of the Martian polar caps from Viking observations. Ph.D. dissertation, California Institute of Technology, 207 pp.

Pollack, J.B. and O.B. Toon (1982) Quasi-periodic climate changes on Mars: A review. Icarus, 50, 2/3, 259-287.

DUST DEPOSITION AND EROSION ON MARS: CYCLIC DEVELOPMENT OF REGIONAL DEPOSITS

Philip R. Christensen, Dept. of Geology, Arizona State University, Tempe, AZ, 85287.

The cycle of dust erosion, transport, and deposition plays an important role in the evolution of the martian surface, both today and in the past. Thermal, radar, and visual remote sensing observations provide important constraints on the surface properties, and have been used to determine the location and physical properties of regional dust deposits. These deposits provide direct clues to the rate and history of dust deposition, and suggest that the martian surface is being actively reworked. The observed dust cycle may be directly related to the cycle of variations in Mars' orbit, with dust continually transported between hemispheres on time scales of 10^5 to 10^6 years.

Major dust deposits are currently located in three northern equatorial regions: Tharsis (-20°S to 59°N, 60° to 190°W), Arabia (-5°S to 30°N, 300° to 360°W), and Elysium (10° to 30°N, 210° to 225°W). They are covered by fine (~2-40 μm), bright (albedo > 0.27) particles, with fewer exposed rocks and coarse deposits than found elsewhere (1,2). These regions also have less bonded material exposed at the surface than found elsewhere (3). Dust deposits may have initially formed due to differences in wind velocity. Once initiated, the burial of sand and rocks would make removal of fines increasingly difficult, enhancing the rate of dust accumulation. Dust is currently deposited uniformly throughout the equatorial region at a rate of ~40 μm/global storm. Over geologic time the rate of accumulation may vary from 0 to 250 μm/year due to changes in atmospheric conditions produced by orbital variations (4). Dust deposited during global storms is subsequently removed only from dark regions, resulting a net accumulation in the low-inertia, bright regions. The evidence for the subsequent removal from dark regions comes from: 1) the observed higher dust content over dark regions than bright regions during clear periods; 2) the post-storm darkening of dark regions (5, this issue); 3) the removal of storm-deposited dust at the Viking lander 1 site during the year following the major 1977 dust storms (6); and 4) the historical persistence of classic dark features. Non-removal of dust from low-inertia, bright regions results in a net accumulation of dust in these areas.

The thickness of the current dust deposits can be estimated from thermal, radar, and visual observations.. The low thermal inertia of the deposits places a lower limit of ~0.1 m on their thickness, while the sparse but ubiquitous presence of exposed rocks and the degree of visible mantling indicates that the thickness is less than 5 meters (7). Dual-polarization radar observations of Tharsis reveal a very rough texture. These measurements can best be reconciled with the other observations by assuming that a relatively thin dust layer buries most of the surface rocks but that the radar samples through this layer to the rough surface below (1). The maximum thickness of this layer can be estimated from the electrical properties of rock powders. For dry powders, the radar energy should penetrate 5 to 50 wavelengths (0.6 to 6 m for the 12 cm radar used) before being attenuated by 1/e (8). The presence of adsorbed water will not affect these results (9). Thus, 12 cm radar could penetrate ~ 1 m, be reflected, and exit the surface with only a 1/e reduction in initial energy. This estimate puts a constraint of 1-2 m on the dust mantle thickness, which agrees well with the value obtained using the exposed rock abundance derived from thermal measurements.

Based on their thickness and rate of accumulation, the age of these deposits is 10^5-10^6 years, suggesting a cyclic process of deposition and removal (1). One possible cause may be cyclic variations in the magnitude and location of maximum wind velocities related to variations in Mars' orbit. At present, perihelion and maximum wind velocities occur in the south whereas regional dust deposits occur in the north, suggesting net transport from south to north. Orbital parameters oscillate with periods ranging from 5×10^4 to 10^6 years. The agreement between these periods and the dust deposit age suggests that there is a possible link. At different stages in orbit

evolution, maximum wind velocities will occur in the north, with subsequent erosion and redistribution of the accumulated fines.

The model proposed here implies that material must be periodically removed from regional dust deposits in order to prevent long-term buildup of fine material in a given location. Thus, the proposed young age of these dust deposits requires mechanisms for eroding extensive deposits of fine material. The burial of sand and rocks makes it increasingly difficult to set particles in motion, with 20 μm particles requiring wind velocities a factor of 2 higher than the most readily moved particles (10). There are, however, several mechanisms for eroding these deposits, including erosion from the edge inward, and increased surface shear stress produced by increased winds (1).

A more plausable mechanism involves the formation of coarse particles as bonded aggregates of dust. Bonding of material has been observed at both Viking landing sites, and globally pervasive crusts have been detected from remote sensing observations (2). These crusts may form during transition periods between obliquity extremes as volatiles carrying adsorbed ions are cycled into and out to the surface (2). This mechanism would link the erosion of the deposits to the same process that leads to their formation. Thus, crusts could form after the deposition of a layer of fine material has been deposited after each obliquity cycle. Such crusted aggregates could provide a source of coarse particles that could be more readily moved by the wind, thereby providing a mechanism for eroding the underlying deposit of dust.

Perhaps the most important process may be surface erosion due to insolation-driven convective vortices (dust devils) of various scales. Experimental work suggests that vortices are very effective in raising particles of all sizes which can then be easily transported by much lower winds (11). There is direct evidence for the occurrence of dust devils on Mars, both through the passage of 5-950 m diameter vortices at the Viking lander sites (12), and through direct observation of dust devils from orbiter images (13). Of the 118 vortices observed at the lander sites, 4 had wind velocities greater than 30 m/sec, which may have been sufficient to raise dust (12). These vortices produced a factor of 2-3 enhancement in the ambient wind velocity. Because dust devils form due to convection in an atmosphere with a superadiabatic lapse rate, they are more frequent during periods of maximum surface heating. This erosion mechanism would be most effective over low-inertia surfaces during summer, and may provide a mechanism for eroding dust from the hemisphere that has the maximum solar insolation during summer. Thus, dust deposited in one hemisphere when the insolation maximum was in the opposite hemisphere would subsequently be eroded when obliquity variations caused the insolation maximum to reverse.

The presence and history of regional dust deposits provide evidence for cyclic processes of deposition outside the polar regions and support models of cyclic variations in martian climate over geologic time. Dust is continually eroded and redeposited, with the location of major deposits shifting on time scales of 10^5 to 10^6 years. In this model much of the uppermost martian surface is young and is being constantly reworked.

References

1) Christensen, P.R., 1986, *J. Geophys. Res.*, in press.
2) Christensen, P.R., 1983, *Icarus, 56,* 496-518.
3) Jakosky, B.M. and P.R. Christensen, 1986, *J. Geophys. Res.*, in press.
4) Pollack, J.B. and O.B.Toon, 1982, *Icarus, 50,* 259-287.
5) Christensen, P.R., 1986, this issue.
6) Arvidson, R.E., E.A. Guinness, H.J. Moore, J. Tillman, and S. D. Wall, 1983, *Science, 222,* 463-468.
7) Harmon, J.K., D. B. Campbell, and S.J. Ostro, 1982, *Icarus, 52,* 171-187.

8) Campbell, M.J. and J. Ulrichs, 1976, *J. Geophys. Res., 84*, 2795-2820.
9) Olhoeft, G.R. and D.W. Strangway, 1974, *Geophys. Res. Lett., 1*, 141-143.
10) Greeley, R., R. Leach, B. White, J. Iversen, and J. Pollack, 1980, *Geophys. Res. Lett., 7*, 121-124.
11) Greeley, R., B.R. White, J.B. Pollack, J.D. Iversen, and R.N. Leach, 1981, *Spec. Pap. Geol. Soc. Am., 186*, 101-121.
12) Ryan, J. A. and R. D. Lucich, 1983, *J. Geophys. Res., 88*, 11,005-11,010.
13) Thomas, P. and P. Gierasch, 1986,*Science, 230*, 175-177.

SURFACE ALBEDO VARIATIONS ON MARS: IMPLICATIONS FOR YEARLY DUST DEPOSITION AND REMOVAL

Philip R. Christensen, Dept. of Geology, Arizona State University, Tempe, AZ, 85287

Dust deposition and removal is an important process in the development and modification of the martian surface. Mars has been known to have variable surface markings from the earliest telescopic views of the planet. These changes have since been seen to be related to aeolian activity, primarily through the reworking of bright dust deposited following major global dust storms (1,2). Viking Infrared Thermal Mapper (IRTM) observations of albedo have also revealed significant changes in surface brightness through time, again primarily associated with major global dust storms (3,4). All of these observations indicate that there is a significant amount of dust that is deposited during the decay of global storms which is subsequently reworked and redistributed. The purpose of this study is to determine the degree, spatial distribution, and timing of the deposition and removal of dust-storm fallout, and to relate the current patterns of dust deposition and removal to the long-term evolution of the martian surface.

A model has been proposed (5, 6 this issue) for the development of regional dust deposits that form through the preferential accumulation of dust-storm fallout into specific northern hemisphere regions. In this model, dust is deposited uniformly during the decay phase of each major storm, but is subsequently removed only from regions that are seen today as classic dark areas. Thus, dark regions remain unmantled by dust, whereas bright regions have developed a 1-2 m thick mantle of fine, bright dust (5). This model can account for the high thermal inertia (coarse) material observed in dark regions, together with their relatively high rock abundance (7), and low albedo. Conversely, bright regions have fine particles (5-40 μm) and fewer exposed rocks, presumably due to mantling of the coarse material by dust.

In order to directly observe the seasonal changes in surface brightness associated with dust deposition and removal, the albedo of specific regions in both hemispheres has been determined through time. The IRTM data were collected into 1° latitude by 4° longitude bins, at 3 hour intervals for each 10° of L_s. Using these data, the albedo changes for a given area have been investigated from the beginning of the Viking mission (L_s 84°), through the first (L_s 190-240°) and second (L_s 270-340°) global dust storms that occurred in 1977. Global data are available through L_s 120° of the second year, allowing a year to year comparison of surface albedo.

The albedo variations as a function of season are shown in Figure 1 for representative bright and dark regions. All of the areas studied show a marked increase in brightness associated with the two global storms, due primarily to the presence of dust in the atmosphere. The increase in brightness, even for bright regions, indicates that the albedo and scattering phase function of suspended dust varies from dust on the surface. The maximum brightness at the peak of the second storm was nearly equal for most bright and dark regions, indicating that the atmospheric dust was optically thick. For some dark regions, however, such as Solis Planum, the albedo remained relatively low even at the height of the storm activity, suggesting that the atmospheric dust was not globally uniform nor well mixed. Many areas show a non-uniform decrease in brightness during the decay phase, again suggesting spatial variations in dust load and non-uniform mixing, possibly due to episodic injection of dust into the atmosphere locally (8).

The albedo of most regions had returned to the pre-storm value by L_s 355°, indicating that the atmosphere had cleared to pre-storm levels by that time. This conclusion is supported by Viking lander observations, which show that the opacity over the two lander sites had decreased to

pre-storm levels by L_S 360° (8). Therefore, surfaces that remained brighter after L_s 360° than they were prior to the two storms are thought to be covered by a thin layer of bright dust fallout.

The distribution of surfaces that remained bright following the storms, and those where the surface quickly returned to its pre-storm albedo follow a consistent pattern. The albedo of bright regions, such as Arabia and Tharsis, rapidly returned to pre-storm values, and was close to the albedo of the previous year (Fig. 1a). Many dark regions also darkened to nearly their pre-storm levels by L_s 360° (Fig. 1b). This pattern holds particularly well for southern hemisphere dark regions. This behavior is consistent with the model of deposition described above; in dark regions the dust is rapidly removed with little net accumulation, whereas in bright regions a dust mantle already exists so that the deposition of additional bright dust does not affect the surface albedo.

There are several dark regions that differ from the general trends described above and provide insight into the level of dust activity that occurs throughout the year. Syrtis Major and Acidalia Planitia are among the few regions that remained significantly brighter at L_s 360° than they were before the global storms began. These areas did, however, continue to darken with time, returning to nearly their pre-storm albedo by L_s 120° (Fig. 1c). It is interesting to note that the albedo of these and some other regions was still slightly higher at this time than it was the previous year, suggesting that some dust still remained on the surface. This finding is consistent with observations at the Viking lander 1 site where dust was deposited following the global storms and was not removed until over a year later (9). These observations support the hypothesis that Syrtis Major and Acidalia Planitia act as local dust sources during inter-storm periods, producing enhanced dust loading in the northern hemisphere (10).

In summary, observations of seasonal changes in surface albedo reveal regional differences in the deposition and subsequent erosion of dust-storm fallout. Southern hemisphere dark areas quickly return to close to their pre-storm albedos, suggesting rapid removal of any dust that was deposited. Northern hemisphere dark regions are brighter post-storm, but gradually darken to pre-storm levels over a Mars year. In doing so they act as local sources of dust during otherwise clear periods. Dust does not appear to be removed from bright regions, resulting in the 1-2 m thick deposits observed today.

References

1) Thomas, P. and J. Veverka, 1979, *J. Geophys. Res., 84*, 8131-8146.
2) Veverka, J., P. Thomas, and R. Greeley, 1977, *J. Geophys. Res., 82*, 4167-4187.
3) Pleskot, L.K. and E.D. Miner, 1981, *Icarus, 45*, 179-201.
4) Lee, S.W., 1986, submitted to Icarus.
5) Christensen, P.R., 1986, *J. Geophys. Res*, in press.
6) Christensen, P.R., 1986, this issue.
7) Christensen, P.R., 1986, submitted to Icarus.
8) Pollack, J.B., D.S. Colburn, R. Kahn, J. Hunter, W. Van Camp, C.E. Carlston, and M.R. Wolfe, 1977, *J. Geophys. Res., 82*, 4479.
9) Arvidson, R.E., E. Guinness, H.J. Moore, J. Tillman, and S.D. Wall, 1983, *Science, 222*, 463-468.
10) Christensen, P.R., 1982, J. *Geophys. Res., 87*, 9985-9998.

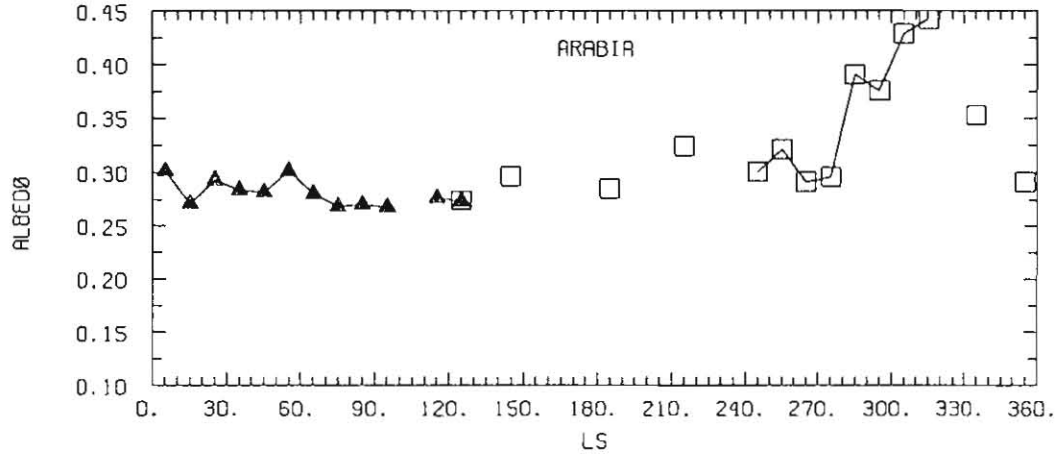

Figure 1. Variation of albedo with season. Open squares represent data from the first year following the arrival of Viking at Mars. a) Arabia, typical of bright region behaviour.

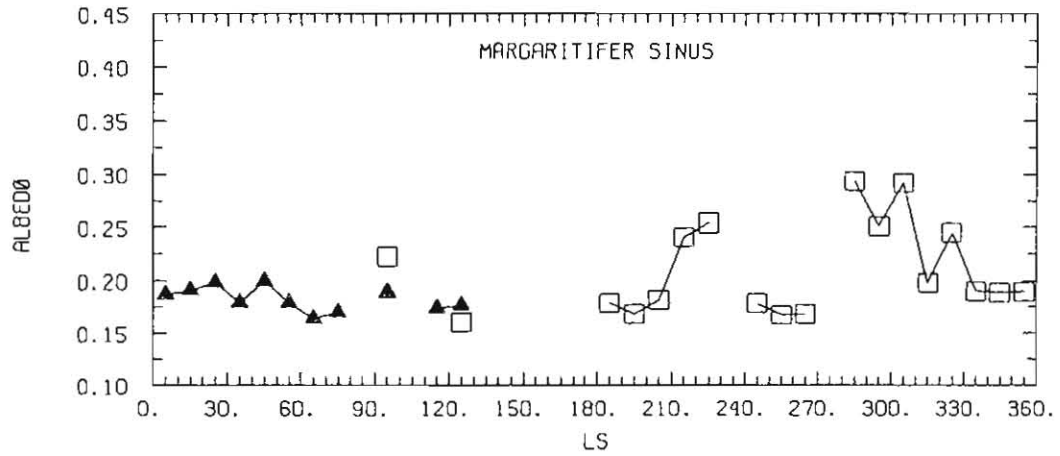

Fig. 1b). Margaritifer Sinus, representative of southern hemisphere dark regions.

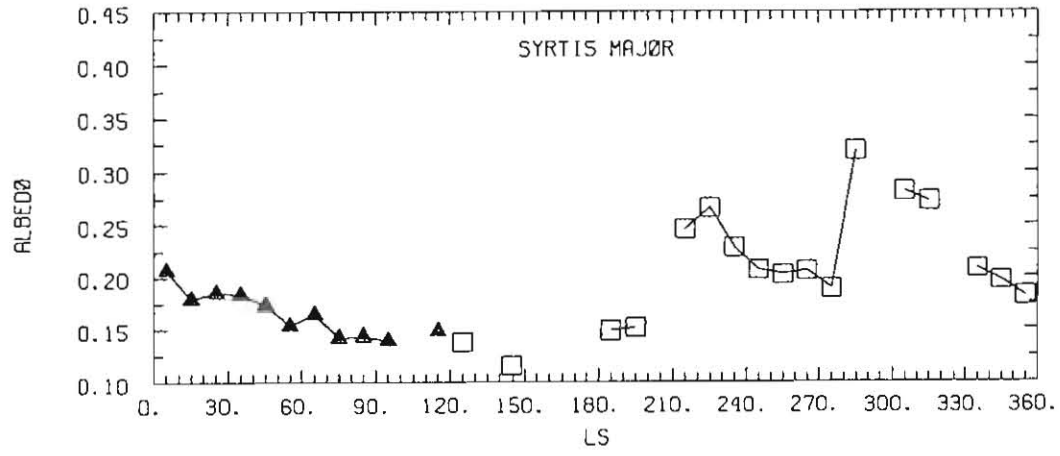

Fig.1c). Syrtis Major, showing the long residence time of dust on the surface in northern hemisphere dark regions following the global dust storms.

INFLUENCE OF DUST ON WATER CONDENSATION AT MARS: D. S. Colburn, J. B. Pollack and R. M. Haberle, NASA Ames Research Center, Moffett Field CA 94035

Mars atmospheric optical depth measurements obtained over 1 1/3 Mars years at the two lander sites are examined to determine the influence of atmospheric dust on water condensation. During certain times of year the morning optical depth is, on the average, larger than the afternoon optical depth, and it is postulated that the minimum is primarily a measurement of atmospheric dust, while the difference (AM-PM) is condensed water vapor which evaporates by the time of the afternoon measurement. The AM-PM difference is examined as a function of the time of year, the amount of dust (indicated by PM values), and the amount of water vapor at the site derived from the Viking Orbiter MAWD experiment (B. Jakowsky, private communication). The time of year is denoted by the solar longitude, with Ls=0 being northern vernal equinox. The span of 1 1/3 years is represented by an Ls range of 100 to 560.

Many sols were found for which an AM-PM difference could be obtained. A running average was created averaging points within + or - 15 sols (Mars days) of each sol. The average was deleted if all points were before (or all after) the indicated sol. As shown in Fig. 1, the smoothed data show few points significantly negative, and the values range from 0 to 0.5 optical depth units. In plots of AM-PM difference vs. Ls, significant peaks in the records are found: five in VL1 and three in VL2 are investigated here. In order to understand the causes of these peaks, one must assess the condensed water in the PM, how much water vapor is available, the amount of dust in the atmosphere, and the solar energy input as a function of time of day and time of year.

To obtain an estimate of condensation, a one-dimensional atmospheric model is used to predict the temperature profile at the appropriate latitude as a function of the time of year and the time of day for an assumed distribution of atmospheric dust. The dust used here is the value determined by the PM optical density measurements, with a mixing ratio independent of altitude. Water vapor determined by the MAWD experiment is assumed to be present, also with a constant mixing ratio. At each pressure level the H2O partial pressure is compared to the vapor pressure for the temperature of that level, and any excess is considered to be ultimately condensed. Thus, condensation is predicted when the temperature falls below the frost point. While the calculation is not completely self-consistent, it demonstrates the relative influence of the various parameters on water condensation.

Three peaks in AM-PM difference are noted in the record for VL2, at Ls values of 217, 355, and 505.

The peak at 217 coincides with the peak of the first dust storm. The dust level is high at this point and drops off gradually. Seasonal variation must be considered here. The latitude of VL2 is relatively high (47.9 N) and the sun is lowest in the sky at Ls 270. Consistent with this, the model shows high values of PM condensation during the period 220-320, while at the lower latitude site of VL1 PM condensation is always small. Temperatures drop to a point, according to the model, at which most of the vapor is condensed all day, and hence an AM- PM variation must necessarily be small. Before and after the cold season, the atmosphere warms through a range at which the AM- PM

variation can be a maximum. After this, during the summer, large AM condensation is less likely. The model shows peaks at 212 and 340, primarily caused by this seasonal effect.

The peak at 217 and the corresponding model peak at 212 also show the effect of the high dust level, which enhances the temperature variation throughout the atmosphere. Thus, PM temperatures at a number of altitude levels were above the frost point while AM temperatures were below it.

The peak at 355 is approximated by a model peak at 340 which again demonstrates the seasonal effect and the tendency at this time of year for a large dust level to enhance condensation.

The peak at 505 is approximated by model peak at 495. In this case the large condensation is attributable to a large water vapor content as measured by MAWD and used by the model.

Profiles have been plotted showing the condensed water overburden as a function of pressure level and altitude. In these plots, the overburden at each altitude is the optical density of the entire column above that point. For the peaks at 217 and 355, they are consistent with the assumed constant mixing ratio, with nearly all of the water vapor condensed in the AM. In these cases the overburden is largest at ground level and drops off nearly exponentially with altitude. At 505, condensation occurs only above 20 km, except for a significant fraction in the lowest pressure layer (approximately 0 to 250 meters, see Fig. 2). This indicates that the middle layer does not cool off enough for condensation to occur.

Five peaks in AM-PM difference are noted in the record for VL1, at Ls values of 212, 312, 393, 455, and 491.

The observed peak at 312 corresponds to a model peak found at 290. This is primarily due to a combination of the high optical depths of the second global dust storm and to a seasonal effect. No significant PM condensation is observed at any time of year at VL1, as the Lander 1 latitude (22.4) is low enough that afternoon temperatures always inhibit condensation. The coldest mornings in the northern hemisphere should occur at Ls=270. The model shows that at this time condensation is enhanced by a large dust optical depth, such as occurred at this time, the start of the second dust storm. The observed peak thus depends both on the season and the dust load.

The observed peak at 491 shows up in the model as a peak at 495. While the dust is fairly low and the season late summer, the water vapor as measured by MAWD became higher than usual, and the model shows this factor as responsible for the peak in condensation.

The minor peak at 455 is reflected in the model and shown to be due to enhanced dust loading, indicated by a peak in the PM optical depth at 457. At this season an increase in dust increases condensation.

The peak at 212 occurs shortly after the northern autumnal equinox. The measured PM optical depth is rising at the beginning of the first dust storm. The model does not show a peak here, and it can only be postulated that the water vapor increased at this point but was not observed due to a MAWD data gap. Correspondingly, an earlier

increase in water vapor at 150 caused a model peak which was not observed due to a data gap in AM-PM observations.

A fifth peak in the VL1 observations, at 393, not as large as peaks at 312 and 491, is not predicted by the model using present parameter inputs.

Profiles for VL1 show most water condensation occurring above an altitude of 15-30 km; occasionally a small fraction of it is ground fog (below 250 m).

In conclusion, the amount of dust in the atmosphere is shown here to influence the diurnal variation in condensation. The extent of this influence depends on season and water vapor as well as other factors.

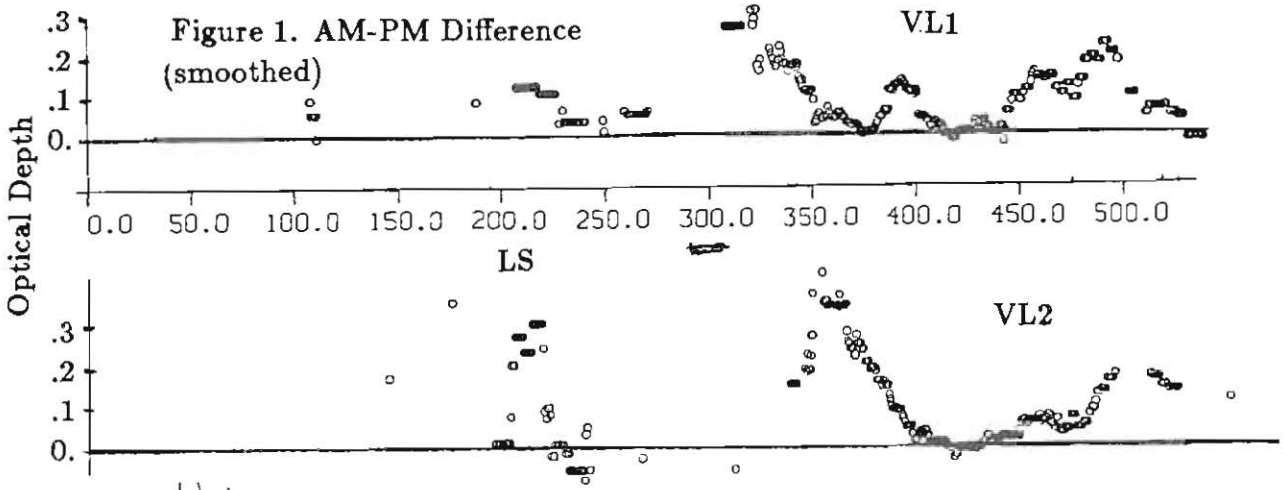

Figure 1. AM-PM Difference (smoothed)

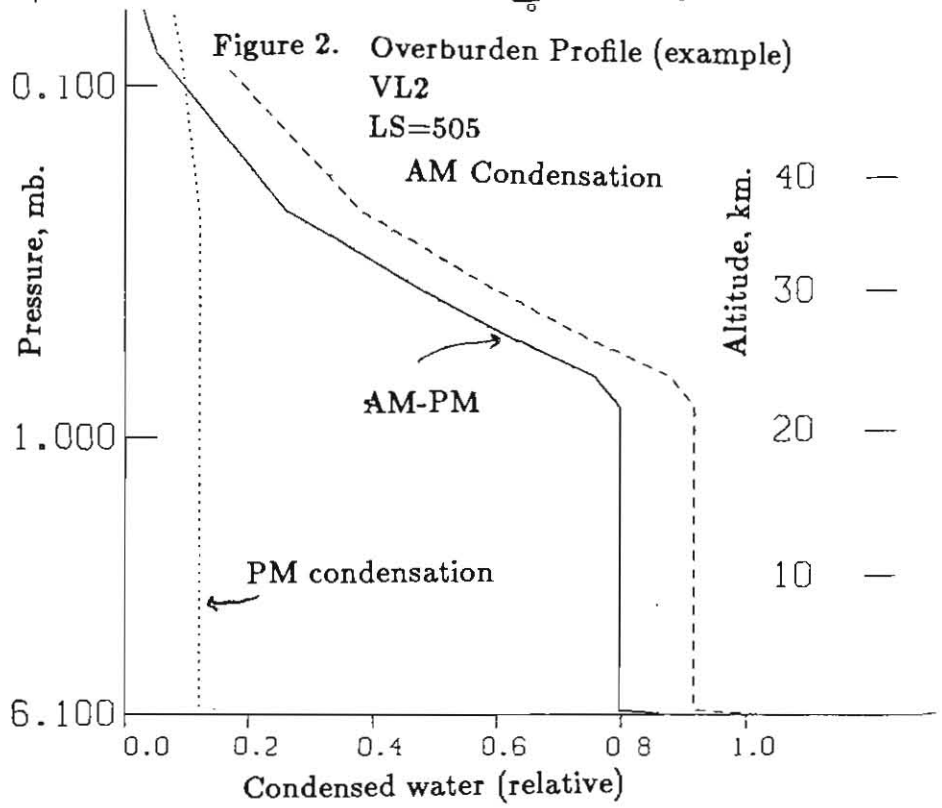

Figure 2. Overburden Profile (example)
VL2
LS=505

CONDENSATION OF FROSTS ON MARTIAN DUST PARTICLES. J. L. Gooding, Planetary Materials Branch, NASA/Johnson Space Center. Houston, TX 77058 USA.

Introduction. Condensation of water-ice and other frosts on Mars should proceed by heterogeneous nucleation on dust particles because. as on Earth. the naturally occurring low degrees of atmospheric water-vapor supersaturation inhibit homogeneous nucleation [1,2]. In contrast with Earth. though, liquid water is, at best. metastable in the Martian surface/atmosphere environment [3] and both the abundances and apparent degrees of saturation of water vapor in the Martian atmosphere are consistent with ice as the condensed-phase buffer [3,4]. Furthermore. very low temperatures and dominance of vapor/solid transitions might favor formation of H_2O-Ic on Mars whereas H_2O-Ih is the common polymorph of water ice on Earth [2,5]. Finally. the major gas in the Martian atmosphere. CO_2, is also condensible as a frost. as is $CO_2 \cdot 5.75\ H_2O$ and possibly other clathrates.

Cloud-chamber experiments have shown that ice-nucleation abilities vary substantially among minerals [1]. Dependence of ice-nucleation threshold temperature on substrate mineralogy has also been demonstrated by low-temperature differential thermal analysis and scanning calorimetry [6,7,10,11] and applied to conceptual studies of ice formation on Mars [8-11].

Heterogeneous Nucleation. Intrinsic properties that determine the favorability of a given substrate toward heterogeneous nucleation of a condensate [1,2] are (1) degree of misfit ("disregistry") between the crystal structures of the substrate and condensate. (2) compatibility of the substrate with condensate in terms of chemical bonds, and (3) abundance of submicroscopic defects in the substrate that would be active sites of assembly for condensate atoms or molecules. Insolubility of the substrate is also a factor when the condensate is water. Among the three principal determinants, disregistry is the parameter that is most easily quantified through direct calculation. Using a modified version of Eqn. (9-32) given by Pruppacher and Klett [2] and crystallographic data from published literature, disregistry was calculated for attempted matches of candidate condensates with each other and with selected mineral substrates. For each condensate/substrate pair, computations proceeded until a minimum was found in the absolute value of disregistry, $/\delta/$. Experimental data indicate that ice-nucleation temperature varies inversely with $/\delta/$ [11].

Comparison of Substrates (Figs. 1-3). Among the major silicates that occur in mafic igneous rocks, orthopyroxenes (e.g., hypersthene; Hy, Fig. 1) appear to be the most favorable substrates although amphiboles (e.g., hornblende, Hbl) might be moderately good substrates. Orthopyroxenes appear to be more favorable than clinopyroxenes (e.g., augite, Aug; pigeonite) and plagioclase (Pl) should be a generally poor nucleator of condensates. Basalt glass is not represented in Fig. 1 (because $/\delta/$ could not be meaningfully calculated) but is known to be a poor ice nucleator [11] and plagioclase glass (i.e., shock-produced maskelynite or residual igneous mesostasis) might be equally poor. Accordingly, the effectiveness of pulverized igneous rocks as condensate nucleators on Mars should vary significantly with the glass/crystal ratio, the plagioclase/pyroxene ratio, and the cpx/opx ratio. However, all of the crystalline igneous silicates should favor H_2O-Ih relative to H_2O-Ic. In addition, olivine (Ol), Hy, and Hbl-variety amphiboles appear to be moderately favorable nucleators of solid CO_2.

Fe-oxides appear to be less favorable nucleators of condensates than are most other mineral groups. Hematite (Hem) and goethite (Gt) appear to be the best potential nucleators of water ice although the former should favor H_2O-Ih whereas the latter should favor H_2O-Ic.

Gooding, J. L.

None of the clay minerals represented in Fig. 1 appear to be especially favorable nucleators, with the possible exception of chlorite (Chl). With respect to H_2O-Ic, though, kaolinite (Kln), Chl, and muscovite (Ms) appear to be potentially good nucleators. It is important to note that, relative to H_2O-Ih, disregistry on {001} forms should not differ substantially from one clay mineral to the next so that observed differences in actual ice-forming effectiveness among clay minerals [6,11] are probably related to disregistries on {100} and {010} forms. Kln, Chl, and Ms are all phyllosilicates with non-expandable structures whereas smectite-group minerals such as montmorillonite (Mnt) and nontronite (Nnt) are characterized by large expansions and contractions along their c-axis directions that occur in response to variations in degree of hydration or by cation exchange involving interlayer sites. Large variations in /δ/ occur for Mnt such that Mnt can appear to be either an extremely favorable or an extremely unfavorable nucleator of water ice, depending upon its degree of structural expansion (Fig. 2).

Chabazite (Cbz), analcite (Anl), and clinoptilolite (Ctl) are common zeolitic alteration products of mafic rocks on Earth and at least the former two species appear to be excellent nucleators of H_2O-Ih. In contrast, clinoptilolite might be an unusually good nucleator of H_2O-Ic and, among the minerals represented in Fig. 1, might be the best potential nucleator of solid CO_2. If they are abundant on Mars, zeolites might be doubly important because of their molecular-sieve properties that permit them to strongly and selectively bind volatile species in unfrozen forms.

Although mineral substrates might serve to initiate condensate formation on Mars, early-formed condensates might also serve as substrates for heterogeneous nucleation of later condensates. Phase H_2O-Ic might be the best overall nucleator of other condensates so that it is important to determine which mineral substrates are the most effective nucleators of H_2O-Ic. As shown in Fig. 1, the most outstanding nucleators of H_2O-Ic might be non-expandable clay minerals and certain zeolites.

Pertinent Observations of Mars. Results from the Mariner 9 IRIS experiment gave no unique solution to the composition of dust in the atmosphere although various combinations of Ms, Mnt, and Pl were favored as model mineral assemblages [12,13]. Among those minerals, Mnt would be the best prospect as a nucleator of H_2O-Ih although its effectiveness should depend significantly on its degree of c-axis expansion (Fig. 2). Because carbonate minerals could not be confirmed [13], there exists no promising substrate for direct nucleation of solid CO_2 among the candidate minerals suggested by IRIS. However, zeolites should be reviewed as important candidates that apparently were not considered in the original IRIS work.

If condensates observed at the Viking 2 landing site nucleated on red dust [14,15], implying that Fe-oxides were important nucleators, Hem and Gt would be the most competitive choices. If identity of the Fe-oxide was known, a case might have been made for the water condensate being either H_2O-Ih (favored by Hem) or H_2O-Ic (favored by Gt). Alternatively, identification of the condensate might have been used to argue for possible identification of the Fe-oxide. If, as suggested by Wall [14], the condensate was a mixture of H_2O and CO_2, a case for Gt might have been made, based on the fact that Gt favors condensation of H_2O-Ic which, in turn, favors condensation of solid CO_2.

More experiments are needed to test these provisional inferences. In addition, direct determination of the mineralogy of Martian dust units of various ages is needed in order to better assess the role of heterogeneous nucleation and condensation as a possible influence on the migration and storage of volatiles throughout Martian geologic history.

Gooding, J. L.

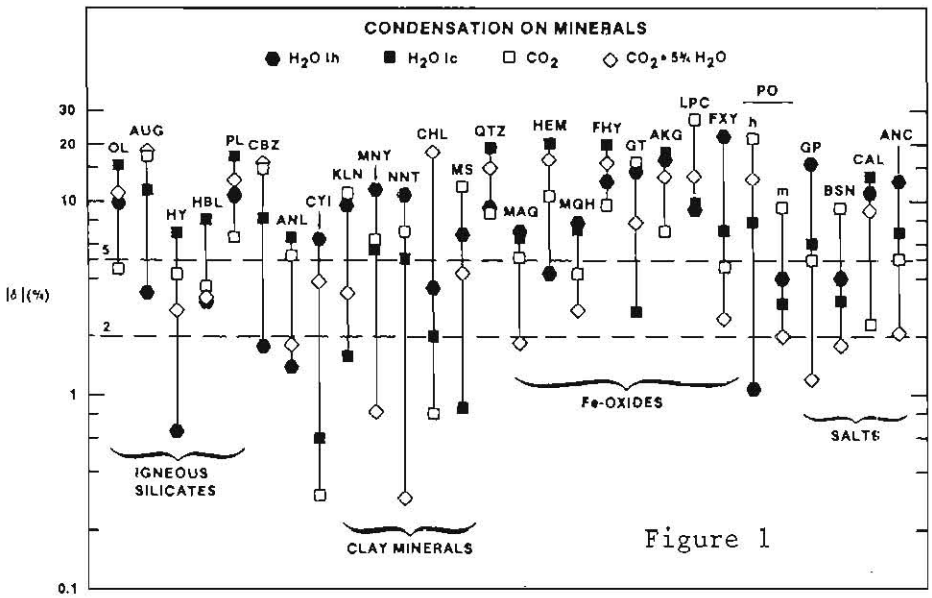

Figure 1

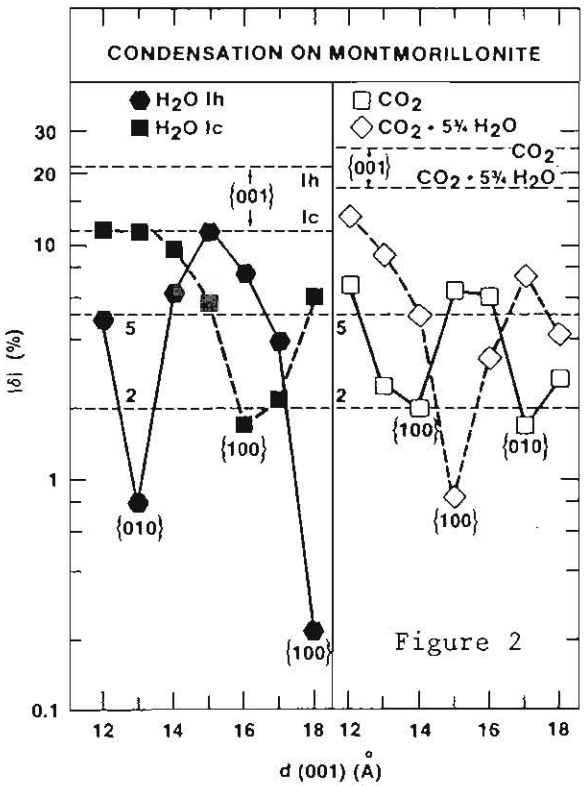

Figure 2

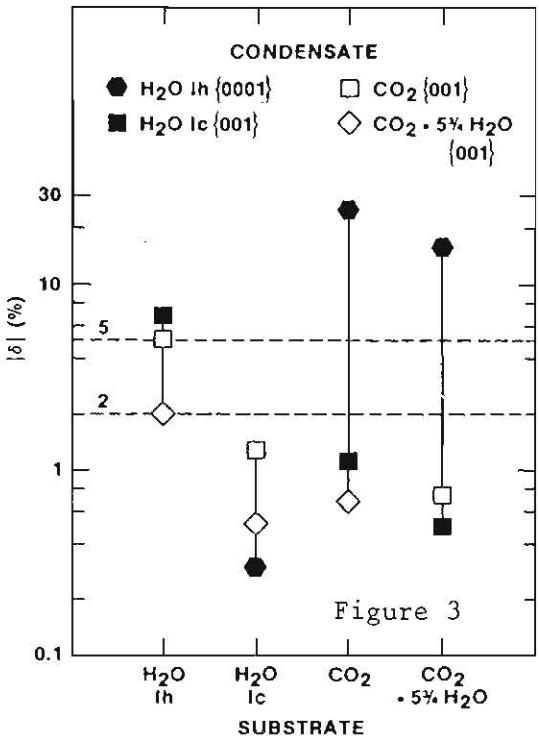

Figure 3

References: [1] Mason B. J. (1971) The Physics of Clouds (second ed.), Clarendon. 671 pp. [2] Pruppacher H. R. and J. D. Klett (1978) Microphysics of Clouds and Precipitation, Reidel, 714 pp. [3] Farmer C. B. (1976) Icarus, 28, 279. [4] Davies D. W. (1979) J. Geophys. Res., 84, 8335-8340. [5] Shumskii P. A. (1964) Principles of Structural Glaciology (D. Kraus. transl.), Dover. [6] Anderson D. M. (1968) Israel J. Chem., 6, 349. [7] Anderson D. M. and Tice A. R. (1971) Soil Sci. Soc. Amer. Proc., 35, 47. [8] Anderson D. M., Gaffney E. F., and Low P. F. (1967) Science, 155, 319. [9] Anderson D. M., Schwarz M. J., and Tice A. R. (1978) Icarus, 34, 638. [10] Gooding J. L. (1985) In Workshop on Water on Mars (S. Clifford, ed.), LPI Tech. Rept. 85-03. Houston, 29. [11] Gooding J. L. (1986) Icarus, 65, in press. [12] Aronson J. R. and Emslie A. G. (1975) J. Geophys. Res., 80, 4925-4931. [13] Toon O. B., Pollack J. B., and Sagan C. (1977) Icarus, 30, 663-696. [14] Wall S. D. (1981) Icarus, 47, 173-183. [15] Clark R. N. (1980) In Lunar. Planet. Sci. XI, LPI, Houston. 160-161.

MARTIAN DUST: THE CASE FOR "PARNA"; Ronald Greeley, Department of Geology, Arizona State University, Tempe, AZ 85287.

The characteristics of martian dust deposits are controversial, especially as the source. However, considerations of terrestrial "dust" deposits may shed light on certain aspects of the problem. Engineers, environmental scientists, planetologists, geologists, and others each tend to have somewhat different meanings for the term "dust". Table 1 shows a classification of windblown particles on Earth; martian atmospheric dust is estimated to be only a few microns in diameter (1) and would fit within the aerosolic dust category. Because the windspeeds needed to initiate particles of this small size are quite high (2), various mechanisms have been proposed to set the dust into motion, other than simple wind shear. These include dust-fountaining (3,4), dust-devils (5), and impact by larger saltating grains such as sand, which is more easily moved by the wind (6,7), as reviewed previously (8). Because sand-size grains may be rare on Mars (9) and may be quickly fragmented by the "Kamikaze" effect (10), it was suggested that dust grains may clump together into larger aggregates (11) which would behave as sand, both for the threshold process and to serve as "triggers" to set finer, non-aggregated dust grains into motion. Windblown aggregates occur on Earth in several forms (Table 1): (a) dune "parna" consist of clay pellets (aggregates) that form dunes on the margins of some dry lakes, (b) volcanic aggregates are formed in clouds of pyroclastic dust during eruption and can be widely dispersed, and (c) sheet parna; although both (a) and (b) may also occur on Mars, sheet parna is the primary type of aggregate discussed here and is proposed as the mantling deposits inferred for many parts of Mars.

"Parna" is an Australian aboriginal word meaning "sandy and dusty ground", used by Butler (12) for the extensive deposits that mantle parts of southeast Australia. The deposits consist of two components, clay or "dust" (~ 2 μm in diameter) and large grains (~ 100 μm) which Butler and Hutton (13) termed as companion sand. Results from field studies (13) of the deposits in the Riverina Plain of SE Australia show prevailing winds when the deposits were formed, possible source regions, and particle size distributions as a function of transport distance. Butler (12) proposed that parna was transported in suspension as aggregates (clay pellets) of a size equal to the companion sands; the occurrence of multiple layered deposits suggests climatic cycles in which clay was produced by chemical weathering during relatively humid periods and then redistributed by winds during more arid periods. Pre-existing sand dunes served as one source for the parna. Dust within the sand dunes was mobilized during arid regimes by the triggering effect of the sand (which then became the "companion" component). Although Butler does not discuss the mode for aggregation, the sand grains may have served as nuclei for the finer grains in the formation of the aggregates. Westerly winds then transported the aggregates in suspension more than 650 km to the east where they settled as a uniform blanket over all terrain features--an aspect cited as evidence for transport via suspension. Once deposited, the pellets disaggregated, forming a matrix containing evenly-distributed sand grains. Dare-Edwards (14) suggests three other sources for sheet parna in Australia: (a) crusty surfaces developed on soil surfaces that have been acted upon by fluctuations of saline groundwater, (b) derivation from mud-cracked surfaces on former lakes (e.g., playas), and (c) alluvial deposits incorporating clay deposits. In all three cases, clay "pellets" are produced which are in the size range (~100-200 μm) easily moved by the winds.

All the potential sources for Australian parna may have martian counterparts. Laboratory experiments under simulated martian conditions have shown that aggregation can occur via electrostatic charging of grains in transport; because the sign of the charge is a function of grain size, the "companion sands" (+ charge) may serve as nuclei for the accretion of dust grains (-charge). Because water has been present in the past on Mars, those processes of parna development associated with the hydrologic cycle may also have occurred. Abundant channels could produce alluvial-related dust; many of the smooth, dark deposits on Mars has been suggested to be martian lakebed deposits; and numerous investigators have suggested subsurface water. With the abundance of salts detected via the Viking landers, saline groundwater interaction would be expected to produce the crusty, clay-pellet surfaces described by Dare-Edwards.

Regardless of their origin aggregates or clay pellets would permit movement of dust by relatively low-speed martian winds. As part of the martian dust cycle (Greeley, this issue), this material--like parna--may be transported in suspension and eventually settle from the atmosphere as a terrain-mantling blanket. Also like parna, some of the deposits may disaggregate to form a relatively stable mass that would be difficult to move unless acted upon again by aggregate-producing processes.

References

(1) Pollack et al. (1977), J. Geophys. Res. 82, 4479-4496.
(2) R. Greeley et al. (1980), Geophys. Res. Lettr. 7, 121-124.
(3) R. Greeley and R. Leach (1979), NASA TM 80339, 304-307.
(4) R. Hugnenin et al. (1979), NASA Conf. Pub. 2072, 40.
(5) P. Thomas and P. Gierasch (1985), Science, 230, 175-177.
(6) A.R. Peterfreund (1981), Icarus, 45, 447-467.
(7) P.R. Christensen (1983), Icarus, 56, 496-518.
(8) R. Greeley (1985), Workshop on Dust on Mars, LPI Tech. Rpt. 85-02, 3-5.
(9) Smalley and Krinsley (1979), Icarus, 40, 276-288.
(10) C. Sagan et al. (1977), J. Geophys. Res. 82, 4430-4438.
(11) R. Greeley, (19__), J. Geophys. Res., 84, 6248-6254.
(12) B.E. Butler (1956), Austral. J. Sci. 18, 145-151.
(13) B.E. Butler and J.J. Hutton (1956), Aust. J. Agric. Res. 7, 536-553.
(14) A.J. Dare-Edwards (1984), Trans. Inst. Br. Geogr. N.S. 9, 337-344.

TABLE 1. WINDBLOWN PARTICLES, EARTH

TERM	SIZE (μm)	TRANSPORT			DEPOSIT/BEDFORM
		DOMINANT MODE	HEIGHT	~RANGE, km	
GRANULES	4000-2000	Creep	Ground level	10^{-3} to 10^{-2}	megaripples
SAND					
Coarse	2000-400	creep/saltation	at/near ground	10^{-3} to 10^{0}	sheets/ripples/dunes
Dune	400-200	saltation	near-ground		
Fine	200-60	suspension/saltation	above ground		
DUST					
Silt	60-4	suspension			mantles
Loess	50-10	suspension	lower troposhere	10^{-1} to 10^{2}	
Aerosolic dust	10-1	suspension	middle-upper troposphere	10^{4} to 10^{6}	
Clay	<4	suspension	upper troposphere	?	
AGGREGATES					
Dune parna	400	saltation	at/near ground	10^{-3} to 10^{0}	dunes
Sheet parna	100	suspension	lower troposphere	10^{1} to 10^{3}	mantles
Volcanic	250-500	suspension	lower troposphere	10^{0} to 10^{3}	mantles

TOWARD AN UNDERSTANDING OF THE MARTIAN DUST CYCLE

Ronald Greeley, Department of Geology, Arizona, Tempe, AZ 85287

Despite more than a decade of study, many of the characteristics of martian dust and the processes associated with it remain enigmatic. The mechanisms for raising dust above the surface into suspension, the mode(s) of settling, and the nature of dust deposits are all subjects of debate. However, observations and measurements of Mars dust, considerations of terrestrial analogs, theoretical models, and results from laboratory simulations permit the formulation of a tentative model of the ***Martian Dust Cycle*** (Fig. 1). The proposed dust cycle consists of three main processes; (a) suspension threshold (the means for raising dust), (b) transportation, and (c) dust settling, or deposition; two associated processes are also included: (d) dust removal and (e) the addition of "new" dust to the cycle.

Suspension threshold. Perhaps the least understood aspect of martian dust storms is the mechanism(s) for putting dust into suspension (1). Because of the low density atmosphere, extremely high winds are required to raise loose dust of the size inferred for martian dust (~ a few μm). Although some dust may be raised by these high winds, most investigators invoke other threshold mechanisms. Dust devils may be one such mechanism; laboratory simulations show that vortical wind shear is very efficient in raising particles (2). With the discovery of dust devils on Mars (3) this possible mode of dust-raising is enhanced. Outgassing of volatiles (CO_2 or H_2O) from the regolith in response to changes in atmospheric temperature/pressure has also been suggested as a means of injecting dust into the atmosphere (4,5). Laboratory experiments show that this process can involve rapid venting of gasses which carry dust particles tens of cm above the surface, depending upon the rapidity of outgassing. Although slow outgassing does not cause dust injection, it can lead to surface fracturing and fissuring, which may be important in the "aggregate" mode of dust-raising discussed below.

Because sand-size grains are more easily moved than dust, it has been suggested that saltating sands could act as "triggers" to set dust into suspension (6,7). Laboratory experiments show this to occur, although in some circumstances, the saltating sands merely "indent" the surface without dislodging the dust (1). Sand "triggering" has been proposed for dust-raising in Australia in reference to "***parna***" (see Greeley, this issue). The third general mechanism of dust-raising involves ***aggregates*** (8) ("dust"-size grains collected into sand- and larger-size clumps). Four sources of aggregates may occur on Mars: (a) deposits settled from the atmosphere as part of the dust cycle, (b) ancient lake bed deposits, similar to clay pellets derived from playas on Earth, (c) aggregates derived from frothy/crusty surfaces generated by fluctuations of saline ground water, and (d) crusty/cloddy weathering surfaces which may be disrupted, as by outgassing (discussed above). Aggregate strength is variable, depending on mode of bonding (electrostatic, cementation, etc.). Because the wind speeds on Mars required to set particles into motion are high, Sagan et al. (9) proposed that holocrystalline grains would be pulverized into fine grains by the "kamikaze" effect. If aggregates were involved, the destruction would be even more effective because of their low strength. Wind tunnel experiments with aggregates show that as they lift above the surface, they rupture into dust clouds (1). Thus on Mars, disaggregation may occur via "kamikaze dust explosions".

Transport The movement of dust in both local clouds and as global transport is documented through earthbased and spacecraft observations. Pollack et al. (10,11) and Haberle et al. (this issue) have developed models to predict the patterns of transport and provide the key to this part of the dust cycle.

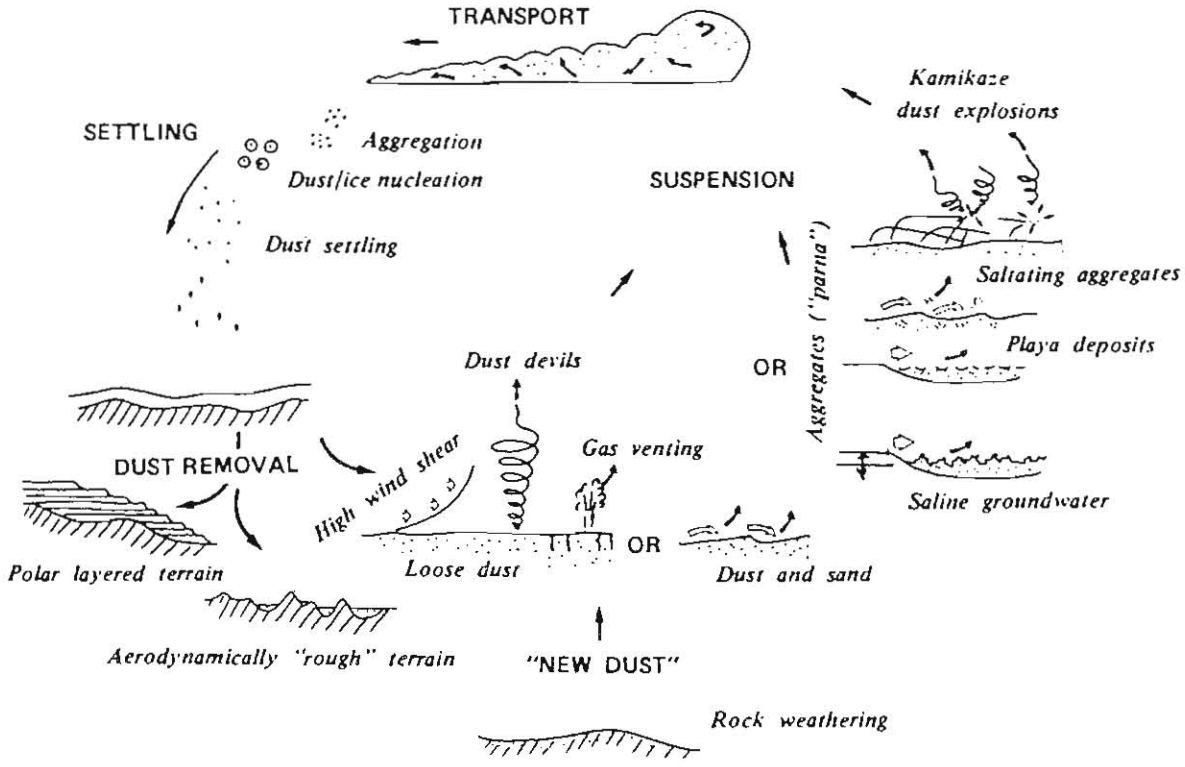

Fig. 1. Diagram of proposed Martian Dust Cycle.

Deposition. With a decrease in driving energy for dust clouds, in time particles settle from the atmosphere. However, because of possible "feedback" mechanisms (11), one of the problems in the dust cycle is how to shut-down dust storms. One mechanism involves the accretion of ice on dust grains (10). Aggregation of grains may also occur via electrostatic bonding, a mechanism demonstrated in laboratory experiments (8) and observed in volcanic dust clouds. Lee has shown (12), however, that the settling rate of larger grains (either ice/dust or dust/dust) is a function of the grain density and diameter, both of which change during accretion.

With settling and deposition, the cycle may be completed and the stage set for dust-raising to initiate the next cycle. However, in addition to the dust threshold, transport, and deposition components of the cycle, dust may be removed from the cycle, and "new" dust may be added.

Dust removal. On Earth, the largest "sinks" for dust removal are the oceans. Although these sinks are lacking on Mars, there are other areas where dust may be removed from the cycle. These include the polar regions (layered deposits) and surfaces that are aerodynamically rough such as impact ejecta fields, terrain that has been severely fractured by tectonic and other processes, and some lava flows. Once deposited on these surfaces, the dust would be difficult to remove until the roughness elements were effectively buried.

"New" dust. Dust may be added to the cycle by a variety of mechanisms on Mars, including chemical and physical weathering (clays are the normal end product of weathering on Earth), impact cratering, volcanism, and tectonism.

In summary, the proposed Martian Dust Cycle (Fig. 1) inter-relates many of the previously proposed aspects of martian dust, and introduces some new concepts, such as "kamikaze dust explosions".

References

(1) Greeley, R., 1985, Dust storms on mars: Mechanisms for dust-raising, in Workshop on Dust on Mars, *LPI Technical Report No. 85-02*, 3-5.
(2) Greeley et al., 1981, *Geol. Soc. Amer. Sp. Pub. 186*, 101-121.
(3) Thomas, P. and P.J. Gierasch, 1985, Dust devils on Mars,*Science, 230*, 175-177.
(4) Greeley, R. and R. Leach, 1979, *NASA TM 80339*, 304-307.
(5) Hugnenin, R. et al., 1979, *NASA Conf. Pub. 2072*, 40.
(6) Peterfreund, A.R., 1981, *Icarus, 45*, 447-467.
(7) Christensen, P.R., 1983, Eolian intracrater deposits on Mars: Physical properties and global distribution, *Icarus, 56*, 496-518.
(8) Greeley, R., 1979, Silt-clay aggregates on Mars, *J. Geophys. Res., 84*, 6248-6254.
(9) Sagan, C., D. Pieri, P. Fox, R. Arvidson, and E. Guinness, 1977, Particle motion on Mars inferred from the Viking lander cameras, *J. Geophys. Res., 82*, 4430-4438.
(10) Pollack, J.B., 1979, Climatic change on the terrestrial planets, *Icarus, 37*, 479-553.
(11) Pollack, J.B., C.B. Leovy, P.W. Greiman, and Y. Mintz,1981, A martian general circulation experiment with large topography, *J. Atmosph. Sci. 38*, no. 1, 3-29.
(12) Lee, S.W., 1984, Influence of atmospheric dust loading and water vapor content on settling velocities of martian dust/ice grains: Preliminary results, *in* Workshop on Dust on Mars, *LPI Technical Report No. 85-02*, 51-52.

THE DEVELOPMENT OF GLOBAL DUST STORMS: THE ROLE OF THE MEAN MERIDIONAL CIRCULATION; R.M. Haberle, NASA Ames Research Center, Moffett Field, CA 94035

Leovy et al. (1984) have identified two distinct regimes that characterize the Martian atmosphere during northern winter. In the first, one or more global dust storms develop which raise dust primarily in the southern subtropics. Haberle et al. (1982) have shown that dust injected into the atmosphere at these latitudes is carried to very high levels and distributed rapidly over much of the planet by a greatly intensified Hadley circulation due to heating by suspended dust. In the second regime, no global dust storms develop. Instead, a shallow layer of dust exists in northern midlatitudes that remains relatively confined. Leovy et al. speculate that traveling baroclinic disturbances, which are much more intense during non dust storm years, generate frequent local dust storms and that these storms are the source of dust during the non dust storm years.

This paper attempts to shed light on why global dust storms occur in some years but not in others. As a working hypothesis, it is assumed that dust enters the atmosphere when surface stresses due to winds become large enough to lift dust by saltation or by other means. The approach taken is to use the zonally symmetric model of Haberle et al., which simulates the mean meridional circulation, to examine how a northern midlatitude source of dust evolves in time, and how it affects the pattern of surface stresses. In particular, we wish to know if dust introduced into northern midlatutes during winter will spread globally, and if not, will its presence strengthen or weaken surface stresses in the southern subtropics? In reality, of course, the mean meridional circulation is but one component of the total dust raising circulation in the southern subtropics; thus, its contribution alone is the focus of this work.

The results of a variety of experiments, to be presented and discussed, suggest that dust does tend to be confined to shallow layers for a source region located in the northern hemisphere. More importantly, however, the presence of dust in northern midlatitudes during winter considerably reduces surface stresses in the southern subtropics -- the region where global dust storms generally originate. The implication is that the occurence of global dust storms may, in fact, be keyed to the behavior of the northern hemisphere midlatitude circulation: if baroclinic wave activity is sufficiently vigorus to create an extensive dust pall in the north, then the contribution to the surface stress by the mean meridional circulation in the southern subtropics is reduced and, presumably, the ability of the total circulation there to raise dust. On the other hand, if the northern midlatitude circulation is unable to raise enough dust, then surface stresses in the southern hemisphere will be maximized and the probability for the development of a global dust storm increased.

While these results are intriguing, they don't in themselves offer an explanation for why global dust storms occur in some years and not in others. Instead, they suggest a competetion between circulations in opposite hemispheres. One possibility is that random meteorological

MARS GLOBAL DUST STORMS

Haberle, R. M.

fluctuations determine which regime will develop, in which case Mars may exhibit a bifurcation phenomenon as suggested by Leovy et al (1984). Another possibility is that dust deposited in northern midlatitudes following a global dust storm provides a source for the baroclinic waves in the following year. Some of the dust is then transported poleward by the waves themselves, while some is moved back into equatorial regions by the mean circulation. After several years, the northern hemisphere source is diminished and the subsequent ability of the mean meridional circulation to contribute to the development of global dust storms is enhanced. This latter possibility will be discussed in more detail.

References:

Haberle, R.M., C.B. Leovy, and J.B. Pollack (1982). Some effects of global dust storms on the atmospheric circulation of Mars. Icarus, 50, 322.

Leovy, C. B., J.E. Tillman, and W.R. Guest (1984). Inerannual variability of Martian weather. Proceedings of the Seymour Hess Symposium, IAMAP, Aug. 1983.

DUST SCATTERING AT THE MARTIAN TERMINATOR DURING THE MARINER 9 MISSION; K. E. Herkenhoff, Division of Geological and Planetary Sciences, California Institute of Technology, Pasadena, CA 91125

Evaluation of martian surface photometry is complicated by aerosol scattering in the martian atmosphere. Surface albedo contrast is often diminished by atmospheric scattering, especially during the early part of the Mariner 9 mission. The usefulness of this dataset for geologic and photometric studies could be greatly enhanced if the atmospheric component of the brightness observed in the images were understood and removed. Our particular interest is in the topography and photometry of the south polar region, which was imaged at highest resolution by Mariner 9. Analysis of images that include the terminator may significantly improve our (presently poor) knowledge of the regional topography in this area. Deviations of the true terminator from the location predicted for a smooth, ellipsoidal Mars are evidence for regional slopes. This technique is very sensitive to small variations in slope, and was used successfully in determining the topography of portions of the lunar surface. Relative slopes within each image of areas near the terminator on the order of 100 km across are best measured by this method, although investigation of the topography of larger regions may also be possible. Mariner 9 A-frames are better suited to this task than Viking images, due to their larger field of view which includes a greater range of incidence angles. However, we plan to compare Mariner 9 and Viking terminator images and investigate possible differences in dust properties and distribution between the two missions.

Recent progress in Mariner 9 television data decalibration has allowed the processing of images to remove residual image effects, light transfer non-linearities, various types of noise, geometric distortions, and to correct for shading. The individual pixel data values in the resulting images are multiplied by an arbitrary scaling factor to approximate the true intensity observed by the camera relative to the solar flux (I/F). Information from the Supplementary Experimental Data Record (SEDR) is used to calculate a profile in each image from any given point toward the sub-solar point (perpendicular to the terminator), yielding a plot of data values vs. incidence angle (Fig. 1). The incidence angles computed in this manner may be in error by as much as 1^{o} due to uncertainties in camera pointing, but may be corrected if surface features can be located and identified in controlled maps and photomosaics.

The theory used to model these data assumes single scattering from dust particles with an exponential density distribution $n(z) = n_{o}\exp(-z/H)$ up to some maximum altitude. This dust distribution, with a scale height of 10 km, was found by Kahn et al. (1981) to be consistent with Viking lander observations of twilight sky brightness. The lander images indicate that the dust particles are strongly forward-scattering, have single-scattering albedos of 0.86, and extend to at least 30 km altitude (Pollack

et al., 1977). Surface scattering is modeled using the Minnaert function given by Thorpe (1977), a lunar surface phase function (Harris, 1961), and a surface albedo of 0.25 (McCord and Adams, 1969). The result shown in Figure 1 does not include surface scattering, but models the data fairly well out to 93° incidence angle. The scale height in this case is 20 km, twice as large as the scale height inferred from Viking lander data. The model optical depth is near unity, about twice as large as the optical thickness at 300 nm estimated by Toon et al. (1977) using IRIS spectra. Scattering observed deeper into the twilight is probably due to small-angle scattering into the geometric shadow.

Clearly, further modeling and image processing are required to better understand this phenomenon. Work is in progress to produce Mariner 9 images that are calibrated in terms of absolute radiometry. The calibration will be applied to images of the martian terminator throughout the Mariner 9 mission to investigate temporal changes in dust distribution. Future modeling of dust scattering at the terminator should include the effects of multiple scattering, in particular the "aureole" around the sun due to the large forward peak in the scattering phase function (Kahn et al., 1981).

References

Kahn, R., R. Goody, and J. Pollack, "The Martian Twilight", J. Geophys. Res. **86**, 5833 (1981).

McCord, T. B. and J. B. Adams, "Spectral Reflectivity of Mars", Science **163**, 1058 (1969).

Pollack, J. B., D. S. Colburn, F. M. Flasar, R. Kahn, C. E. Carlston, and D. Pidek, "Properties and Effects of Dust Particles Suspended in the Martian Atmosphere", J. Geophys. Res. **84**, 2929 (1979).

Pollack, J. B., D. S. Colburn, R. Kahn, J. Hunter, W. Van Kamp, C. E. Carlston, and M. R. Wolf, "Properties of Aerosols in the Martian Atmosphere, as Inferred From Viking Lander Imaging Data", J. Geophys. Res. **82**, 4479 (1977).

Thorpe, T. E., "Viking Orbiter Observations of Atmospheric Opacity During July - November 1976", J. Geophys. Res. **82**, 4151 (1977).

Thorpe, T. E., "Viking Orbiter Photometric Observation of the Mars Phase Function July Through November 1976", J. Geophys. Res. **82**, 4161 (1977).

Toon, O. B., J. B. Pollack, and C. Sagan, "Physical Properties of the Particles Composing the Martian Dust Storm of 1971-1972", Icarus **30**, 663 (1977).

MARINER 9 TERMINATOR DUST SCATTERING

HERKENHOFF, K. E.

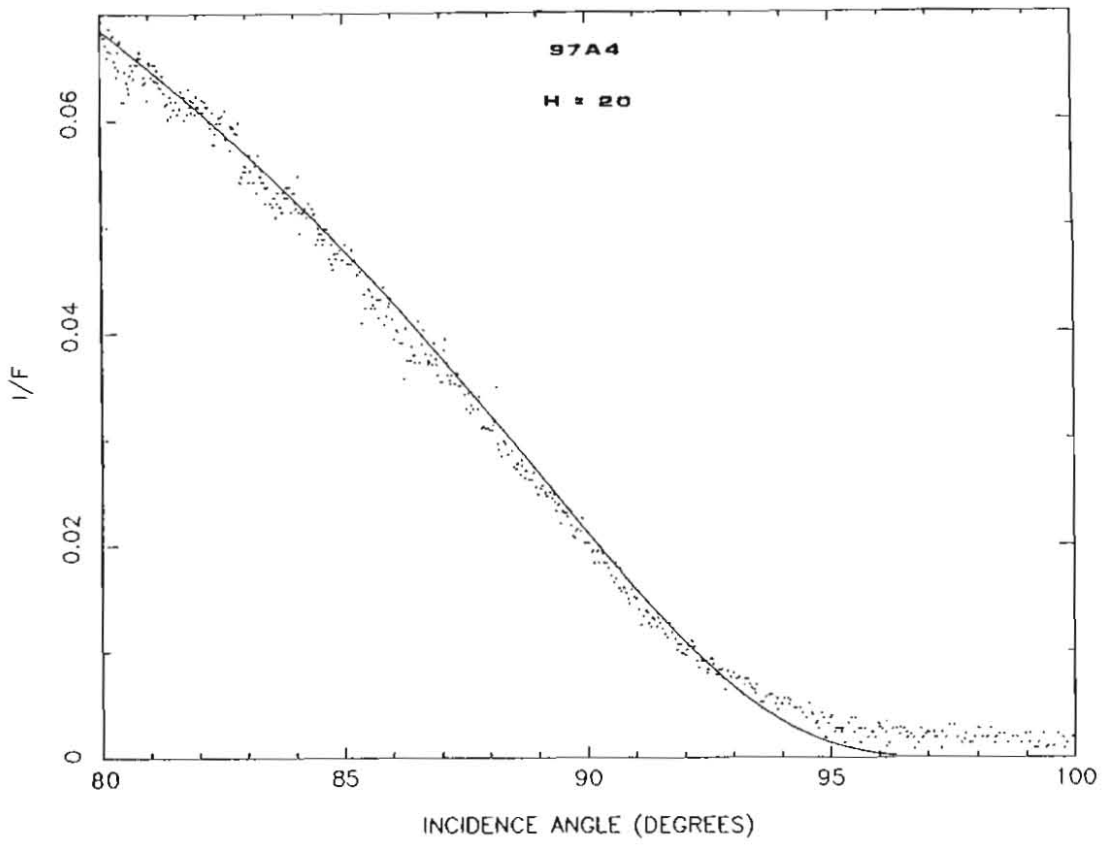

Figure 1. Individual pixel data values (points) and atmospheric dust scattering model (solid line) for orbit 97, frame A 4 (orange filter). Maximum dust height is 60 km, with a total optical thickness of about 1. The cosines of the emission and phase angles are 0.7 and 0.86, respectively.

ARE THE VIKING LANDER SITES REPRESENTATIVE OF THE SURFACE OF MARS?

Bruce M. Jakosky, Laboratory for Atmospheric and Space Physics, University of Colorado, Boulder, CO 80309, and Philip R. Christensen, Department of Geology, Arizona State University, Tempe, AZ 85287.

The detailed nature and physical structure of the martian surface has been observed directly only at two lander sites, with observations providing resolution as fine as a few millimeters over about 5 x 10^{-7} percent of the surface. Remote-sensing observations, on the other hand, provide information on the centimeter- to meter-scale structure of the surface on a global basis. We compare the properties of the two lander sites, as observed directly and as inferred from remote-sensing data, with global properties inferred from remote-sensing observations; this will allow us to determine whether the observed properties at these locations are representative of the entire surface, and whether the entire range of surface processes extant are represented at the two lander sites.

In-situ observations at the lander sites show a boulder-strewn surface with abundant fine material, and they show evidence for the abundant occurrence of aeolian processes. The VL-1 site contains numerous large drifts of fine material, in some cases encroaching on and partly covering up large rocks and what appear to be outcrops of bedrock; although it has abundant fines, the VL-2 site has none of these large drifts. Trenching operations show that the fine material beneath the surface at both sites is darker than the surface, suggesting the presence of a thin veneer of bright dust at the surface. In addition, deposition of additional dust onto the surface was observed after the global dust storms, in amounts sufficient to change the reflectance of the surface; this added dust appears to have been eroded away at VL-1 in a subsequent year. A duricrust is present at both lander sites, consisting of a case-hardened bonding together of the fine material. Due to the high salt content within the duricrust at both sites, it is likely that the salts act as the cementing agent to hold the grains together.

Remote-sensing observations of Mars, including of the regions which contain the two lander sites, have been made from the Viking Orbiter using thermal infrared, broadband albedo, and color imaging techniques. Observations from Earth have been obtained using radar and spectral reflectance techniques. Although the spatial resolution element in each case is greater than several kilometers, each measurement is sensitive to the properties of the uppermost meter or less of the surface. Viking orbiter images suggest that the regions containing the lander sites are homogeneous at scales up to tens of kilometers; we can therefore compare the remote-sensing observations with what is seen in the immediate vicinity of the landers themselves.

Each of the remote-sensing data sets provides a somewhat non-unique interpretation of the nature of the surface. For instance, spatial variations in the surface thermal inertia can be explained equally well by variations in the particle size of a homogenous surface, variations in the abundance of rocks covering the surface, or variations in the degree of formation of a bonded duricrust. By examining all of the available data sets, we can use the various constraints placed by each of the data sets to better describe the nature of the surface. Globally, the analyses which most constrain the surface are the abundance of surface rocks as estimated by thermal-infrared

spectral observations, and the correlation between the thermal inertia and the radar cross section.

The fact that the thermal inertia correlates with the radar cross section indicates that the process that causes the thermal conductivity to vary spatially also causes the bulk density to vary spatially. Packing geometry or particle size variations cannot explain the variations, but they can be explained either by a spatially-varying duricrust or by a varying abundance of small rocks mixed in with the fine material. In the latter case, up to 50 % of the surface would need to be covered by rocks in the regions of high thermal inertia. The estimates of rock abundance provided by infrared techniques indicate, however, that the surface rock abundance is nowhere high enough to explain these observations; additionally, they indicate a unimodal distribution of rocks rather than a bimodal distribution that would explain the distribution of thermal inertia. The simplest geologically-plausible explanation for these data is that the surface of Mars is covered by fine material that is unconsolidated in some places and has in some places been bonded together to form a duricrust. Rocks are present on the surface everywhere, but their abundance does not change drastically from place to place and they generally do not cover a significant fraction of the surface.

The fact that the thermal inertia correlates well globally with both the 12.5- and 70-cm radar cross section suggests that the duricrust in regions of high thermal inertia dominates the uppermost meter of the surface. Observations of the VL-1 site show that region to fit into the general correlation of thermal inertia with 12.5-cm radar cross section, but to not fit the correlation with 70-cm cross section. Therefore, that location appears to have a duricrust that dominates the uppermost ten centimeters but does not dominate the uppermost meter of the surface. This appears to be consistent with the observations at the site which show it to have a relatively thin and variable duricrust. The VL-2 site is too far north to be examined by Earth-based radar. Both lander sites have a relatively high albedo and do not fit the general trend of albedo with thermal inertia, suggesting that there is a thin layer of bright dust overlying the surface. Again, this is consistent with the lander imaging of these locations.

Regions which do not fit into the general trend of albedo with thermal inertia are Chryse, Utopia, Hellas, Argyre, and Isidis. Notice that these regions are all low-elevation basins. Because the landers were targeted to low regions, they were therefore destined to land in an anomalous region. The lander sites appear to be intermediate in properties and processes between classical bright and dark regions of the planet. Deposition of dust onto the surface occurs globally each year. Dark regions remain dark because dust is rapidly removed after the annual dust storms. Bright, low-inertia regions retain the dust over a longer time, accumulating it to a thickness of at least several centimeters. The VL-1 site retains enough dust to raise the albedo, but the dust is removed before it becomes thick enough to dominate the surface morphology and thermal behavior. Thus, the VL-1 site differs primarily due to the timescale on which dust deposition and removal occurs. It may be a region of incipient formation of a low-thermal-inertia surface.

INTERANNUAL VARIABILITY IN MARS' SOUTH POLAR RECESSIONS AND POSSIBLE CORRELATIONS WITH MAJOR DUST STORMS; P. B. James and L. J. Martin, Lowell Observatory and University of Missouri-St. Louis, St. Louis, MO 63121.

There are three principal cycles present in the seasonal martian climate system: the CO_2 and H_2O volatile cycles and the dust cycle. The amount of interannual variability in these cycles has been a matter of considerable interest and debate during the last two decades as has the degree of correlation between cycles. Although some excellent spacecraft data sets exist, they represent isolated seasons and do not provide an opportunity for interannual comparisons. Telescopic observations provide data spanning a greater number of years although, because they are obtained only near opposition, they are far from continuous.

The data pertaining to the spring recession of the south polar cap offer the greatest potential for revealing interannual variations in the CO_2 cycle. Telescopic views of this particular season are superior because it is viewed at favorable apparitions with relatively high resolution and because there is relativelty less surface/hood ambiguity. Modern data sets which pertain to the south cap recession include: the Lowell plate collection encompassing the years 1907 to 1958 (Fischbacher et al., 1969); International Planetary Patrol pictures from 1971 and 1973 (James and Lumme, 1982); Viking images from 1977 (James et al., 1979); and data sets obtained Iwasaki et al. (1986) and Dollfus (1965). Intercomparisons of data sets are not straightforward. For example, the IPP data were reduced to average diameters for 1° L_S intervals while the much less extensive Lowell data were binned in 10° L_S intervals; the globe spanning IPP network often permitted coverage of the entire cap boundary in a day, while only a much more limited longitude range was viewed in the earlier Lowell studies. Other observers have used different measurement and data reduction techniques.

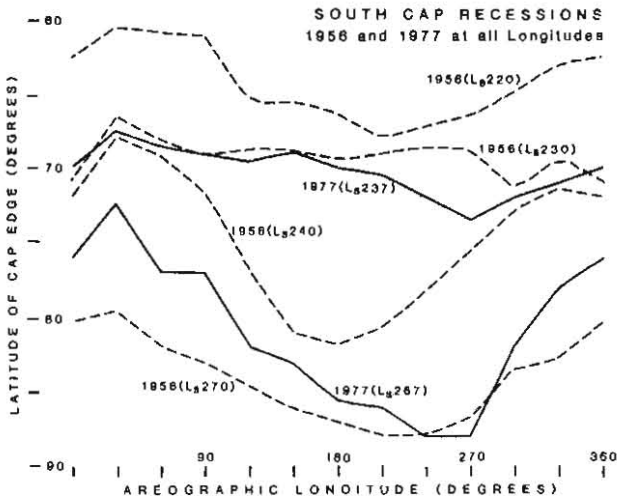

FIGURE 1

We have therefore re-examined some of these data in order to facilitate comparisons between years. In order to avoid possible systematic errors associated with intercomparisons of data acquired on different systems analyzed in different ways, we have confined the study to the Lowell and IPP data, which were measured in the same manner on the same equipment. Significant differences are revealed between 1956 and 1977 in the longitude by longitude comparison shown in Figure 1. A fixed longitude comparison between 1971 and 1973 confirms the report of differences between these years by Iwasaki et al (1986). The preliminary conclusion is that the 1956 and 1973 recessions seem to be advanced relative to the median for all recessions while 1971 and 1977 seem to be retarded.

The following Table I lists global and semi-global dust storm events which have been well documented photographically (Martin, 1984). Inasmuch as all of these years featured at least one global dust storm event, polar regression data for these years may provide insights into possible correlations with the observed duststorm patterns.

PHOTOGRAPHICALLY DOCUMENTED STORMS THAT EXPANDED

BEGINNING DATE	L_s	APPARENT DIAMETER	INITIAL LOCATION	COMMENTS
10 July 1922	192°	19°	Margaritifer Sinus	Observed for 4 days only
19 Aug 1956	250°	23°	Hellespontis	Planet encircling
29 May 1969*	163°*	19°	Hellospontis*	Size unknown
10 July 1971	213°	21°	Hellespontis	Two weeks duration
22 Sept 1971	260°	19°	Hellespontis	PLANETWIDE
13 Oct 1973	300°	22°	Solis Planum	Planet encircling
		VIKING ORBITER IMAGING		
15 Feb 1977*	204°*		Solis Planum*	Planet encircling
27 May 1977*	268°*		Solis Planum*	Planet encircling

*Estimated; earliest clouds may not have been observed.

TABLE I

Fischbacher, G. E., L. J. Martin, and W. A. Baum (1969). Martian polar cap boundaries. Lowell Observatory Report (unpublished).

James, P. B. and K. Lumme (1982). Martian south polar cap boundary: 1971 and 1973 data. Icarus 50, 368-380.

Dollfus, A. (1965). Etude de la planete Mars de 1954 a 1958. Ann. Astrophys. 28, 722-746.

Iwasaki, K., Y. Saito, and T. Akabane (1986). Martian south polar cap 1973. Publ. Astron. Soc. Japan (in press).

Martin, L. J. (1984). Clearing the martian: The troubled history of dust storms. Icarus 57, 317-321.

THE VERTICAL DISTRIBUTION OF AEROSOLS DURING THE GROWTH PHASE OF A GLOBAL DUST STORM; F. Jaquin, Cornell University

Vertical reflectance profiles were constructed from Viking Orbiter images of the martian limb, and inverted to reveal the distribution of aerosols above 30 Km. Data obtained during the growth phase of the first Viking global dust storm ($170 < L_S < 210$) fall into three bands near latitudes 15N, 0, and 25S. Limb profiles from the southern band, historically a source region of global dust storms, indicate a predominantly two-component aerosol distribution. The first component occupies a region of large opacity ($\tau > 1$) between the surface and about 30 Km and grows in elevation at a rate of about .5 Km/sol, to a maximum elevation of 50 Km. Above this, the second component, a high elevation detached haze between 50 and 70 Km, is observed that does not change elevation as the large opacity region below it does. The lower elevation haze component is interpreted to be the product of the growing dust storm. The high elevation detached haze may have been formed by transport of dust from other latitudes, perhaps by the ascending branch of the cross-equatorial Hadley cell, that subsequently settles, leaving a detached haze structure. Alternately, the condensation of water vapor related to the diurnal atmospheric tide could produce the observed structure. Both possibilities are discussed.

The Varying Properties of Martian Aerosols; R. Kahn, Dept. of Earth and Planetary Sciences and McDonnell Center for the Space Sciences, Washington University, St. Louis, MO 63130

Indications from existing data sets are that aerosols in the Martian atmosphere exhibit variable but at least to some degree systematic behavior with changing season, elevation, and region. Derived optical properties and particle spatial distributions for "ice-like" and "dust-like" components are summarized and compared in this study. Observations show variability in both dust and ice particle size, but a picture emerges in which condensates are most evident at all latitudes during northern spring and summer, while the relative importance of dust increases in southern spring and summer. The aerosol differences will need to be considered when constructing atmospheric radiative transfer models, and also may contain clues about the location of reservoirs of dust and water.

The use of only two parameters, the single scattering albedo (w) and the scattering asymmetry factor (g), to describe aerosol scattering properties is consistent with the little that is currently known about Martian atmospheric properties. Values derived by the Viking Lander 1 (VL1) imaging sky brightness experiment, performed in low northern latitudes during early northern summer, are w = 0.86 and g = 0.79, averaged over the solar spectrum (1). These numbers, which are consistent with dust particles a few microns in size, have been used as the standard for atmospheric modeling (2). The spatial distribution of clouds as viewed from orbit suggests that thicker hazes are present only at higher northern latitudes in this season, and that clouds with morphologies indicative of condensates are common near the equator over the Tharsis ridge (3). Models of the effect of atmospheric haze on Orbiter views of Mars surface texture near VL1 in late northern spring seem to require values nearer w = 0.95 and g = 0.85 using the clear filter (4), similar to those of water ice particles (5). Analysis of the VL1 site twilight reflectance, which samples higher in the atmosphere than the sky brightness observation, also requires the product (wg) to be larger than the standard and views a bluer sky than predicted using the standard particle parameters (6).

The importance of condensates at high elevations and globally during northern spring and summer is most evident in the cloud morphology data (3) and the Mariner 9 (7) and Viking Orbiter (8) limb studies. Early indication of high condensate haze was obtained from the decreased red to blue ratio (R/B) in the Mariner 9 television limb scans (7). Using the more extensive and better constrained Viking Orbiter limb data, detached condensate hazes are found surmounting a more dust-like haze at nearly all locations except sometimes during spring and summer in the southern hemisphere (8; Fig. 1). Condensates are identified from R/B, from the detached and vertically well defined nature of the layers, and from the relationship between inferred condensation level and the observed local column water vapor abundance. For the cases so far examined, all in mid latitudes between late southern summer and late northern summer (avoiding the dustier season), the condensation level decreases and the mean condensate particle size increases with increasing column water vapor abundance. This implies an active cloud formation process which may be used to constrain the interaction between vertical mixing and temperature structure in the column. (9)

Notes:
1) Pollack et al. (1979) JGR 84, 4479-4497;
2) Zurek (1982) Icarus 50, 288-310;
3) Kahn (1984) JGR 89, 6671-6688;
4) Kahn, Guinness, and Arvidson (1986) Icarus, in press;
5) Asano and Sato (1980) Appl. Opt. 19, 962-974;
6) Kahn, Goody, and Pollack (1981) JGR 86, 867-880;
7) Anderson and Leovy (1978) JAS 35, 723-734;
8) Jaquin, Kahn, and Gierasch (1986) submitted to Icarus;
9) Continuing work on this subject is supported in part by NASA grant NAGW 660 to Washington University, St. Louis.

Figure Caption: Three color limb profile showing absolute reflectance from Viking Orbiter images 131B52, 62, and 72, taken in late southern winter, low latitude. The refectance spectra of the detached haze at 55 km and near the base of the profile at 10 km are given in the inset.

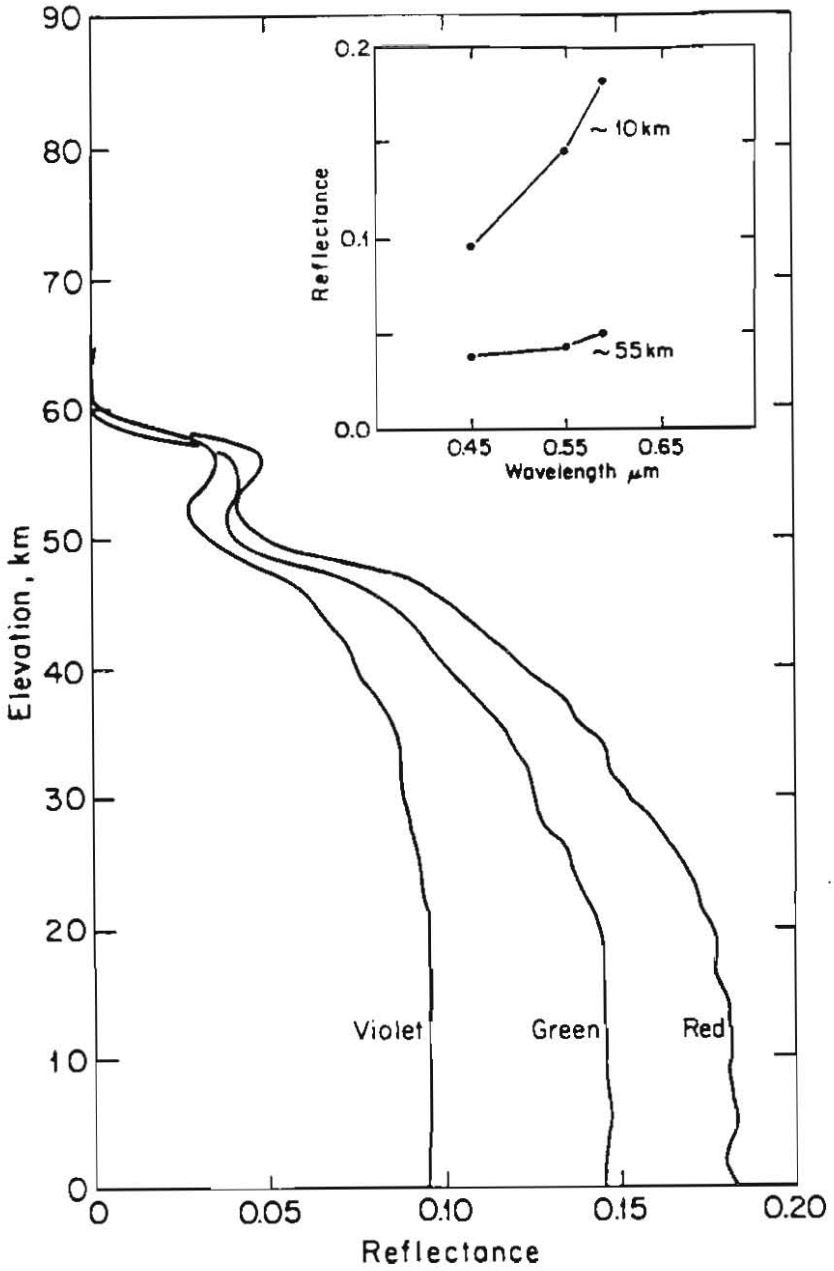

VIKING OBSERVATIONS OF REGIONAL SOURCES AND SINKS OF DUST ON MARS

Steven W. Lee, Department of Geology, Arizona State University, Tempe, AZ 85287

Seasonal variability of classical martian albedo features has long been noted by terrestrial observers [1,2]. Spacecraft observations of such features have shown them to be related to aeolian transport of bright dust into and out of regions, primarily in association with major dust storms [cf. 3,4]. Investigation into the amount and direction of dust transport related to variable features can reveal regions which, at present, act as either sources (net erosion of dust from an area) or sinks (net deposition) [5,6].

A study of seasonal variations of albedo features in the Solis Planum and Syrtis Major regions has been based on Viking Orbiter data obtained over more than one complete martian year. Contour maps of Lambert albedo and single-point thermal inertia have been constructed from the Infrared Thermal Mapper (IRTM) experiment data, and Orbiter images have been used to determine the pattern and variability of regional winds (inferred from wind streak orientations). Coupled with ground-based radar data, these data sets allow the regional sediment transport direction, surface properties (texture, morphology, and roughness), and the implications of the observed seasonal and longer term dust redistribution, to be investigated. The results of this study are outlined below.

Solis Lacus, the most prominent dark albedo feature in Solis Planum, extends over approximately 20° of longitude and 10° of latitude (centered at 25°S, 85°W), and contains and is surrounded by a conspicuous pattern of bright and dark wind streaks. The albedo feature is highly variable in extent and contrast with its surroundings, generally being most distinct during southern spring and summer (minimum Lambert albedo ~0.13) and less distinct during southern fall and winter (minimum albedo ~0.16). The regional thermal inertia values (~8-10 x 10^{-3} cal/cm^2/sec$^{1/2}$/°K) are indicative of a surface covered by particles larger than ~100 μm [7]. A seasonal dust-transport cycle has been proposed to explain these observations: 1) During late southern spring and summer, bright dust is eroded from the surface (possibly ejected by a saltation triggering mechanism) and transported from the region by local dust storms (several were detected by Viking, and have been commonly observed from Earth). Removal of dust over a wide area results in the dark, distinct, Solis Lacus feature. 2) Following cessation of dust-storm activity, sedimentation from the atmospheric dust load occurs over the entire region, decreasing the contrast of the albedo feature with its surroundings. 3) The cycle may be renewed by dust-storm activity the following year. The retention of some albedo features throughout the year, plus the constancy of the regional thermal inertia, requires that the albedo features do not involve erosion or deposition of substantial deposits; cycling of, at most, a few tens of μm of dust is indicated. Differences in time of occurrence, severity, and longevity of dust-storm activity may lead to the observed year-to-year changes in Solis Lacus.

Dramatic seasonal variability is also characteristic of Syrtis Major (~5°S - 25°N, 275° - 300°W). The feature lies on the low-albedo slopes of a volcanic shield [8] (generally darker than ~0.2 in albedo), the darkest area (albedo ~0.1) being closely associated with a mass of dunes located near the crest of the shield. Thermal inertias of ~8 x 10^{-3} cal/cm^2/sec$^{1/2}$/°K, plus the observed dunes, argue strongly for a sandy surface. Syrtis Major increases in albedo immediately following global dust storms, then darkens steadily through the balance of the year until reaching its pre-storm albedo (also confirmed in [9]). The observed trend of bright and dark streaks is in response to winds generally directed upslope and to the west. The dust-transport cycle consistent with these observations is: 1) Enhanced deposition from global dust storms increases the regional albedo. 2) The relatively mobile surface coupled with effective regional winds (possibly

reinforced by the global circulation) results in ejection of dust from the surface and net transport to the west during the remainder of the year, yielding a decreased regional albedo. 3) Initiation of another global dust-storm cycle begins the process again. Such a transport cycle provides a mechanism for significantly enhanced deposition in the neighboring low thermal inertia region, Arabia (as suggested in [10]).

These observations indicate that very different levels of aeolian activity give rise to the noted seasonal variability of these two regions: 1) In Solis Lacus, local dust storms result in net removal of dust from the area, while deposition occurs from the atmospheric dust load throughout the remainder of the year. Solis Planum serves as a source region of dust only during the limited period (dust storm season) when regional winds are capable of inducing dust ejection from the surface. Significant contributions to the global dust load may occur only when local storms grow into major global dust storms. 2) Syrtis Major presents a picture of a considerably more active aeolian enviornment. Deposition occurs only during and immediately following major dust storms, while during the rest of the year regional winds are apparently effective agents of dust ejection and transport. Syrtis Major thus acts as a dust source region through most of the year, possibly supplying the neighboring dust sink region of Arabia.

REFERENCES

[1] Slipher, E.C., 1962, *A Photographic History of Mars, 1905-1961*, Northland Press, Flagstaff, AZ.
[2] De Mottoni, G., 1975, *Icarus 25*, 296-332.
[3] Sagan , C. et al., 1973, *J. Geophys. Res. 78*, 4163-4196.
[4] Thomas, P. and J. Veverka, 1979, *J. Geophys. Res. 84*, 8131-8146.
[5] Lee, S.W. et al., 1982, *J. Geophys. Res. 87*, 10025-10041.
[6] Lee, S.W., 1986, submitted to *Icarus*.
[7] Kieffer, H.H., et al., 1977, *J. Geophys. Res. 82*, 4249-4295.
[8] Schaber, G.G., 1982, *J. Geophys. Res. 87*, 9852-9866.
[9] Christensen, P.R., 1986, this abstract volume.
[10] Christensen, P.R., 1982, *J. Geophys. Res. 87*, 9985-9998.

DUST CLOUDS OF A DIFFERENT NATURE, L. J. Martin, Planetary Research Ctr, Lowell Observatory; and P. B. James, University of Missouri - St. Louis

At four different times, Viking images showed clouds over a tributary canyon near the head of Echus Chasma (1°N, 81°W). These pictures were taken on Orbiter I revolutions 648, 682, 696, and 701 during the second Mars' year of the mission, between 27 March and 19 May 1978. There were no other Viking images of this area during that 53-day interval, making it uncertain whether this was a single, continuous cloud or part of a series of multiple events. It is unlikely that this cloud activity was restricted to the four dates for which we have images. Other Viking images of this area taken before and after that period do not show similar clouds, even though several images were taken near or within the same seasonal interval (L_s 66° - 88°) during other Mars' years.

We assume that these were dust clouds since they all were bright on red-filter images and because two of the four clouds had the accepted characteristic appearance of dust clouds (Briggs **et al.** 1979). In two cases of the four, we have overlapping violet-filter images which have also show these clouds as bright. We therefore suggest that they may also contained water. Nearby transitory bright albedo streaks may have been formed by associated dust-cloud activity. These dust clouds differ from others because of their persistence over the same location and their association with the small canyon. We are not aware of any similar cases. They are also of interest since each of the four clouds is different in appearance from the others. It is assumed that similar circumstances must have led to their formation or that they resulted from the continuation of the same set of events. IRTM data do not show any obvious events over this area, although there were no observations on the dates of these clouds (Lee 1986). The IRTM observations within that time interval suggest that these clouds may not have persisted through night hours.

Several mechanisms seem to play an important role in the generation of Martian local dust storms. A common denominator for many storms seems to be local circulations induced by the large regional slopes which occur in several areas of Mars (James 1985). Such katabatic winds probably contribute to the entrainment of dust in the local storms along the edge of the south polar cap, are one of the major factors in creating dust storms in the Solis Planum area [Magalhaes and Gierasch (1982); Peterfreund and Kieffer (1979)], and appear to play a role in generating storms in the Chryse basin such as the one observed by Viking Orbiter I (James and Evans 1981). The storms reported in this paper occur on one of Mars' largest regional slopes. An averaged slope of 0.006 from ENE to WSW stretches upward for roughly 1400 km from Echus Chasma to Noctis Labyrinthus. Ascraeus Mons and Pavonis Mons may also contribute downslope winds to this system. Once these winds reach the canyon, the sudden fall over a steep wall should accelerate their velocity and create considerable turbulence. This slope is similar to the nearby slope from Lunae Planum to the Chryse Basin, which seems to be effective in generating dust storms, and is steeper than the regional slope in the Solis Planum area. It is also important to note that the observations reported here were made during the season in which bore waves (Hunt **et al.** 1981; Kahn and Gierasch 1982) were observed in the Tharsis region. Inasmuch as the bore-wave

phenomenon is almost certainly a result of katabatic winds generated by the large thermal contrasts in the region, the fact that both effects are observed in the same general spatial and temporal locations seems to favor a common origin. For all these reasons, it seems reasonable to assign to slope winds an important role in the dynamics of generation of this group of storms.

References

Briggs, G. A., Baum, W. A., and Barnes, J. (1979). Viking Orbiter imaging observations of dust in the Martian atmosphere. **J. Geophys. Res.** 84, 2795-2820.

Hunt, G. E., Pickersgill, A. O., James, P. B., and Evans, N. (1981). Daily and seasonal Viking observations of Martian bore wave systems. **Nature** 293, 630-633.

James, P. B. (1985). Martian local duststorms. In **Recent Advances in Planetary Meteorology** (G. Hunt, ed.), pp. 85-100. Cambridge University Press, Cambridge, U.K.

James, P. B., and Evans, N. (1981). A local duststorm in the Chryse region of Mars: Viking Orbiter observations. **Geophys. Res. Lett.** 8, 903-906.

Kahn, R., and Gierasch, P. (1982). Long cloud observations on Mars and implications for boundary layer characteristics over slopes. **J. Geophys. Res.** 87, 867-880.

Lee, S. (1986). Private communication.

Magalhaes, J., and Gierasch, P. (1982). A model of Martian slope winds: Implications for aeolian transport. **J. Geophys. Res.** 87, 9975-9984.

Peterfreund, A. R., and Kieffer, H. H. (1979). Thermal infrared properties of the Martian atmosphere. 3. Local dust clouds. **J. Geophys. Res.** 84, 2853-2863.

INFRARED OPACITY OF DUST IN THE MARS ATMOSPHERE; T. Z. Martin, Jet Propulsion Laboratory

The work carried out between 1980 and 1984 to derive dust opacities from Viking IR Thermal Mapper data has led to the production of several interesting datasets: a zonal mean opacity history for over a Mars year; opacity time histories for the Lander sites; global opacity maps during the period near the 1977a major storm; and an opacity histogram for the planet (Martin, 1986).

The zonal mean opacity was derived from the Mars Average Data Set (Martin, 1981) and covers L_s 90-90-226 (1.4 Mars years). Major dust storms in 1977 affected the atmosphere between areocentric solar longitudes (L_s) 200 to 360. The highest opacities occurred in a broad equatorial zone during the 1977b storm; an opacity mean of 2.8 (at 9 μm) was found; locally higher values are implied. The clearest atmosphere occurs during L_s 50-150 in northern latitudes 10 to 60 degrees, where the opacity at 9 μm is about 0.03. The Viking lander sites experienced opacities considerably below the equatorial values.

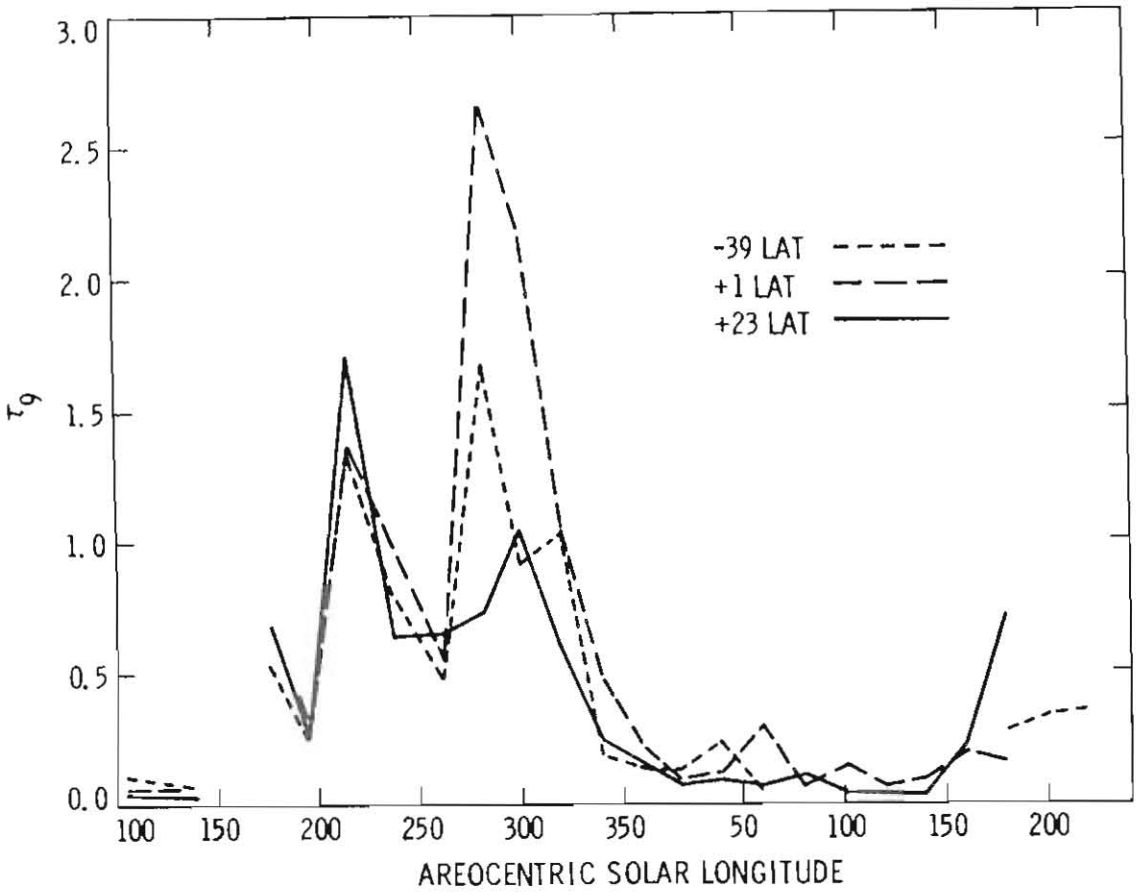

Fig. 1. Zonal mean opacities for three selected 2-degree wide latitude bands.

A histogram of opacity for one Mars year, generated from the zonal mean data, shows a very skewed distribution in which the most common value, 0.056, is well below the mean of 0.51. Thus, Mars may be considered "clear" most of the time and for most places, but when storms occur, their effects are dramatic.

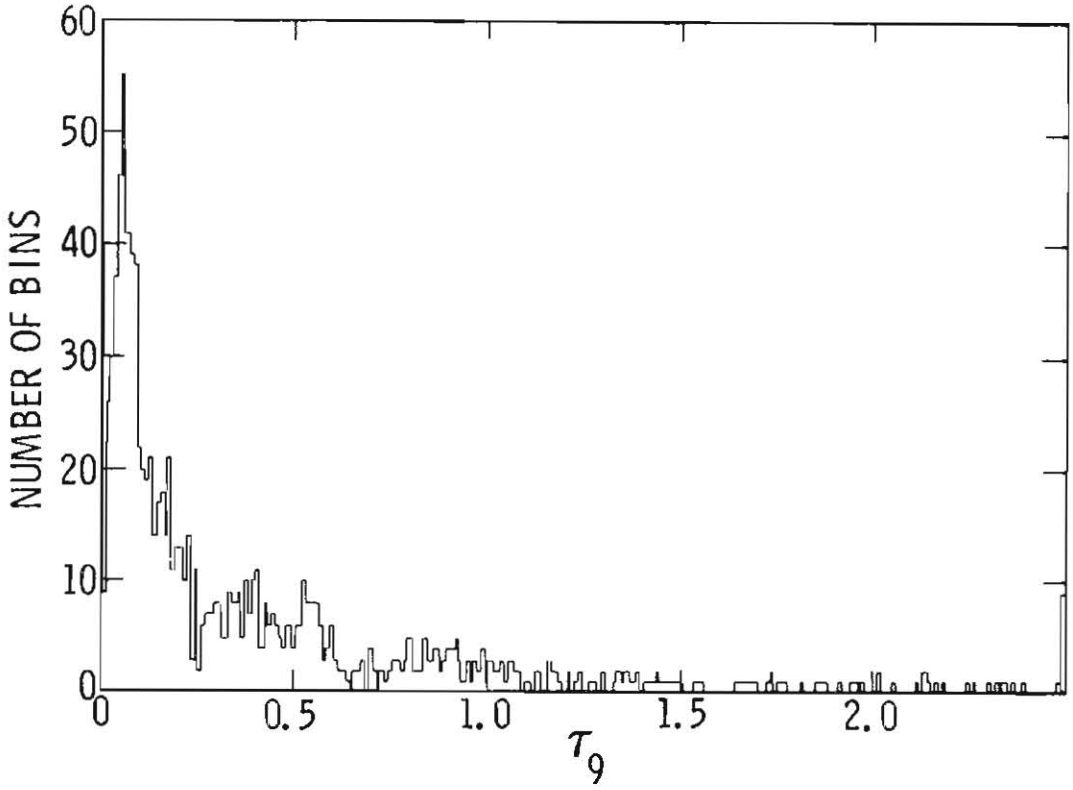

Fig. 2. Histogram of 9 μm opacity for one Mars year. Points are weighted by area of each zonal mean bin.

Time histories of opacity within 5 by 5 degree lat/lon bins centered at the two Viking Lander sites agree in form with those found by observations from the surface; however, the scale factor between the two methods is about 2.5 (larger opacity in the visual than at 9 μm). This ratio implies that the size distribution of particles found satisfactory for fitting Mariner 9 IRIS spectra and Viking Lander data is inadequate; larger particles are required to affect the 9 μm opacities, or smaller ones to affect the visible opacities.

Opacity maps have been generated for the whole planet in approximately 10 degree L_s increments from L_s 168 prior to the storm 1977a and continuing through L_s 270. These show high opacity near the south polar cap edge throughout the period, probably related to local storm activity there. The 1977a storm affected opacities globally; however, the time of peak opacity varied with location. Hellas did not show an opacity maximum until after L_s 230.

Martin, T. Z. (1981), Mean thermal and albedo behavior of the Mars surface and atmosphere over a Martian year, Icarus 45, 427-446.

Martin, T. Z. (1986), Thermal infrared opacity of the Mars atmosphere, Icarus, in press.

Acknowledgment. The research described in this paper was performed by the Jet Propulsion Laboratory, California Institute of Technology, under contract with the National Aeronautics and Space Administration.

OBSERVATIONS OF DUST FROM MARS OBSERVER

D. J. McCleese and R. A. West

Jet Propulsion Laboratory
Pasadena, CA

This paper describes the scientific objectives and measurement approach of the Pressure Modulator Infrared Radiometer (PMIRR) in the study of Martian atmospheric dust from Mars Observer. PMIRR comprises nine channels in the 0.3 to 50 μm spectral interval, and obtains high vertical resolution profiles of the atmosphere by limb sounding and surface observations via nadir scans. PMIRR provides temporally and spatially coincident vertical profiles of temperature, dust, water vapor and condensates as a function of pressure, with additional measurements of surface temperature and polar radiative balance.

Table 1 shows the spectral characteristics and measurement functions of each of the PMIRR channels.

Table 1. PMIRR Channel Sectral Characteristics and Measurement Functions

Channel Number	Bandpass	Central wavelength μm	Channel Type (1)	Measurement Function
1	1,230-1,400	7.6	PMR(CO_2)+WB	Temperature 0-20 km
2	725-745	13.6	PMR(CO_2)+WB	Temperature 20-50 km
3	670-700	14.6	PMR(CO_2)+WB	Pressure 30-50 km & Temperature 50-80 km
4	1,400-1,500	6.9	PMR(H_2O)+WB	Water Vapor 0-35 km
5	820-870	11.8	WB	
6	460-510	20.6	WB	
7	290-340	31.7	WB	Dust & Condensates 0-80 km. Radiative Balance
8	190-240	46.5	WB	
9	3,333-33,333	0.55	WB	

(1) PMR denotes a radiometer channel which uses a pressure modulator cell containing the specified gas. WB denotes a wideband or filter channel.

Limb sounding techniques are employed by PMIRR to obtain 5 km vertical resolution profiles of the atmosphere with enhanced sensitivity to atmospheric constituents, independent of atmospheric temperature gradients. Aerosol extinction profiles are determined in all eight of the PMIRR thermal infrared spectral channels from 7 to 50 μm together with temperature profiles with the same spatial resolution. The channels at 12 and 21 μm are chosen for their high sensitivity to small amounts of dust and H_2O ice. The

channel at 32 μm is located in a spectral interval that is influenced little by gaseous absorption, and the ratio of the radiance at 32 μm to that at 7 μm is relatively insensitive to the particle size and composition (dust and/or ice). The 32 μm channel is, therefore, a good reference for total opacity due to airborne particulates.

Given the vertical profile of temperature as a function of pressure, profiles of dust and condensate extinction coefficients can be derived from the measurements of atmospheric thermal emission made in each of the PMIRR infrared channels. Two processes contribute to the emitted radiance: thermal emission by gas and dust, and scattering by dust. Primary scattering of upwelling radiation from the surface dominates the scattering source function since the single scattering albedo is low and multiple scattering is negligible at these wavelengths. Our approach to modelling the effects of primary scattering, and emission and extinction by dust and gas, is to use a modified Emissivity Growth Approximation technique. This has been used successfully to retrieve profiles of sulfuric acid aerosol mass loading in the terrestrial stratosphere from Solar Mesospheric Explorer limb radiance measurements. The multispectral extinction data is used to distinguish between dust and condensate aerosols and to estimate particle size.

The independent retrieval of temperature profiles in the presence of dust is essential to this approach, and is made possible by the use of the PMIRR CO_2 pressure modulator temperature sounding channels. The contrast in CO_2 optical depth in the atmospheric path for the wideband and pressure modulated signal components of these channels allows thermal emission from aerosols and CO_2 to be differentiated.

Figures 1a, b and c show the results of simulated retrievals of temperature and dust using PMIRR. The vertical optical depth of dust at visible wavelengths τ_{vis} for each profile is shown in the figures. The figures compare individual profiles composed of dust models and temperature profiles measured by the Viking I and II Landers during entry and the Viking Orbiter radio science experiment with corresponding dust and temperature profiles retrieved by PMIRR. Individual vertical profiles of dust extinction coefficient were retrieved at 7.6 μm and scaled to visible wavelengths.

PMIRR can obtain aerosol extinction profiles at all levels in the atmosphere from the surface to 80 km in all its infrared channels for most of the Martian year. During the dustiest periods of the great dust storms, extinction profiles at the longer wavelengths are still obtained, but accurate results at shorter wavelengths are only available above 10 km. Only during the great dust storms, when nadir opacities at visible wavelengths are well in excess of 2.0, are limb sounding results limited to a lower boundary of 15-20 km. At these times, however, the nadir sounding measurements, which form part of the nominal PMIRR scan pattern, will still provide low vertical resolution (10 km) measurements of temperature and estimates of aerosol opacity at the lowest levels.

The research described in this paper was performed by the Jet Propulsion Laboratory, California Institute of Technology, under contract with the National Aeronautics and Space Administration.

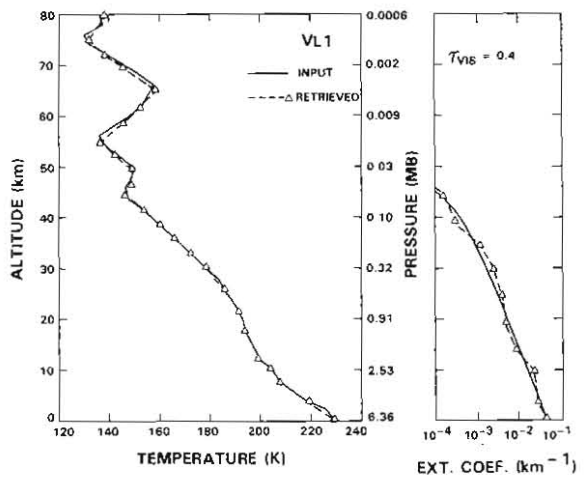

1(a) Profiles at Viking Lander 1

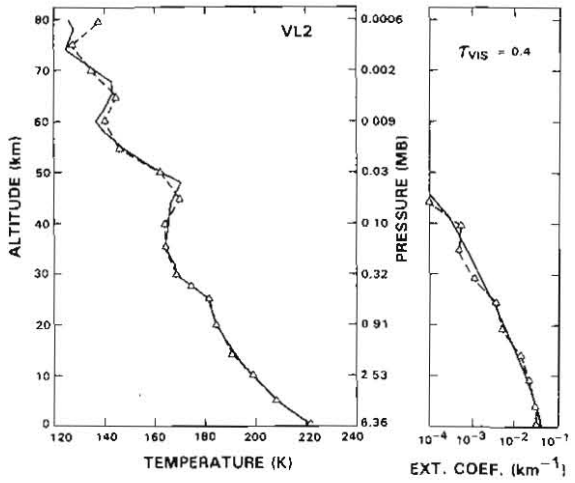

1(b) Profiles at Viking Lander 2

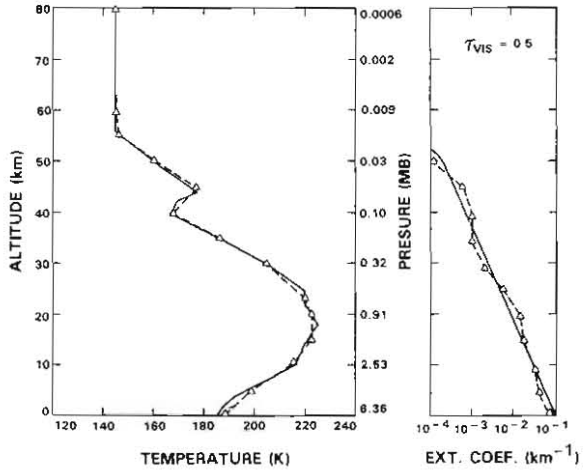

1(c) Profiles from Viking Radio Science Experiment

Figure 1. Retrieved Temperature and Airborne Dust Profiles

MARTIAN MINIATURE SLOPE FAILURES, MUTCH MEMORIAL STATION

Henry J. Moore, U.S. Geological Survey, Menlo Park, CA., 94025

Two slope failures occurred at the Mutch Memorial Station (Lander 1) about 8 and 25 m from the lander [1,2,3]; the failures are about 0.15 and 0.20m wide. There are several questions in regard to the slope failures. (1) What are the geometrical relations between the failed units of the materials and the local topography? (2) Do the slope failures correlate with seasonal changes or other processes? (3) What are the mechanical properties of the materials that failed? (4) What are the origins of the materials that failed? (5) Why did the materials fail? (6) Do the materials correspond to any materials sampled or tested by the lander?

The slope failure 25 m away is too distant for adequate description, much less measurement. The timing of the failure is well constrained by images to sometime between Sols 767 and 771. These Sols correspond to the beginning of the last quarter of the second summer (L_s 147°-150°) witnessed by the lander. At this time, atmospheric pressures attain a seasonal low of slightly less than 700 Pa and atmospheric temperatures attain a seasonal high near 250 K. The slope failure 8 m away produced a miniature landslide with three units: a scar, a runout tongue, and a runout mound. The slide was only viewed by camera 1 which precludes stereometric measurements. The relief of the scar is uniform and about 0.01 m; the relief of the runout tongue is 0.01-0.02 m; the relief of the runout mound is 0.04 m. Shadows and viewing conditions suggest that the slope is near 30°, the scar and the runout tongue are about 0.4 m long. The timing of the slide is poorly constrained by images to sometime between midsummer to very early fall (L_s 134°-191°) of the first year witnessed by the lander. For this period, atmospheric pressures reach seasonal lows less than about 720 Pa and atmospheric temperatures reach seasonal highs of about 245 K - 250 K.

The uniform relief of the scarp suggests that a uniformly thick layer of relatively weak material overlies a stronger substrate. This uniform relief also constrains the relation between geometry of the failure surface and the local topography as well as the mode of failure.

For a marginally stable slope, the cohesion of a frictionless material need only be about 18-20 Pa. Internal friction further reduces the cohesion required for stablity. When the angle of internal friction is greater than the slope angle, the slope is stable regardless of the cohesion. If a slope toe is involved, the slope is stable for angles of internal friction greater than about 23° regardless of the cohesion. Thus, the materials of the slope failures must be substantially weaker than in situ, undisturbed materials measured by the sampler in the sample field which have cohesions near 1 kPa or larger [4].

The failures probably occurred in layers formed by the accumulation of reworked dust from major and global dust storms on protected lee slopes downwind of rocks. The accumulations of dust are superposed on drifts.

MARTIAN MINIATURE SLOPE FAILURES

Moore, H. J.

Elsewhere, thin dust deposits from major and global dust storms are easily moved by light winds, and so the cohesions of such deposits must be very small.

The reasons for initiating the slope failures are unclear but may involve factors related to seasonal changes because both failures occurred during the summer. The failures could have been initiated by (1) an increase in thickness of the layers beyond a critical thickness, (2) positive pore pressures generated by desorption of CO_2 gas from warmed surfaces of grains or by humidification, (3) marsquakes, (4) wind stresses, (5) chemical changes that altered the mechanical properties, or (6) some combination of the above factors.

The simplest mechanism that will initiate failure is to allow the layer to thicken until the body forces exceed the surface forces due to cohesion and internal friction when the angle of internal friction is sufficiently small. For simple translational failure (without a slope toe), a layer of a frictionless material with a cohesion of 20 Pa is stable when it is 0.01 m deep, but it is no longer stable when it thickens to 0.011 m.

If the martian materials are similar to nontronite in their CO_2 adsorption properties [5], positive pore pressures of CO_2 gas from warmed surfaces of grains in confined units of the material could initiate slope failure. BET equations [6] fit to published curves for CO_2 adsorption on nontronite at three temperatures [5], empirical correlations of the unimolecular-layer parameters (Vm) and the parameters related to heats of adsorption (C) [6], and footpad 2 temperatures suggest that pore pressures in this confined unit of material could range from (+) 700 Pa to (-) 500 Pa above or below the ambient pressure. Such pressures are large enough to reduce the effective coefficient of friction to zero and disrupt materials with cohesions of several hundred Pa.

Desorption of CO_2 by humidification could develop pore pressures as large as 80 kPa (800 mb) [7], if sufficient amounts of water vapor were made available. Apparently, the introduction of rather modest amounts of water vapor (a few micrograms of H_2O) could displace or desorb enough CO_2 to generate pore pressures of about 1 kPa.

Marsquakes with trivial accelerations could initiate failure if the layers were marginally stable. With increased cohesions and angles of internal friction, the accelerations required to initiate failure increase.

The roles of wind stresses and chemical changes have not been assessed at this time.

Irrespective of how they form, miniature landslides may represent an

important step in the dust cycle on Mars. Miniature landslides and slope failures disrupt the surface materials and produce surface configurations that are no longer in equilibrium with respect to martian winds [3,8].

REFERENCES CITED

[1] Jones, Kenneth L. and others, 1979, One Mars year: Viking lander imaging observations: Science, v. 204, p. 799-805.

[2] Guinness, Edward A., and others, 1982, Two Mars years of surface changes seen at the Viking landing sites: J. Geophys. Res., v. 87, p. 10,051-10,058.

[3] Arvidson, R.E., and others, Three Mars years: Viking Lander I imaging observations: Science, v. 222, p. 463-468.

[4] Moore, H.J., Clow, G.D., and Hutton, R.E., A summary of Viking sampler trench analyses for angles of internal friction and cohesions: J. Geophys. Res., v. 87, p. 10,043-10,050.

[5] Fanale, F.P., and Cannon, W.A., 1979, Mars: CO_2 adsorption and capillary condensation on clays-significance for volatile storage and atmospheric history: J. Geophy. Res., v. 84, p. 8404-8414.

[6] Brunauer, S., and others, 1938, Adsorption of gases in multimolecular layers: J. Amer. Chem. Soc., v.60, p. 309-319.

[7] Huguenin, R., Harris, S., and Carter, R., 1985, Freeze/thaw injection of dust into the martian atmosphere: Lunar and Planetary Science XVI, part 1, p. 376-377.

[8] Moore, H.J., 1985, The martian Dust Storm of Sol 1742: Proceedings of the 16th Lunar and Planetary Sci. Conf., Part 1, J. Geophys. Res., v. 90 (Supplement), p. D163-D174.

SPECTRAL PROPERTIES OF "DUST" PRODUCED IN THE DRY VALLEYS OF ANTARCTICA: A MARTIAN ANALOGUE? Richard V. Morris[1], Howard V. Lauer, Jr.[2], David G. Agresti[3], and Jeffery A. Newcomb[3]. [1]SN4, NASA-JSC, Houston, TX 77058, [2]LEMSCO, Houston, TX 77058, and [3]Dept. of Physics, University of Alabama at Birmingham, Birmingham, AL 35294.

Introduction. The Dry Valleys are a deglaciated set of valleys located in southern Victoria Land, Antarctica. Physical weathering processes dominate there because the low temperatures and paucity of liquid water limit chemical weathering and also participation by biological activity. Chemical weathering does occur [e.g.,1,2], although at very slow rates. Basically, it is characterized by the decomposition of primary silicate minerals into clay minerals and amorphous to crystalline ferric oxides [e.g.,1,2]. The cold, dry climate of the Dry Valleys is probably the best terrestrial approximation to the climate of contemporary Mars [summarized by 3]. It is possible that weathering processes dominant in the Dry Valleys are also active on the martian surface. We are studying the spectral manifestations of weathering in Dry Valley soils as an analogue for interpreting martian spectral data in terms of primary and secondary mineralogies.

Samples and Methods. A large suite of soils was collected in Wright Valley at an air temperature of approximately -6°C in 1979 and kept in cold storage since then [4]. We consider here results for 10 soils; 9 were from a one meter deep soil pit on Prospect Mesa and one was a surface soil (WV481) collected near Don Juan Pond. We warmed aliquots of soil to room temperature where they had a loose consistency and did not appear wet. Each soil was then dry sieved to pass 1 mm. A portion of the <1 mm soil was then washed with H_2O to remove soluble salts and sieved at 45 um to give two size fractions. Spectral data were acquired at room temperature with a Cary 14 configured with an integrating sphere. Some Mossbauer spectra were also obtained with an Elscint spectrometer.

Results and Discussion. For the H_2O-washed samples from the soil pit, the mass fraction of <1 mm soil in the <45 um size fraction is approximately 21% for the 7 soils collected above the boundary of the permanently frozen zone (40 cm) and approximately 10% for the three soils below it. We attribute this difference to the action of the freeze-thaw cycle. For WV481, the corresponding figure is 67%.

The spectral data for WV222, the uppermost soil (0-1 cm) from the soil pit, are shown in Figure 1 for both H_2O-washed and not washed <1 mm size fractions. The minimum near 0.95 um and the suggestion of a broad band at longer wavelengths are consistent with pyroxene and probably are due to the clinopyroxene observed petrographically in the soil-pit soils [3]; this is consistent with their Mossbauer spectra which show mostly ferrous iron. The feature near 0.45 um is probably due to ferric iron. Although the features due to iron are the same in both washed and not washed samples, the features due to H_2O are not. For the H_2O-washed sample, the minima are at approximately 1.40 and 1.90 um. For the other sample, the features are more complex and and have minima near 1.45 and 1.95 um and strong inflections corresponding to unresolved bands at 1.40 and 1.90 um. This suggests that the unwashed sample contains a water-soluble and H_2O-bearing phase that is not present in the H_2O-washed sample. Although other possibilities exist, a water-soluble material that has H_2O bands in the right place [5] and has been identified petrographically and by SEM analysis in the unwashed soils [3] is

gypsum ($CaSO_4.2H_2O$). The intensity of the 1.45 and 1.95 um features decreases from the surface, and they are not evident in spectra of soils from deeper than approximately 40 cm in the permanently frozen zone.

In Figure 2 we plot the spectra of three soils; WV222 and WV481 are surface soils and WV214 was collected approximately 57 cm beneath WV222 in the permanently frozen zone. The absorption edge moves to longer wavelengths in the order WV214<WV222<WV481 suggesting increasing amounts of ferric iron in that order. This is consistent with preliminary Mossbauer results that indicate that the area ratio of ferric to ferrous doublets increases in the same order. For the soil pit samples, these results show that differential weathering has occurred between the surface and the permanently frozed zone with the surface slightly more oxidized (weathered) Presumably, all three spectra represent a sequence in which the progressively longward shifts in the absorption edge are due to increasingly larger amounts of weathering-induced oxidation of ferrous to ferric iron. Note that the band near 0.95 um for WV214 and WV222 is a composite band centered near 0.91 um for WV481. Presumably, this additional structure is due to the ferric weathering product which for WV481 is optically thick enough in this spectral region. A band for many ferric oxides and oxyhydroxides typically occurs between 0.85 and 1.0 um [6].

What are the implications for the interpretation of martian spectral data? (1) The position of the absorption edge for spectral data of the martian bright regions [e.g.,8] is longward of that for WV481, which indicates more highly oxidized material on Mars, assuming analogous weathering processes. Age estimates for the Antarctic soils are needed to determine the rate of weathering there and , after appropriate scaling, estimate the rate of similar weathering expected on Mars. Antarctic-style weathering on Mars can then be measured against competing processes. (2) By analogy with the WV481, the 0.87 band in the martian spectra is associated with a ferric weathering product, possibly a hematite-like phase.

References. [1] Ugolini and Jackson, Ant Geo, 1101, 1982; [2] Bockheim, Soil Sci 128, 142, 1979; [3] Gibson et al., Pl3LSC, A912, 1983; [4] Gibson, pers comm, 1986; [5] Hunt et al., Mod Geo 3, 1, 1971; [6] Morris et al., JGR 90, 3126, 1985.

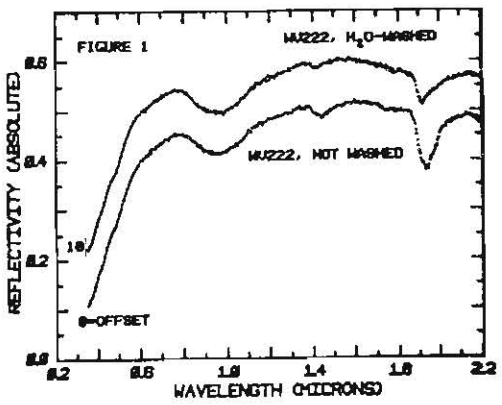

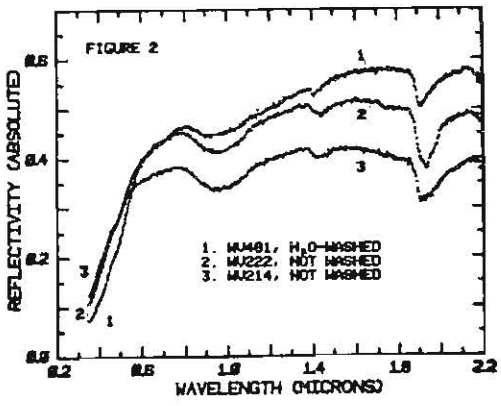

DUST IN THE SPRING SEASON POLAR ATMOSPHERES: A NORTH-SOUTH COMPARISON; D. A. Paige†, California Institute of Technology, Jet Propulsion Laboratory, Pasadena, CA 91109

The Viking IRTM observations provide a great deal of information concerning the behavior of dust in the Martian polar regions during the spring seasons. Surface temperatures remain fixed at low temperatures due to the presence of CO_2 frost, while the dusty polar atmospheres are heated by the sun throughout the day. Large temperature contrasts between surface and atmosphere during spring cause brightness temperatures in the IRTM infrared channels to be highly sensitive to changes in dust opacity with temperature within the atmospheric column. Although the absence of simultaneous independently derived atmospheric temperature profiles and dust optical properties makes it impossible to "invert" the IRTM observations to obtain unique dust opacity profiles, the IRTM 15μ atmospheric temperature channel data provide enough additional information to constrain the suite of possible interpretations of these observations to a manageable level. Although qualititive in nature, the results of this type of work may eventually provide insights into the dynamical processes that bring dust into the martian polar regions each year.

Figures 1 and 2 show the IRTM brightness temperature observations of the near-polar north and south study regions[1] in condensed form. The data have been separated into low emission angle observations ($\theta \leq 60°$), and high emission angle observations ($\theta > 60°$). During spring, all the measured brightness temperatures in the north and south are significantly higher than ~145K, the expected temperature of surface CO_2 frost deposits. Radio occultation profiles[2] and the IRTM T_{15} observations indicate strong temperature inversions over both polar caps during spring. T_7 , T_9 , T_{11} and T_{20} are higher than surface CO_2 frost temperatures during this season due to of the presence of aerosols (dust and/or water ice) in the warm polar atmospheres.

A one-dimensional atmospheric radiative-dynamic equilibrium model was used to interpret the IRTM polar spring observations[3]. The model includes the effects of anisotropic-nonconservative scattering by atmsopheric aerosols and absorption by CO_2 gas at solar wavelengths, and anisotropic-nonconservative scattering and emission by atmospheric aerosols at infrared wavelengths, emission and absorption by CO_2 in the strong 15μ band, heat conduction between surface and atmosphere and atmospheric heating due to dynamical motions. For a given set of atmospheric and surface properties, the model calculates atmospheric thermal equilibrium temperature profiles and IRTM brightness temperatures at the top of the atmosphere in a self-consistent manner.

The model results show that most of the major features of the IRTM spring season observations of the north and south can be simulated by assuming Toon-Pollack dust optical properties[4,5], and small amounts of of dynamic heating in the lower atmosphere. The dominance of atmospheric solar heating over atmospheric dynamic heating during spring is also clear from the data alone, which show increasing brightness temperatures with decreasing solar zenith angles. Pure water ice clouds can not explain the IRTM observations in the north because water ice particles do not absorb enough solar energy to heat the atmosphere to the observed temperatures. The observed values of T_9 in the north and south are diagnostic of the dominant influence of atmospheric dust on infrared cooling rates as well. The effects of rapid increases in dust opacity during the first and second great dust storms of 1977 are quite apparent in the south polar data. There was a similar,

but less intense dust injection event at the north pole at L_s 29.8 which was probably due to local dust storm activity at the edge of the retreating polar cap.

The most challenging aspect of these observations to model were the measured values of T_{15} at low emission angles relative to the brightness temperatures in the surface sensing channels. Model results predict that T_{15} should be considerably higher than the other brightness temperatures for Toon-Pollack dust uniformly distributed with pressure. Extensive fiddling with the input parameters revealed that if the dust in the south was confined to the lowest 5km of the atmosphere, then a better agreement between model brightness temperatures and the observations could be achieved. In the north, the low T_{15} problem is even more serious, and even more fiddling was required to fit the observations. A satisfactory fit was finally achieved by not only confining the dust to the lowest 5km, but suspending all atmospheric dynamic heating above 5km and doubling the assumed ratios of dust optical depths at infrared wavelengths to those at solar wavelengths. The observations in the north could also be matched without radically altering the canonical dust optical properties by assuming the atmosphere above 10km was cooled by dynamic motions rather than heated. Upper atmospheric cooling could also be achieved in the north by the addition of water ice clouds, which do not heat the atmosphere at solar wavelengths, but cool the atmosphere in the infrared. This last effect is the most likely explanation for the low upper atmospheric temperatues.

Calculated values of T_{20} relative to the other brightness temperatures could be made to better agree with the observations in both the north and the south if basalt infrared optical properties were assumed for $\lambda > 20\mu$. This adjustment is in accordance with the fits to the IRIS data in original paper by Toon et al. and with the results of Hunt[6] and Kahn[7] using IRTM data.

The results of this study have confirmed much of what has been learned about dust optical properties at lower latitudes and have provided some new, but somewhat ambiguous information concerning the behavior of dust in the martian polar regions during spring. The principal conclusions are:

1. Dust in the north and south polar atmospheres is similar in composition and to that observed at lower latitudes.
2. Dust in the north polar atmosphere during spring is confined to the lowest atmospheric scale height.
3. Low upper atmospheric temperatures in the north during spring are most likely caused by the presence of high altitude water ice clouds.

REFERENCES

1. Paige, D. A. and A. P. Ingersoll, *Science* **228**, 1160 (1985).
2. Lindal, G. F. et al., *J. Geophys. Res.* **84**, 8443 (1979)
3. Paige, D. A., Ph.D. Thesis, California Institute of Technology (1985).
4. Toon, O. B., J. B. Pollack and C. Sagan, *Icarus* **30**, 663 (1977).
5. Pollack, J. B. et al. *J. Geophys. Res.* **84**, 2929 (1979).
6. Hunt, G. E., *ibid,* p. 2865.
7. Kahn, R., Ph.D. Thesis, Harvard University (1980)

† National Research Council Resident Research Associate

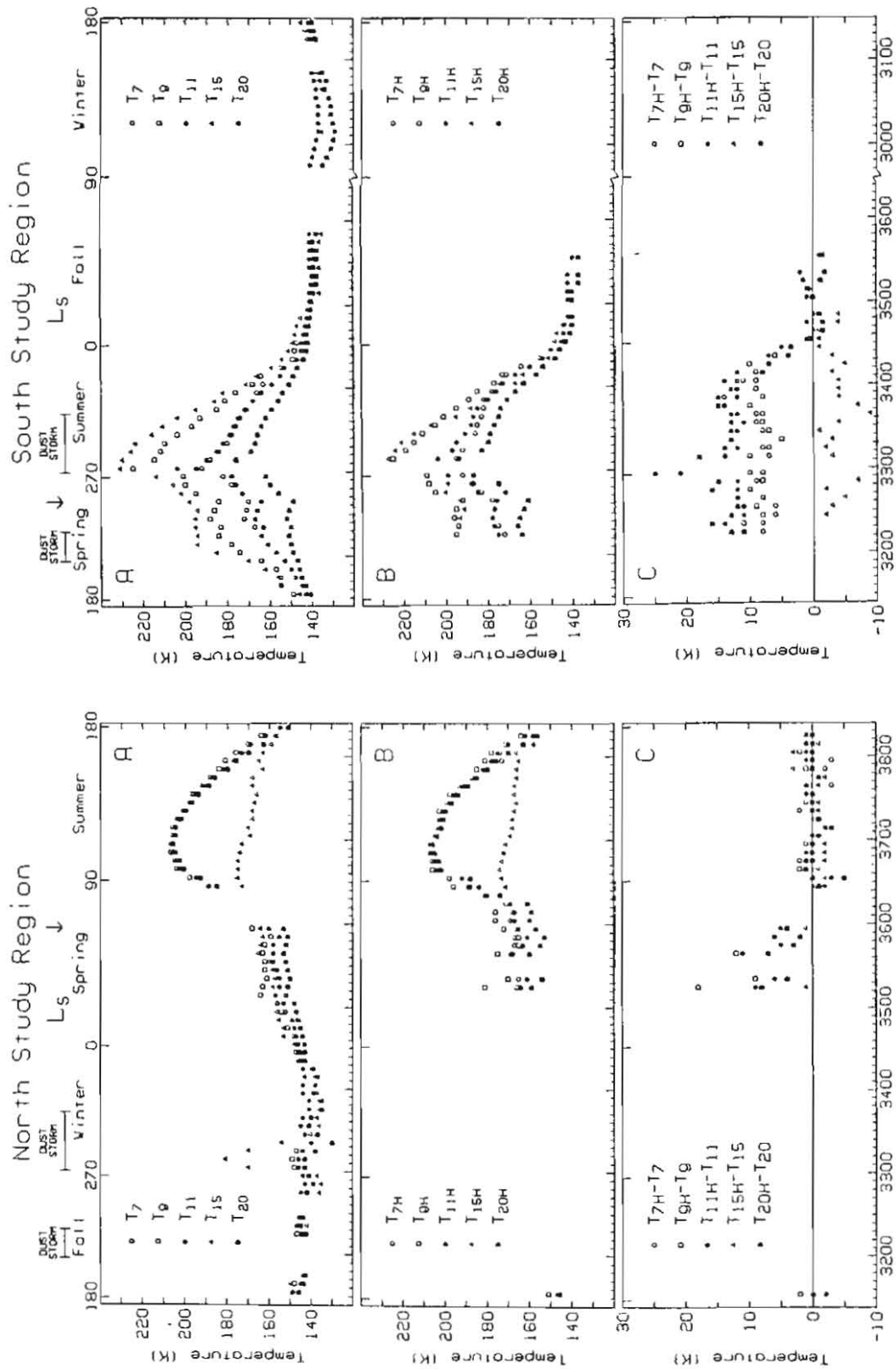

Figs. 1 and 2. 10-day averaged IRTM north and south study region[1] brightness temperatures. (A) T_7, T_9, T_{11}, T_{15} and T_{20} for emission angles $\theta \leq 60°$. (B) T_{7H}, T_{9H}, T_{11H}, T_{15H} and T_{20H} for emission angles $\theta > 60°$. (C) Differences between the 10-day averaged IRTM brightness temperatures for $\theta > 60°$ and $\theta \leq 60°$.

INFLUENCE OF DUST ON THE GENERAL CIRCULATION OF THE MARTIAN ATMOSPHERE: J. B. Pollack, R. M. Haberle, NASA Ames Research Center, J. Barnes and M. Schlesinger, Oregon State University, R. Zurek, J.P.L., C. B. Leovy, University of Washington, J. White, J. Schaeffer, and K. Bilski, Informatics, Inc.

Measurements conducted from the Viking landers have shown that radiatively significant quantities of fine dust particles are present at all times in the Martian atmosphere (1, 2). In particular, dust optical depths range from several tenths during the summer season in the northern hemisphere to several at times of global dust storms(1). In order to investigate the influence of dust on various components of the atmospheric circulation, we have initiated a series of numerical experiments with a general circulation model (GCM).

The MARS GCM is a version of a model developed at UCLA for the Earth's atmosphere that has been adapted to Mars (3). Hence, it allows for the condensation of carbon dioxide in the winter polar regions, for example. We have previously used it to assess the influence of topography on the circulation for dust free conditions (3). Thus, a sigma coordinate system was employed.

We have made a number of improvements and modifications to the above version of the Mars GCM so that it could be used to study the influence of dust on the circulation. First, the model is now capable of having a large number of vertical layers, in contrast to the 3 vertical layers used in the earlier simulations. Such a capability is needed both because dust is mixed to high altitudes and because a resolution of one half a scale height or better is needed to adequately resolve thermal tides. In our present simulations, we use 6 vertical layers that extend from the surface to about an altitude of 40 km.

A second improvement to the GCM has involved incorporating the radiative effects of dust in the heating algorithms. In the case of solar radiation, we have used radiation properties of the dust derived from relevant Viking and Mariner 9 data (1, 4) to define the optical and microphysical properties of the dust and have carried out a series of multiple scattering calculations with an adding/doubling program. The results from these calculations are incorporated into a look-up table that defines the net solar flux as a function of altitude. In a similar way, we have used a delta-Eddington code to define an effective emissivity for dust in two broad spectral regions of the thermal infrared: inside and outside the spectral domain of the 15 micron band of carbon dioxide.

Finally, we have improved algorithms used to treat subgrid scale turbulence within the free-atmosphere due to shear instabilities and subgrid scale turbulence within the planetary boundary layer.

The numerical experiments consisted of defining a temporally constant, ubiquitous dust loading of the atmosphere and running the model for a long enough time to define a statistically, steady-state circulation. The dust mixing ratio is assumed to be independent of altitude in the troposphere.

The present simulations were conducted at summer solstice in the southern hemisphere for globally averaged dust optical depths of 0 and 1. Thus, they are directed at assessing the magnitude of the enhancement of the atmospheric circulation caused by dust just before the start of global dust storms at this season.

In accord with previous studies (2, 5, 6) the radiative effects of dust lead to a significant strengthening of the Hadley circulation and thermal tides, and to a weakening of baroclinic eddies. Furthermore, the static stability in the summer hemisphere increased, the latitudinal temperature gradient at midlatitudes of the winter hemisphere increased, and the strong jet in the winter hemisphere strengthened and shifted poleward in the dust simulations as compared to the dust-free simulations. In both simulations, there are strong winds near the surface at subtropical latitudes of the summer hemisphere and beneath the winter jet.

References:

(1) Pollack, J. B., D. S. Colburn, F. M. Flasar, R. Kahn, C. E. Carlston, and D. Pidek (1979). Properties and effects of dust suspended in the Martian atmosphere. J. Geophys. Res. 84, 2929.
(2) Zurek, R. and C. B. Leovy (1981). Thermal tides in the dusty Martian atmosphere: a verification of theory. Science 213, 437.
(3) Pollack, J. B., C. B. Leovy, P. W. Greiman, and Y. Mintz (1981). A Martian general circulation experiment with large topography. J. Atmos. Sci. 38, 3.
(4) Toon, O. B., J. B. Pollack, and C. Sagan (1977). Physical properties of the particles composing the Martian dust storm of 1971-72. Icarus 30, 663.
(5) Haberle, R. M., C. B. Leovy, and J. B. Pollack (1982). Some effects of global dust storms on the atmospheric circulation of Mars. Icarus 50, 322.
(6) J. R. Barnes (1984). Linear baroclinic instability in the Martian atmosphere. J. Atmos. Sci 41.

RADAR REFLECTIVITY OF A VARIABLE DUST COVER, L.E. Roth, R.S. Saunders, and T.W. Thompson, Jet Propulsion Laboratory, California Institute of Technology, Pasadena, California 91109.

This study represents an attempt at finding an answer to the following questions: What are the surface characteristics that are required for radar, a remote sensing instrument operating in the 1cm (K_a-band) to 30cm (L-band) wavelength range, to detect the temporal and spatial fluctuations in the depth of a dust cover assumed to envelop a planetary surface? What is the minimum detectable fluctuation? Can the areal extent of the cover be determined and its changes detected? What is the optimum wavelength to be used in a radar experiment designed to monitor the eolian regime over a given surface segment? The original motivation for the study came from the effort to formulate an alternate interpretation of the apparent seasonal reflectivity variations noted in the Goldstone Mars radar data (1,2,3). The results are applicable to any vegetation-free geologic surface that satisfies conditions (a) through (e) given below.

Central to this work was modeling of reflectivities associated with configurations that consisted of stacks of layers resting on a dielectric half-space. The formalism developed for that purpose is a multi-layer extension, based on (4,5), of the one-layer-atop-a-half-space model considered in the early lunar radar work (6) and treated in detail in literature (e.g., 7). The multi-layer models are equally suited for investigating the eolian activity at the top of the stack (variable: d_1, the depth of the top layer) (Figs. 1,2,3) and the hypothetical thawing of the water-ice at the bottom (variable: ε_1, the dielectric constant of the half-space). Due to the large number of free parameters in multi-layer models (see the caption of Fig. 2), the interpretation of the calculated reflectivities is ambiguous. The multi-layer models, however, are the only available approximation to an analytically untractable configuration consisting of a variable-depth layer resting on a variable-permittivity half-space (8,9,10).

Conclusions: (a) Subtle changes in the depth of a dust layer resting atop a planetary surface are, in principle, detectable if the geometry admits validity of the one-layer-atop-a-half-space model. (b) The free-space/layer and layer/half-space interfaces have to be planar on the scale of the (foreshortened) wavelength in the layer. (c) The dielectric constants of both the layer and the half-space should be isotropic, i.e., the magnitudes of both constants should be independent of the location in the medium. (d) The magnitude of the dielectric constant of the layer has to be close to the geometric mean of the dielectric constants of the free space and the half-space. (e) Reflectivity is insensitive to variations in depth if the magnitudes of those variations are close to even multiples of the quarter-wavelength in the layer; it is most sensitive to variations that are close to the odd multiples. (f) A static eolian cover is indistinguishable from a bare half-space. (g) At S-band, the minimum detectable change in depth of a dust layer is about 0.05cm to 0.10cm; at X-band it is about 0.01cm. (h) In the case of the Goldstone Solar System Radar, the observations aimed at detecting eolian activity on Mars have to be conducted both at S- and X-bands. Addition of the K-band capability would be beneficial. Longer-wavelength radars are less useful for the stated purpose. (i) The predictions of the layered-models theory have not been experimentally verified.

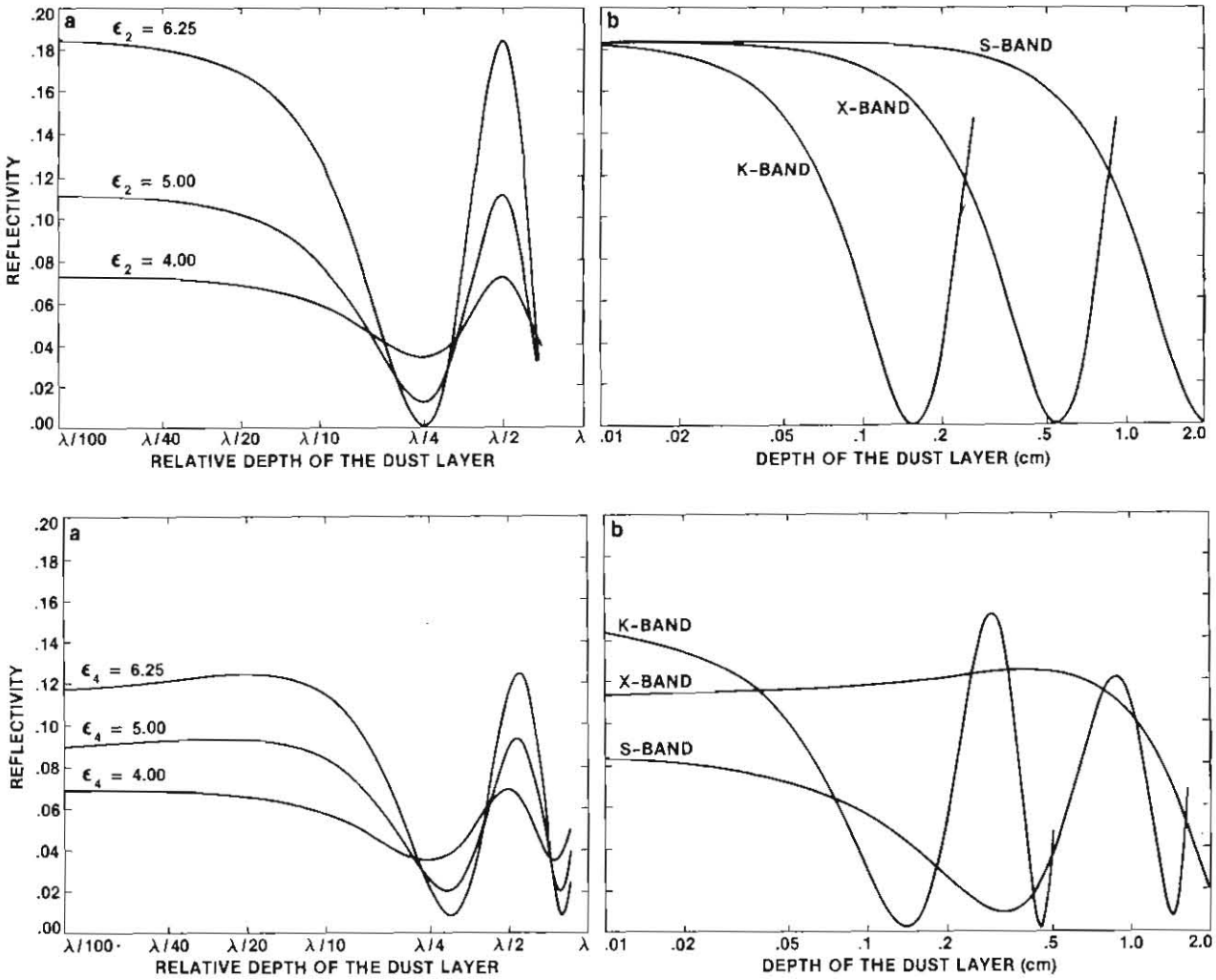

Fig. 1. (a) Reflectivity of a one-layer-atop-a-half-space configuration vs. depth of the layer relative to the wavelength in the layer, λ, for three different values of the dielectric constant of the half-space, ϵ_2; dielectric constant of the layer ϵ_1=2.50. (b) Reflectivity of the same configuration vs. depth of the layer, d_1, for three different wavelengths; ϵ_1 the same as in (a); ϵ_2=6.25.

Fig. 2. (a) Reflectivity of a three-layers-atop-a-half-space configuration vs. depth of the top layer relative to the wavelength in that layer, λ, for three different values of the dielectric constant of the half-space, ϵ_4; dielectric constants and depths of the intermediate layers ϵ_2=3.00, ϵ_3=3.50, d_2=5.00 cm, d_3=5.00 cm. (b) Reflectivity of the same configuration vs. depth of the layer, d_1, for three different wavelengths; ϵ_1, ϵ_2, ϵ_3, d_2, d_3 the same as in (a); ϵ_4=6.25.

References: (1) Downs, G.S., Reichley, P.E., Green, R.R. (1975) Icarus 26, 273. (2) Zisk, S.H., Mouginis-Mark, P.J. (1980) Nature 288,735. (3) Roth, L.E., Saunders, R.S., Schubert, G. (1985) Lunar and Planetary Science XVI, 712. (4) Kong, J.A. (1975) Theory of electromagnetic waves, Wiley. (5) Ulaby, F.T., Moore, R.K., Fung, A.K. (1981) Microwave remote sensing, Vol. 1, Addison-Wesley. (6) Hagfors, T. (1970), Radio Sci. 5,189. (7) Born, M., Wolf, E. (1970) Optics, 4th Ed., Pergamon. (8) Evans, D.D. (1973) Radio Sci. 8,1083. (9) Engheta, N., Papas, C.H. (1983) Appl. Phys. B 30,183. (10) Lincoln Laboratory (1967) Radar studies of the moon, Final Report, no # given.

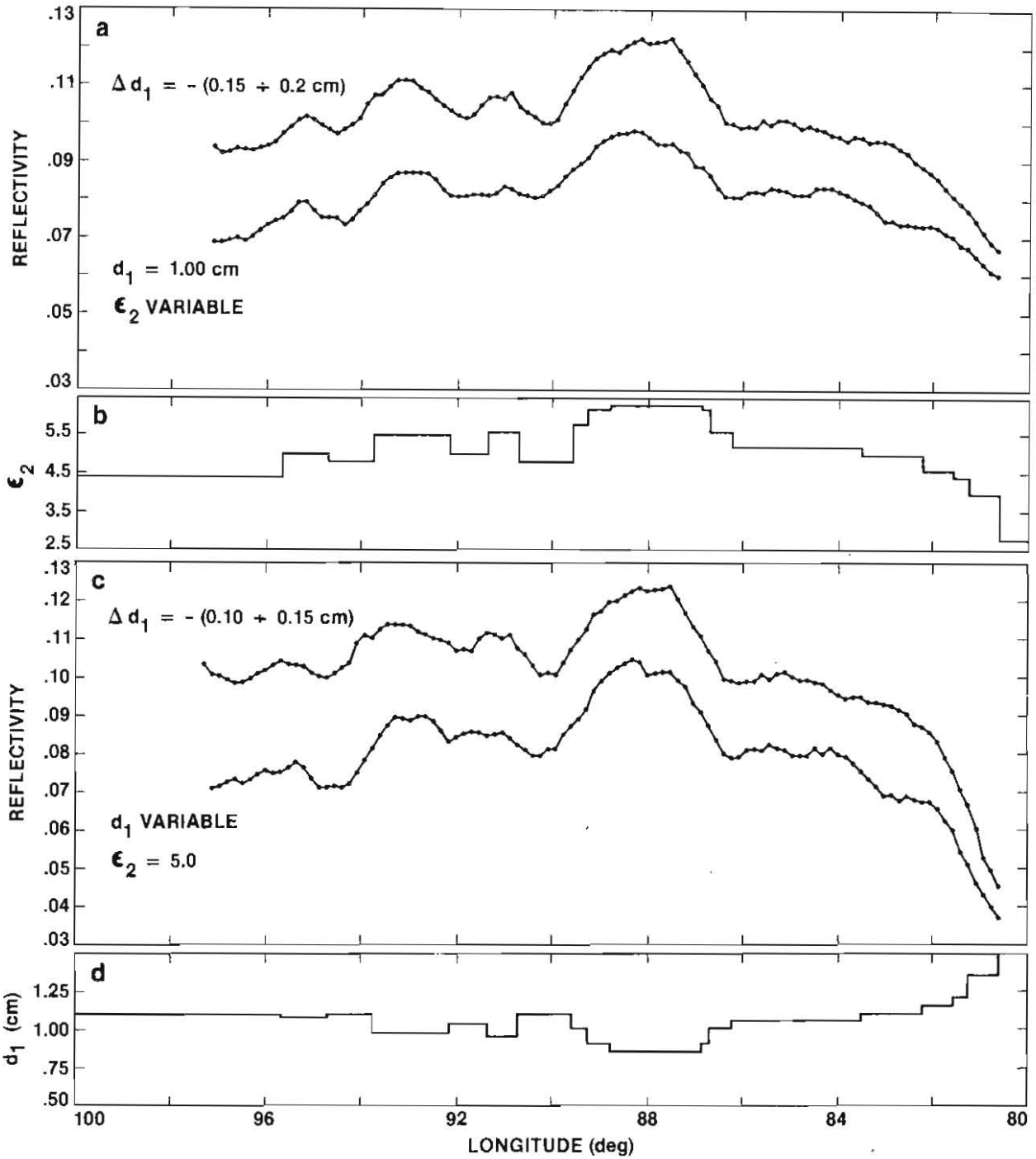

Fig. 3. Simulated reflectivity vs. longitude, of the Goldstone Mars scans #41 (6 Oct 73, -15.94° lat., $L_s=295.59^{\circ}$) and #42 (24 Sept 71, -15.93°, $L_s=260.81^{\circ}$). Calculated reflectivities randomized in the gaussian sense, then smoothed via running averages; bins of 7. (a) Lower line: Reflectivity of the configuration consisting of a variable dielectric-constant, ε_2, half-space (see (b)) coated with a uniform layer of dust, d_1=1.00 cm; ε_1=2.60. Upper line: Reflectivity of the same configuration after removal of 0.15 to 0.20 cm of dust. (b) Assumed dielectric profile in the source area of the data. Dielectric constants ε_2 range from 2.80 to 6.30. (c) Lower line: Reflectivity of the configuration consisting of a constant dielectric-constant half-space, ε_2=5.00, coated with a nonuniform layer of dust (see (d)). Upper line: Reflectivity of the same configuration after removal of 0.10 to 0.15 cm of dust. (d) Assumed nonuniform dust cover in the source area of the data. Depths d_1 range from 0.85 to 1.50 cm.

THE MARS ATMOSPHERE SPECTROMETER FOR MARS OBSERVER; D.W. Rusch, B.M. Jakosky, R.T. Clancy, C.A. Barth, A.I.F. Stewart, G.M. Lawrence, and W.E. McClintock, Laboratory for Atmospheric and Space Physics, University of Colorado, Boulder, CO., and L.J. Paxton, Naval Research Laboratory, Washington, DC.

The Mars Atmosphere Spectrometer Experiment (MASE), proposed for the Mars Observer (MO) Mission, is a scanning spectrometer with channels in the ultraviolet, visible, and near-infrared region of the spectrum. Its principal objectives are to provide vertical profiles of ozone and aerosol abundances in the Mars atmosphere as a function of time and place. Aerosol composition and scattering properties will also be measured. The MASE has 10 channels which measure Rayleigh scattering in the ultraviolet from 250 nm to 322 nm, 4 channels to measure visible radiation from 330 nm to 550 nm, and 2 channels in the near-infrared at 1.23 and 1.27 μm.

The UV channels will measure ozone by its absorption of radiation in the Hartley continuum. The visible light channels will be used to define the properties of airborne dust scattering. The IR channel at 1.27 μm measures the photolysis rate of ozone and the 1.23 μm channel the background dust properties in the IR.

The MASE will scan the atmosphere of Mars in the plane of the orbit using a scanning mechanism that articulates the field of view from above one limb of the planet, through the nadir, and off the opposite limb, thus giving information on the planet's limb and on the surface at a variety of scattering angles.

Dust plays an important role in the radiative balance and dynamics of the atmosphere. The MASE will provide information on the radiative prop-

erties of the dust by measuring the wavelength dependence of its absorption properties and its angular scattering function. The dust content of the atmosphere will be determined as a function of time, latitude, and altitude. The MASE will also obtain vertical profiles of atmospheric condensate which can be used to constrain the vertical mixing rate in the atmosphere.

The atmospheric opacity due to air-borne dust is probably always greater than the Rayleigh scattering opacity at visible wavelengths. The dust is both highly absorbing and forward scattering. The wavelength dependence of the dust scattering function (phase function x single-scatter albedo) will be measured from the UV into the IR.

In terms of the transport of dust, the relevant physical measurement by MASE is the vertical profile of dust abundance in the atmosphere for each location where data are obtained. Data will be limited to the sunlit portion of the planet but will provide information at up to 12 longitudes each day with a latitude resolution of about 5 deg. Measurements of the distribution of the dust will be used to constrain estimates of the vertical mixing of dust in the atmosphere, the origin and evolution of dust storms of global and near-global scale, any net transport of dust into the polar regions, and the annual redistribution of dust raised from the surface. Profiles of dust obtained by MASE will play a key role in mapping the sources of this dust and its distribution at the onset of the dust storms.

Observations by MASE will also yield information on the wavelength and phase-angle dependence of scattering by dust. These measurements provide information on the particle size distribution of the dust. From the scat-

tering and absorption properties of the dust, we can calculate the amount of sunlight absorbed in the atmosphere. This is important in understanding the radiative balance of the atmosphere and the surface. Application to the polar heat balance is of special interest due to the possible influence of the dust on CO_2 frost condensation and sublimation rates. Application at the start of dust storms will help constrain the efficacy of any radiative feedback in promulgating the effects of the dust storms.

POSSIBLE GOLDSTONE RADAR OBSERVATIONS OF MARS: 1986 AND 1988 OPPOSITIONS

T. W. Thompson, R. F. Jurgens, L. Roth, and L. Robinett,
Jet Propulsion Lab., California Institute of Technology, Pasadena, CA 91109

Mars has been target for earth-based radar observations at the Goldstone and Arecibo Observatories since the late 1960's and early 1971's. Previous observations at Goldstone have occurred in the 1971, 1973, 1978, 1980, and 1982 oppositions. In the next few years, oppositions of Mars occur in 1986, 1988, 1990, 1993, and 1995 as shown in Figure 1. Since radar echo strength is proportional to the inverse fourth power of the Earth-Mars distance, the 1986 and 1988 oppositions are better than the 1990, 1993, and 1995 oppositions. This is illustrated further in Table 1 by the number of days that Mars is less than 0.6 and 0.8 AU.

Earth-based radar observations of Mars over several oppositions extend across the equatorial region from 24° north to 24° south, about 42 percent of the surface. The favorable oppositions of 1986 and 1988 will greatly extend our southern hemisphere coverage as shown in Figure 1. Existing coverage from the 1971 and 1973 oppositions extends from 14° to 22° south. New coverages of 1986 covers 3° to 12° south and 1988 covers 20° to 25° south.

In addition to favorable geometries for the next two oppositions, there has been a substantial upgrade to the Goldstone radar in the last few years. The existing S-band (wavelength = 12.5 cm) radar is being supplemented with an X-band radar (wavelength = 3.5 cm). This may help in the detection of liquid water since the dielectric constant of liquid water changes dramatically between X- and S-band as shown in Figure 2. In addition, the on-site hardware has been upgraded to an all digital radar. One consequence is that the number of range bins will be doubled and range resolution will be halfed. Also, the new observations will have resolutions comparable to that of the proposed Mars Orbiter Radar Altimeter as shown in Figure 3. Goldstone S-band and X-band resolutions are 8 x 80 km and 4 x 40 km, respectively, while the Mars Observer Radar Altimeter will have circular spot sizes of 2 and 20 km diameters at K- and L-band (wavelengths = 0.8 and 30 cm).

In summary, the upcoming 1986 and 1988 Mars oppositions present an excellent opportunity to extend our knowledge of Mars via earth-based radar observations using the Goldstone radar. The planet coverage is south of the equator and will extend from 3° to 25° when combined with the 1971 and 1973 data. The Goldstone radar has been upgraded permitting better resolution than before, and X-band observations will be added to supplement the existing S-band system.

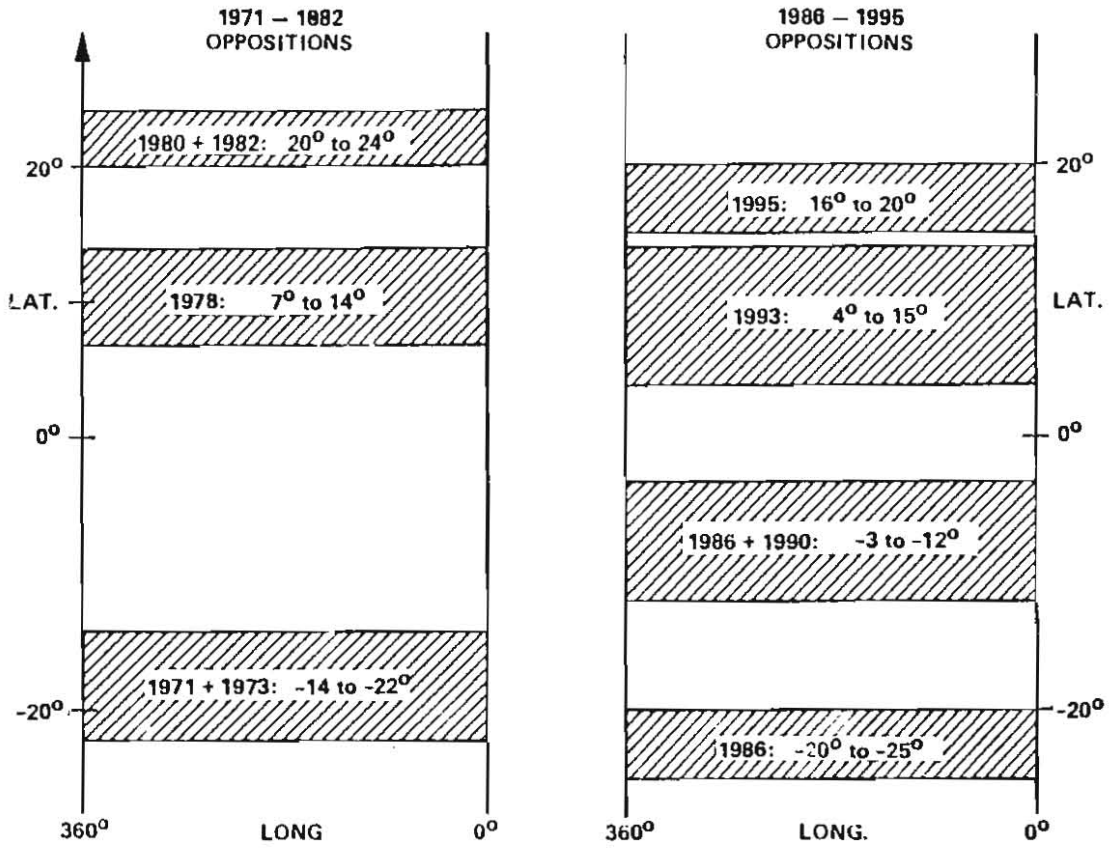

Figure 1. Latitude-Longitude Coverages for Earth-based Radar Observations of Mars (1971-1995).

OPPOSITION	DAYS (0.4-0.6 AU)	DAYS (0.6-0.8 AU)	LATITUDE COVERAGE	DECLINATION
16 JULY 1986 (0.404 AU)	115	63	-3° - -10°	-28°
22 SEPTEMBER 1988 (0.393 AU)	119	63	-20° - -25°	-1°
20 NOVEMBER 1990 (0.517 AU)	64	65	-3° - -13°	+22°
04 JANUARY 1993 (0.626 AU)	0	89	+4° - +12°	+25°
13 FEBRUARY 1995 (0.676 AU)	0	70	+17° - +21°	+18°

Table 1. Summary of Upcoming Mars Oppositions (1986-1995).

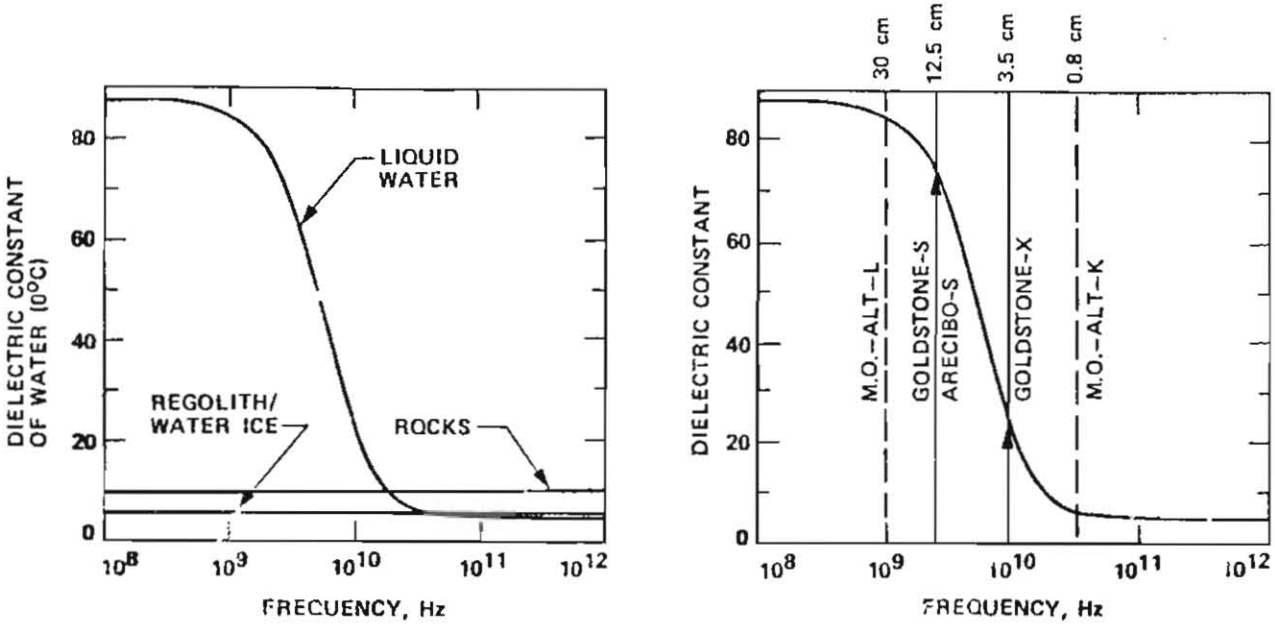

Figure 2. Variation of Dielectric Constant of Liquid Water Versus Frequency.

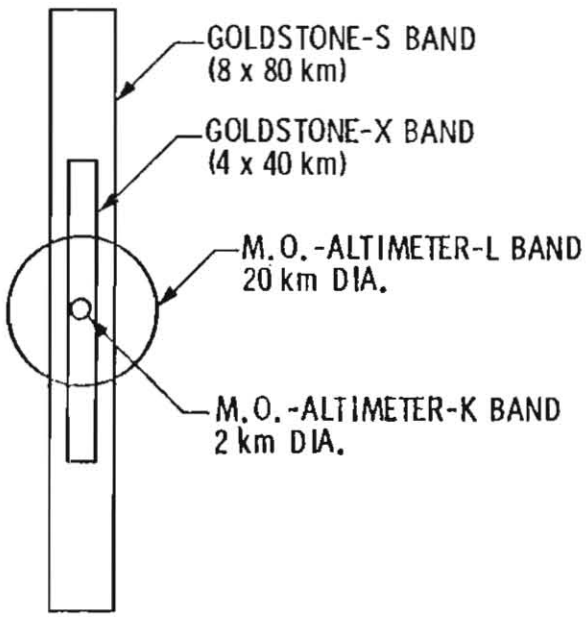

Figure 3. Scales for Earth-based and Mars Orbiter Radar Observations of Mars.

MARTIAN ATMOSPHERIC DUST PROCESSES OVER THREE YEARS AS INFERRED FROM LANDER METEOROLOGY MEASUREMENTS; JAMES E. TILLMAN, Viking Computer Facility, Dept. of Atmos. Sci., AK-40 University of Washington, Seattle, WA 98195

Atmospheric pressure measurements at the Viking 1 Lander site imply at least two different yearly dust storm regimes. In the first year, the moderate "1977 A" storm began about L_s 208 while the more intense "1977 B" storm began about L_s 282. The onset of the A storm was quite rapid with pressure variations doubling within two sols, while the B storm was more intense but built up slowly over seven sols. During the second and third years, no similar global storms were detected by the landers. However, year three had high enough winds to move soil at the lander 1 site (1). During year 4, a large (1.3 mb) transient pressure variation was observed about L_s 204 which decayed prior to a two week communication break (2,3). At the resumption of communications, L_s 217, Lander imaging indicated an intense global storm and pressure measurements suggest that it was in the decaying phase.

Footpad temperature measurements from this period in year 4 indicate that the minimum temperatures were similar to the previous year at this season, a year without global storms, but the afternoon maximum temperatures are significantly reduced. During year 4, the afternoon maximum's remain within 225 to 228 ^{o}K between L_s 217 to 226 while during the previous year they range from 230 to 248 ^{o}K for the same season.

Harmonics of the diurnal variation for both landers, analyzed on a sol by sol basis, will be used to illustrate the year to year variations in global dustiness. Even though there is a major interannual variation in global dustiness, the harmonics and daily average pressures are quite similar between L_s 60 and L_s 120 indicating a similarity of CO_2 in the southern polar cap and regolith which is independent of the presence or absence of global storms in a given year.

References:

(1) Arvidson, R.E., E.A. Guinness, H.J. Moore, J. Tillman and S.D. Wall, 1983, Three Mars Years: Viking Lander 1 Imaging Observations, Science, Vol. 222, 463-468.

(2) Tillman, James E., Martian Meteorology and Dust Storms from Viking Observations, 1985, in Case for Mars II, V 62, Science and Technology, American Astronautical Society, ed. Christopher P. McKay, 333-342.

(3) Leovy, C.B., J.E. Tillman, W.R. Guest and J. Barnes, 1985, Interannual Variability of Martian Weather, in Recent Advances in Planetary Meteorology, ed. Garry E. Hunt, Cambridge Univ. Press, 69-84.

PHYSICAL PROPERTIES OF AEOLIAN FEATURES IN THE ELYSIUM-AMAZONIS REGION OF MARS. James R. Zimbelman, Lunar and Planetary Institute, 3303 NASA Road 1, Houston, Texas, 77058.

Aeolian features are abundant in the Elysium Planitia and Amazonis Planitia regions of Mars. Global maps of the distribution of bright and dark wind streaks [1], yardangs and dune masses [2], and dark splotches within craters [3] show high concentrations of these features within the area of study (30^{o}S to 30^{o}N, 157.5^{o}W to 225^{o}W). Physical properties of wind streaks [4] and dark splotches [5] have been previously described in the context of global studies; this work presents the physical properties of aeolian features as determined from high spatial resolution thermal infrared data.

Wind streaks and dark patches are the most common aeolian features in the Elysium-Amazonis region [6] (Fig. 1). The high resolution data missed the Cerberus streak but the Pettit streak (discussed below) and an unnamed crater with an associated streak (3^{o}N, 198^{o}W, center left margin of Fig. 1) were observed. The upwind interior of the unnamed crater has high thermal inertia (9×10^{-3} cal cm^{-2} $s^{-1/2}$ K^{-1}) and is relatively bright in comparison to the surrounding plains [6]. Several small, bright streaks were crossed along the groundtracks of the thermal data; the bright streaks are most numerous adjacent to and north of the Pettit streak (Fig. 1). These streaks are small enough that they are not actually resolved in the thermal data but they are detected wherever a significant portion of the streak is within the field of view of the instrument. All of the bright streaks detected have an enhanced thermal inertia (+1) relative to that of the surrounding plains. These results suggest that the increased albedo at visual wavelengths is not indicative of the streak surface at the cm scale; the materials in the bright streaks are more compacted/indurated or (more likely) larger in average size than the fine dust covering the plains.

The Pettit wind streak is large enough for both the dark and bright portions of the streak to be resolved in the thermal data [7]. The highest thermal inertias (6-7) correspond to the dark (central) portion of the streak but the bright streak materials have thermal inertias (3-4) higher than the surrounding plains (Fig. 2). The Pettit bright streak results are consistent with the bright streak results discussed above. The streak thermal inertias correspond to effective grain diameters representative of fine and very fine sand (dark and bright streak components, respectively). Spectral differences between the thermal bands of the IRTM allow an assessment to be made of the abundance of high thermal inertia materials ('blocks') within the field of view of the instrument [8]; the Pettit streak shows no difference in block abundance between the streak and the plains. This indicates that the enhanced thermal inertias of the streak are not due to increased exposure of competent material within the streak.

One group of yardangs (Fig. 3) has high thermal inertias (8-10) and high block abundances (15-25%) relative to the surrounding plains. These values are consistent with the erosion of fairly competent materials within the yardangs; the large block abundances suggest that the competent materials are still quite exposed in the yardangs so that erosion of the features could be recent or even ongoing.

References: 1) P. Thomas and J. Veverka, JGR 84, 8131-46, 1979. 2) A.W. Ward, JGR 84, 8147-66, 1979. 3) P. Thomas, Icarus 57, 205-27, 1984. 4) A.R. Peterfreund, Icarus 45, 447-67, 1981. 5) P.R.Christensen, Icarus 56, 496-518, 1983. 6) L.A. Leshin and J.R. Zimbelman, LPS XVII, 1986. 7) J.R. Zimbelman, Icarus, 1986. 8) P.R. Christensen, JGR 87, 9985-98,1982.

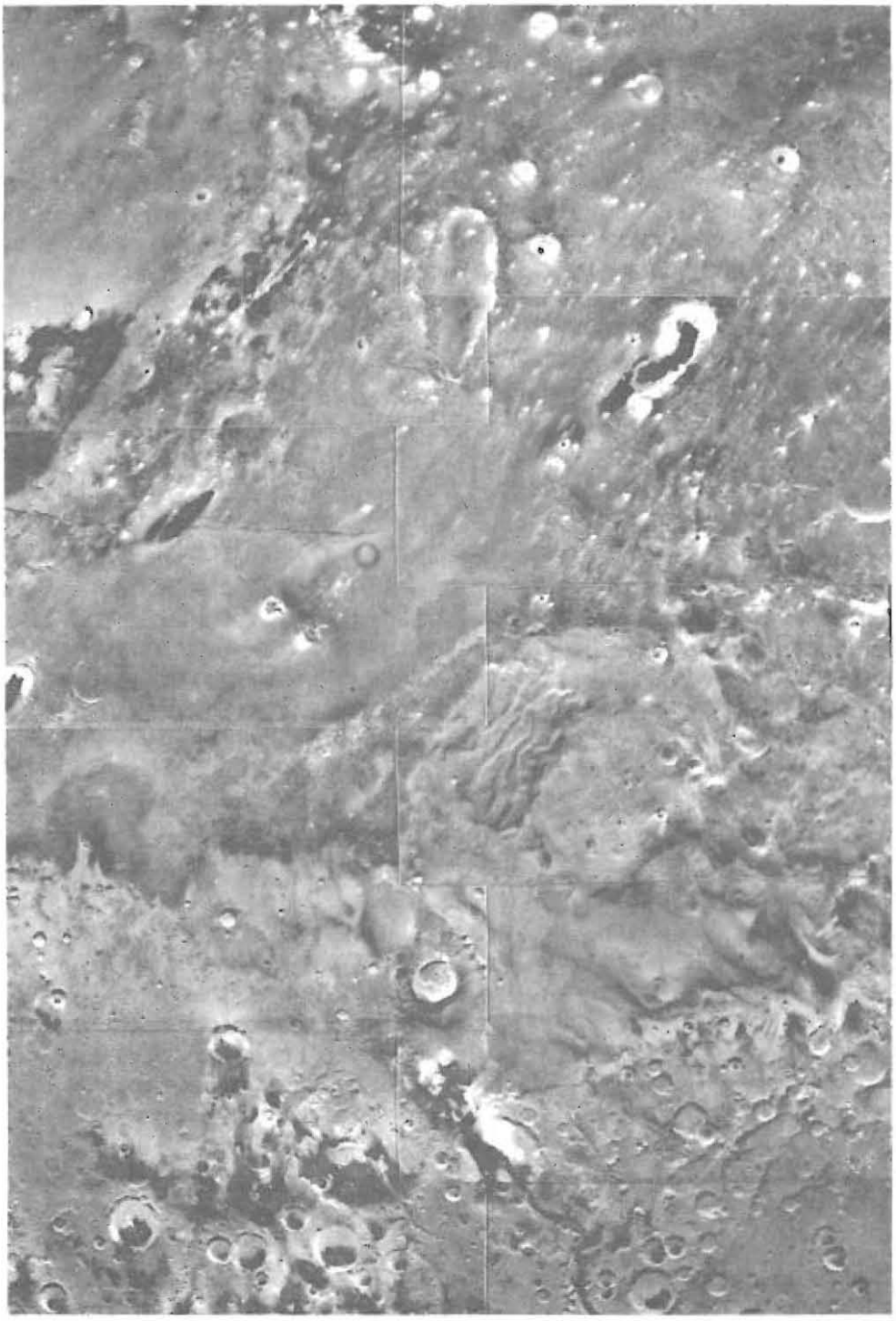

Fig. 1. Low-resolution view of a portion of the Elysium-Amazonis region. The prominent crater-associated dark streaks near the center of the figure are the Cerberus (left) and Pettit (right) streaks. Note the large number of small, bright streaks in the vicinity of Pettit as compared to the area around Cerberus. (323S37-45, width at center is 900 km, area shown covers 15^{o}S to 25^{o}N, 170^{o}W to 200^{o}W).

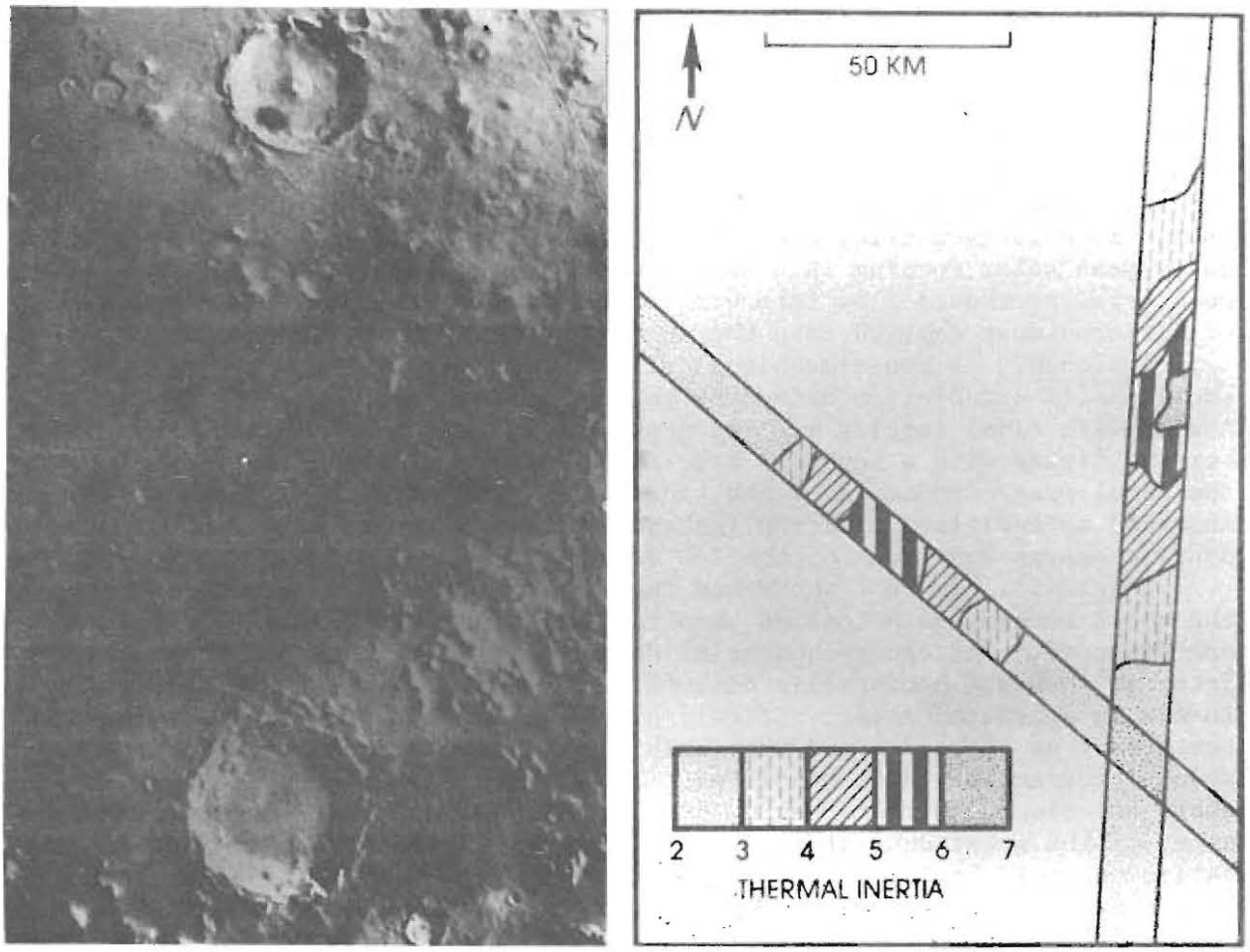

Fig. 2 (top). Thermal inertias of the Pettit streak. Comparison of thermal inertias with visual features (left, 387X08, centered at 11°N, 176°W: right, vertical track, daytime data from orbit B514; diagonal track, nighttime data from orbit A534).

Fig. 3. Yardangs having high thermal inertias (I=8-10) and block abundances (15-25%) as compared to the surrounding plains (I=2.5 and 5% block cover). (886A11, area shown is 140 km across, centered at 12°N, 160°W).

CROSS-EQUATORIAL TRANSPORT DURING A MARTIAN GREAT DUST STORM.
Richard W. Zurek, Jet Propulsion Laboratory, California Institute of Technology, Pasadena, CA 91109, and Robert M. Haberle, NASA/Ames Research Center, Moffett Field, CA 94035.

Introduction. As the opacity of the airborne dust haze increases over low latitudes during a planetary-scale dust storm on Mars, the convergence of the zonal-mean fluxes of heat and momentum due to atmospheric tides may break up the zonally symmetric, cross-equatorial (Hadley) circulation driven by the daily-mean solar forcing in a dusty atmosphere. This break-up of the cross-equatorial northward flow into hemispheric Hadley cells may limit the amount of airborne dust carried into the northern hemisphere.

Approach. A two-dimensional circulation model (1) was used to compute the diabatic circulation driven by the solar heating of a global dust haze. Atmospheric tidal forcing was included in the model by computing the daily varying fields with a separate atmospheric tidal model (2) and then computing the zonal-mean components of the tidal flux-convergences (3). These were inserted as additional forcing functions into the two momentum and the thermodynamic energy equations of the 2-D atmospheric circulation model.

Results. Figure 1 shows how the low-latitude circulation computed by the model becomes more complex when the atmospheric tidal flux-divergences are included. The cross-equatorial Hadley circulation has been nearly split into two separate hemispheric circulations. Since the tidal forcing at these levels is generated almost entirely by the solar heating of the airborne dust, the effect of the tides and the inhibition of the cross-equatorial flow is reduced for smaller dust opacities. These results are computed as steady-state solutions, so that they do not apply to the initial, rapidly evolving onset of the great dust storm. They do suggest that the opacity at northern latitudes would begin to decrease sooner than at sites in the southern hemisphere.

References. (1) Haberle, Leovy and Pollack, Icarus 50, 322, 1982. (2) Zurek, Icarus 45, 202, 1981. (3) Zurek, to appear in J. Atmos. Sci., 1986.

The research described here was performed in part by the Jet Propulsion Laboratory, California Institute of Technology, under contract with the National Aeronautics and Space Administration.

Fig. 1. The steady state, zonally averaged northward wind computed for a global dust haze of uniform optical depth τ: (top) $\tau = 5$, but without atmospheric tidal flux-convergences; (middle) $\tau = 5$ and with tidal effects; (bottom) $\tau = 2$ and with tidal effects.

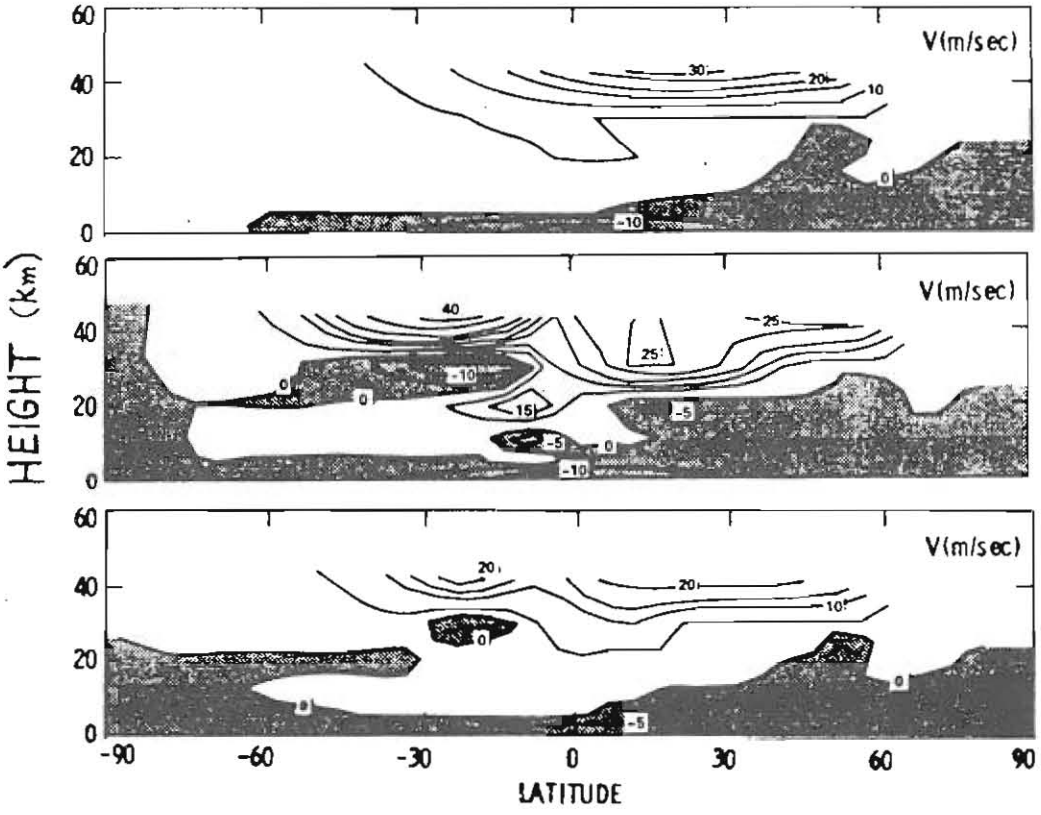

List of Registered Attendees

Edward Albin
Arizona State University

Raymond Arvidson
Washington University

Amos Banin
Hebrew University

Jeffrey Barnes
Oregon State University

Grady Blount
Arizona State University

Philip Christensen
Arizona State University

David Colburn
Ames Research Center

Robert Craddock
Arizona State University

Dave Crown
Arizona State University

Larry Esposito
University of Colorado

James Gooding
Johnson Space Center

Maureen Geringer
Arizona State University

Ronald Greeley
Arizona State University

Robert Haberle
Ames Research Center

Kenneth Herkenhoff
California Institute of Technology

Vicki Horner
Arizona State University

Bruce Jakosky
University of Colorado

Philip James
University of Missouri, St. Louis

Fred Jaquin
Cornell University

Linda Jaramillo
Arizona State University

Ralph Kahn
Washington University

Nicholas Lancaster
Arizona State University

Jeff Lee
Arizona State University

Steven Lee
Arizona State University

Baerbel Lucchitta
U. S. Geological Survey, Flagstaff

Leonard Martin
Lowell Observatory

Terry Martin
Jet Propulsion Laboratory

Henry Moore
U. S. Geological Survey, Menlo Park

Richard Morris
Johnson Space Center

David Paige
Jet Propulsion Laboratory

Alan Peterfreund
University of Massachusetts

James Pollack
Ames Research Center

Ladislav Roth
Jet Propulsion Laboratory

David Scott
NASA Headquarters

Robert Sullivan
Arizona State University

Eilene Theilig
Arizona State University

Peter Thomas
Cornell University

Thomas Thompson
Jet Propulsion Laboratory

James Tillman
University of Washington

Robert West
Jet Propulsion Laboratory

Steven Williams
Arizona State University

James Zimbelman
Lunar and Planetary Institute

Richard Zurek
Jet Propulsion Laboratory

U.S. GOVERNMENT PRINTING OFFICE: 1986—669-014/40335